

Finding flavons at colliders

Gauhar Abbas^{a1}
 Ashutosh Kumar Alok^{b2}
 Neetu Raj Singh Chundawat^{b3}
 Najimuddin Khan^{c4}
 Neelam Singh^{a5}

^a Department of Physics, Indian Institute of Technology (BHU), Varanasi 221005, India

^b Indian Institute of Technology Jodhpur, Jodhpur 342037, India

^c Department of Physics, Aligarh Muslim University, Aligarh-202002, India

Abstract

We conduct a comprehensive investigation into the flavor phenomenology and collider signatures of flavon of $\mathcal{Z}_N \times \mathcal{Z}_M$ flavor symmetries for the soft symmetry-breaking scenario and a new symmetry-conserving mechanism at the high-luminosity LHC, high energy LHC, and a 100 TeV hadron collider. The flavor physics of quark and leptonic observables places different bounds on the parameter space of flavons of $\mathcal{Z}_N \times \mathcal{Z}_M$ flavor symmetries. On the collider side, the decay $t \rightarrow ca$ can be probed by the high-luminosity LHC, high energy LHC, and a 100 TeV hadron collider for the $\mathcal{Z}_8 \times \mathcal{Z}_{22}$ flavor symmetry. The inclusive production signatures can be used to probe the flavon of all the $\mathcal{Z}_N \times \mathcal{Z}_M$ flavor symmetries for the soft symmetry-breaking scenario for a heavy flavon at a 100 TeV collider. Flavons of all the $\mathcal{Z}_N \times \mathcal{Z}_M$ flavor symmetries can be probed at high energy LHC and a 100 TeV collider for a low mass in the case of soft symmetry-breaking. The di-flavon production is within reach of the high-luminosity LHC, high energy LHC, and a 100 TeV collider only for a light flavon. The 14 TeV high-luminosity LHC can probe only the $\mathcal{Z}_2 \times \mathcal{Z}_5$ and $\mathcal{Z}_8 \times \mathcal{Z}_{22}$ flavor symmetries for a few specific inclusive signatures. The symmetry-conserving scenario remains beyond the detection capabilities of any collider.

¹email: gauhar.phy@iitbhu.ac.in

²email: akalok@iitj.ac.in

³email: chundawat.1@iitj.ac.in

⁴email: nkhan.ph@amu.ac.in

⁵email: neelamsingh.rs.phy19@itbhu.ac.in

1 Introduction

The enigma of fermion masses and quark mixing has persisted since the advent of the Standard Model [1, 2]. This challenge has been further exacerbated by the inclusion of neutrino masses and mixing. Potential resolutions to this issue may arise from various theoretical frameworks. Among these are the dark technicolor model, which addresses the problem through hierarchical vacuum expectation values (VEVs) manifested as sequential multi-fermion chiral condensates [3, 4, 5, 6], continuous flavor symmetries [7, 8, 9, 10, 11, 12, 13, 14, 15, 16, 17, 18, 19, 20], discrete symmetries [21, 22, 23], and alternative frameworks [24, 25, 26, 27].

The $\mathcal{Z}_N \times \mathcal{Z}_M$ flavor symmetry [21] is capable of explaining the masses and mixing of fermions through the different realizations of the Froggatt-Nielsen (FN) mechanism [7]. This symmetry is a subset of a more generic $\mathcal{Z}_N \times \mathcal{Z}_M \times \mathcal{Z}_P$ flavor symmetry, which naturally emerges in a dark technicolour framework [4, 1].

The FN mechanism is built upon the idea that an Abelian flavor symmetry $U(1)_F$ can differentiate among the different flavors among inter and intra-fermionic generations of the SM. A flavon field, χ , is employed for this purpose, which couples with the top quark at tree-level, and the masses of other fermions originate from the higher dimensional non-renormalizable operators constructed using the flavon field and choosing the appropriate charges of the fields under the flavor symmetry $U(1)_F$. For instance, if the charges of the fermions fields ψ_i^c and ψ_j are θ_i and θ_j , respectively, under the $U(1)_F$ flavor symmetry, and the Higgs field is assigned zero charge, the Yukawa Lagrangian for the masses of fermions takes the form of non-renormalizable operators,

$$\begin{aligned} \mathcal{O} &= y \left(\frac{\chi}{\Lambda} \right)^{(\theta_i + \theta_j)} \bar{\psi}_i \varphi \psi_j, \\ &= y \epsilon^{(\theta_i + \theta_j)} \bar{\psi}_i \varphi \psi_j = Y \bar{\psi}_i \varphi \psi_j \end{aligned} \quad (1)$$

where y denotes the dimensionless coupling constant, Λ represents the scale of the flavor symmetry, $\epsilon = \frac{\langle \chi \rangle}{\Lambda}$, $Y = y \epsilon^{(\theta_i + \theta_j)}$ stands for the effective Yukawa coupling, and the transformation of the gauge singlet flavon scalar field χ under the $SU(3)_c \times SU(2)_L \times U(1)_Y$ symmetry of the SM is given by,

$$\chi : (1, 1, 0). \quad (2)$$

The VEV of the flavon field χ breaks the $U(1)_F$ flavor symmetry spontaneously. The scale Λ , where the higher dimension operators appearing in equation 1 get renormalized, is not predicted by the FN mechanism, and it can be anywhere between the weak and the Planck scale. The essential requirement for the FN mechanism is that the flavor symmetry is broken in a way such that the ratio $\frac{\langle \chi \rangle}{\Lambda} < 1$.

The flavor phenomenology of the flavon field is determined by the scale Λ . The flavon field can impact flavor observables such as neutral meson mixing and CP -violation, meson decays, and charged lepton flavor violating effects. These effects could be detectable if the scale Λ is relatively low, closer to the weak scale. In such a scenario, it would also be possible to investigate the direct production of flavons in hadron colliders, like the Large Hadron Collider (LHC). Therefore, a critical question is how low the scale Λ can be, while still satisfying constraints from flavor physics data. This question also hinges on the nature of the flavor symmetry implementing the FN mechanism. For a continuous symmetry such as the $U(1)_F$ flavor symmetry, it is essential to determine whether it is a global or gauged symmetry. If $U(1)_F$ is a gauged symmetry, the flavor and collider phenomenology of the flavon field will include contributions from the exchange of the corresponding gauge boson. Conversely, a global $U(1)_F$ flavor symmetry would face the issue of a massless Goldstone boson.

The $\mathcal{Z}_N \times \mathcal{Z}_M$ flavor symmetry creates the FN mechanism through the product of two discrete symmetries. This results in a flavor structure of the SM, which is written in terms of the small parameter ϵ . The neutrino masses and mixing can also be recovered in this framework [22]. The theoretical origin of the $\mathcal{Z}_N \times \mathcal{Z}_M$ flavor symmetry may be traced back to an underlying Abelian or non-Abelian continuous symmetry or their products. For instance, in the dark technicolour framework, this symmetry is the result of the breaking of the two $U(1)$ axial symmetries [4, 1].

The flavor phenomenology of two simple prototypes of the $\mathcal{Z}_N \times \mathcal{Z}_M$ flavor symmetries is investigated in reference [22] where $N = 2$ and $M = 5, 9$ are used. The choice $N = 2$ is inspired by the use of the discrete \mathcal{Z}_2 symmetry in different scenarios, such as the two-Higgs-doublet model (2HDM) and the minimal supersymmetric SM

(MSSM), as well as the left-right symmetric mirror models [28, 29, 30, 31]. There are extensive phenomenological investigations of the flavon field in literature. For instance, for flavor phenomenology, see references [22, 32, 33, 34, 35, 36], and for collider studies, see the references [37, 38, 39, 40, 41, 42, 23, 43, 44, 45].

In this work, we conduct a comprehensive investigation into the flavor phenomenology and collider signatures of the flavon associated with $\mathcal{Z}_N \times \mathcal{Z}_M$ flavor symmetries, extending beyond established prototypes. We examine quark flavor constraints through neutral meson mixing and decays and derive constraints on the flavon of $\mathcal{Z}_N \times \mathcal{Z}_M$ flavor symmetries from a wide range of observables in diverse decay channels, specifically focusing on the quark-level transition $b \rightarrow s\mu^+\mu^-$. Additionally, we investigate the muon forward-backward asymmetry in $B \rightarrow K\mu^+\mu^-$ decays, which is predicted to be zero within the SM. Furthermore, we explore the bounds from future sensitivities of lepton flavor violation experiments such as MEG-II, Mu3e, PRISM/PRIME, DeeMe, Mu2e, and COMET. We demonstrate that these upcoming experiments have the potential to constrain the parameter space of the flavon associated with $\mathcal{Z}_N \times \mathcal{Z}_M$ flavor symmetries by orders of magnitude compared to existing limits.

In the conventional approach, flavor and collider studies of flavon physics involve imparting mass to the pseudoscalar component of the flavon field through a soft symmetry-breaking term [22, 32, 33, 35, 36]. We investigate the flavor phenomenology and collider signatures of the flavon associated with $\mathcal{Z}_N \times \mathcal{Z}_M$ flavor symmetries using both the conventional approach and a novel symmetry-conserving mass mechanism for the pseudoscalar component of the flavon field. This novel scenario proves to be highly predictive.

For the collider signatures, our primary focus is on the High Luminosity LHC (HL-LHC), the High-Energy Large Hadron Collider (HE-LHC) [46], and a future high-luminosity 100 TeV hadron collider such as FCC-hh [47]. We classify the search for flavons into low and high-mass regions, with the low-mass region being particularly sensitive to the new symmetry-conserving mass mechanism of the pseudoscalar flavon. We utilize inclusive decay channels such as $\ell\bar{\ell}$, $b\bar{b}$, and $t\bar{t}$, as well as associative production channels like $t\bar{t}a \rightarrow t\bar{t}t\bar{t}$, $gg \rightarrow ab\bar{b} \rightarrow \tau\tau b\bar{b}$, and $gb \rightarrow ab \rightarrow \tau\tau b$ to identify the flavon of different $\mathcal{Z}_N \times \mathcal{Z}_M$ flavor symmetries. Additionally, we investigate di-flavon production for both light and heavy flavon to determine the sensitivities of flavon models associated with $\mathcal{Z}_N \times \mathcal{Z}_M$ flavor symmetries. Throughout our investigation, we do not assume any specific ultraviolet (UV) completion of the $\mathcal{Z}_N \times \mathcal{Z}_M$ flavor symmetries, and we conduct our phenomenological studies in a model-independent manner.

This work will be presented along the following track: In section 2, we discuss different $\mathcal{Z}_N \times \mathcal{Z}_M$ flavor symmetries and their motivations. The scalar potential with the soft symmetry-breaking and the symmetry-conserving scenarios is presented in section 3. In section 4, bounds on the parameter space of the flavon of different $\mathcal{Z}_N \times \mathcal{Z}_M$ flavor symmetries from quark flavor physics are derived. We discuss constraints from lepton flavor violation experiments in section 5. We discuss the hadron collider physics of the flavon of the $\mathcal{Z}_N \times \mathcal{Z}_M$ flavor symmetries in section 6. In section 7, we summarize this work.

2 The $\mathcal{Z}_N \times \mathcal{Z}_M$ flavor symmetry

In this section, we present different realizations of the $\mathcal{Z}_N \times \mathcal{Z}_M$ flavor symmetry, for which we investigate the flavor phenomenology and collider signatures of the flavon field. A minimal form of the $\mathcal{Z}_N \times \mathcal{Z}_M$ flavor symmetry, $\mathcal{Z}_2 \times \mathcal{Z}_5$, was first proposed in reference [21], and flavor bounds on this minimal form, along with a non-minimal form, $\mathcal{Z}_2 \times \mathcal{Z}_9$, are derived in reference [4].

The theoretical origin of the $\mathcal{Z}_N \times \mathcal{Z}_M$ flavor symmetry may come from spontaneous breaking of a $U(1) \times U(1)$ symmetry, which could be a global or a local symmetry. It is also possible that this symmetry contains only one $U(1)$ factor as a local symmetry. The crucial difference between the FN mechanism based on the $\mathcal{Z}_N \times \mathcal{Z}_M$ flavor symmetry and the FN mechanism based on a $U(1)$ symmetry is that the $\mathcal{Z}_N \times \mathcal{Z}_M$ flavor symmetry may also originate from the breaking of a global $U(1)_A \times U(1)_A$ symmetry. This keeps apart the FN mechanism based on the $\mathcal{Z}_N \times \mathcal{Z}_M$ flavor symmetry from that based on the conventional $U(1)$ symmetry. Such a theoretical scenario is discussed in the appendix.

The FN mechanism is produced by imposing the $\mathcal{Z}_N \times \mathcal{Z}_M$ flavor symmetry on the SM. This provides the following mass Lagrangian for fermions,

$$-\mathcal{L}_{\text{Yukawa}} = \left[\frac{\chi(\text{or } \chi^\dagger)}{\Lambda} \right]^{n_{ij}^u} y_{ij}^u \bar{\psi}_{L_i}^q \tilde{\varphi} \psi_{R_j}^u + \left[\frac{\chi(\text{or } \chi^\dagger)}{\Lambda} \right]^{n_{ij}^d} y_{ij}^d \bar{\psi}_{L_i}^q \varphi \psi_{R_j}^d$$

$$+ \left[\frac{\chi(\text{or } \chi^\dagger)}{\Lambda} \right]^{n_{ij}} y_{ij}^\ell \bar{\psi}_{L_i}^\ell \varphi \psi_{R_j}^\ell + \text{H.c.}, \quad (3)$$

The complex singlet scalar field χ acquires VEV $\langle \chi \rangle = f$, and the Lagrangian corresponding to the SM fermions (charged leptons and quarks) mass is given by

$$-\mathcal{L}_{\text{Yukawa}} = Y_{ij}^u \bar{\psi}_{L_i}^q \tilde{\varphi} \psi_{R_j}^u + Y_{ij}^d \bar{\psi}_{L_i}^q \varphi \psi_{R_j}^d + Y_{ij}^\ell \bar{\psi}_{L_i}^\ell \varphi \psi_{R_j}^\ell + \text{H.c.}, \quad (4)$$

where i and j show the generation indices, ψ_L^q, ψ_L^ℓ are left-handed doublets of the quark and leptonic fields, $\psi_R^u, \psi_R^d, \psi_R^\ell$ are the right-handed up, down-type quarks and leptons, $\tilde{\varphi} = -i\sigma_2 \varphi^*$, φ represent the SM Higgs doublet, and σ_2 is the second Pauli matrix. The couplings Y_{ij} stand for the effective Yukawa couplings such that $Y_{ij} = y_{ij} \epsilon^{n_{ij}}$, where $\frac{\langle \chi \rangle}{\Lambda} = \frac{f}{\sqrt{2}\Lambda} = \epsilon < 1$.

2.1 $\mathcal{Z}_2 \times \mathcal{Z}_5$ flavor symmetry

The first minimal realization of the $\mathcal{Z}_N \times \mathcal{Z}_M$ flavor symmetry is the $\mathcal{Z}_2 \times \mathcal{Z}_5$ flavor symmetry. This can produce the charged fermion masses and mixing along with that of neutrinos. This is an essential criteria for a solution to the flavor problem [4]. The transformations of the scalar and fermionic fields under this symmetry are provided in table 1.

Fields	\mathcal{Z}_2	\mathcal{Z}_5
u_R, c_R, t_R	+	ω^2
$d_R, s_R, b_R, e_R, \mu_R, \tau_R$	-	ω
$\psi_{L_1}^q$	+	ω
$\psi_{L_2}^q$	+	ω^4
$\psi_{L_3}^q$	+	ω^2
$\psi_{L_1}^\ell$	+	ω
$\psi_{L_2}^\ell$	+	ω^4
$\psi_{L_3}^\ell$	+	ω^2
χ	-	ω
φ	+	1

Table 1: The charges of left and right-handed fermions of three families of the SM, right-handed neutrinos, Higgs, and singlet scalar fields under \mathcal{Z}_2 and \mathcal{Z}_5 symmetries, where ω is the fifth root of unity.

The $\mathcal{Z}_2 \times \mathcal{Z}_5$ flavor symmetry enables us to write the mass Lagrangian for charged fermions as,

$$\begin{aligned} -\mathcal{L}_{\text{Yukawa}} = & \left(\frac{\chi}{\Lambda}\right)^4 y_{11}^u \bar{\psi}_{L_1}^q \tilde{\varphi} u_R + \left(\frac{\chi}{\Lambda}\right)^4 y_{12}^u \bar{\psi}_{L_1}^q \tilde{\varphi} c_R + \left(\frac{\chi}{\Lambda}\right)^4 y_{13}^u \bar{\psi}_{L_1}^q \tilde{\varphi} t_R + \left(\frac{\chi}{\Lambda}\right)^2 y_{21}^u \bar{\psi}_{L_2}^q \tilde{\varphi} u_R \\ & + \left(\frac{\chi}{\Lambda}\right)^2 y_{22}^u \bar{\psi}_{L_2}^q \tilde{\varphi} c_R + \left(\frac{\chi}{\Lambda}\right)^2 y_{23}^u \bar{\psi}_{L_2}^q \tilde{\varphi} t_R + y_{31}^u \bar{\psi}_{L_3}^q \tilde{\varphi} u_R + y_{32}^u \bar{\psi}_{L_3}^q \tilde{\varphi} c_R + y_{33}^u \bar{\psi}_{L_3}^q \tilde{\varphi} t_R \\ & + \left(\frac{\chi}{\Lambda}\right)^5 y_{11}^d \bar{\psi}_{L_1}^q \varphi d_R + \left(\frac{\chi}{\Lambda}\right)^5 y_{12}^d \bar{\psi}_{L_1}^q \varphi s_R + \left(\frac{\chi}{\Lambda}\right)^5 y_{13}^d \bar{\psi}_{L_1}^q \varphi b_R + \left(\frac{\chi}{\Lambda}\right)^3 y_{21}^d \bar{\psi}_{L_2}^q \varphi d_R \\ & + \left(\frac{\chi}{\Lambda}\right)^3 y_{22}^d \bar{\psi}_{L_2}^q \varphi s_R + \left(\frac{\chi}{\Lambda}\right)^3 y_{23}^d \bar{\psi}_{L_2}^q \varphi b_R + \left(\frac{\chi}{\Lambda}\right) y_{31}^d \bar{\psi}_{L_3}^q \varphi d_R + \left(\frac{\chi}{\Lambda}\right) y_{32}^d \bar{\psi}_{L_3}^q \varphi s_R \\ & + \left(\frac{\chi}{\Lambda}\right) y_{33}^d \bar{\psi}_{L_3}^q \varphi b_R + \left(\frac{\chi}{\Lambda}\right)^5 y_{11}^\ell \bar{\psi}_{L_1}^\ell \varphi e_R + \left(\frac{\chi}{\Lambda}\right)^5 y_{12}^\ell \bar{\psi}_{L_1}^\ell \varphi \mu_R + \left(\frac{\chi}{\Lambda}\right)^5 y_{13}^\ell \bar{\psi}_{L_1}^\ell \varphi \tau_R \\ & + \left(\frac{\chi}{\Lambda}\right)^3 y_{21}^\ell \bar{\psi}_{L_2}^\ell \varphi e_R + \left(\frac{\chi}{\Lambda}\right)^3 y_{22}^\ell \bar{\psi}_{L_2}^\ell \varphi \mu_R + \left(\frac{\chi}{\Lambda}\right)^3 y_{23}^\ell \bar{\psi}_{L_2}^\ell \varphi \tau_R + \left(\frac{\chi}{\Lambda}\right) y_{31}^\ell \bar{\psi}_{L_3}^\ell \varphi e_R \\ & + \left(\frac{\chi}{\Lambda}\right) y_{32}^\ell \bar{\psi}_{L_3}^\ell \varphi \mu_R + \left(\frac{\chi}{\Lambda}\right) y_{33}^\ell \bar{\psi}_{L_3}^\ell \varphi \tau_R + \text{H.c.} \end{aligned}$$

The mass matrices for up- and down-type quarks and charged leptons read,

$$\mathcal{M}_u = \frac{v}{\sqrt{2}} \begin{pmatrix} y_{11}^u \epsilon^4 & y_{12}^u \epsilon^4 & y_{13}^u \epsilon^4 \\ y_{21}^u \epsilon^2 & y_{22}^u \epsilon^2 & y_{23}^u \epsilon^2 \\ y_{31}^u & y_{32}^u & y_{33}^u \end{pmatrix}, \mathcal{M}_d = \frac{v}{\sqrt{2}} \begin{pmatrix} y_{11}^d \epsilon^5 & y_{12}^d \epsilon^5 & y_{13}^d \epsilon^5 \\ y_{21}^d \epsilon^3 & y_{22}^d \epsilon^3 & y_{23}^d \epsilon^3 \\ y_{31}^d & y_{32}^d & y_{33}^d \end{pmatrix}, \mathcal{M}_\ell = \frac{v}{\sqrt{2}} \begin{pmatrix} y_{11}^\ell \epsilon^5 & y_{12}^\ell \epsilon^5 & y_{13}^\ell \epsilon^5 \\ y_{21}^\ell \epsilon^3 & y_{22}^\ell \epsilon^3 & y_{23}^\ell \epsilon^3 \\ y_{31}^\ell & y_{32}^\ell & y_{33}^\ell \end{pmatrix}, \quad (5)$$

where $\epsilon = 0.1$ can produce the required masses of the fermions.

The masses of the charged fermions can be written as[48],

$$\{m_t, m_c, m_u\} \simeq \{|y_{33}^u|, \left|y_{22}^u - \frac{y_{23}^u y_{32}^u}{|y_{33}^u|}\right| \epsilon^2, \quad (6)$$

$$\left|y_{11}^u - \frac{y_{12}^u y_{21}^u}{|y_{22}^u - y_{23}^u y_{32}^u / y_{33}^u|} - \frac{y_{13}^u |y_{31}^u y_{22}^u - y_{21}^u y_{32}^u| - y_{31}^u y_{12}^u y_{23}^u}{|y_{22}^u - y_{23}^u y_{32}^u / y_{33}^u| |y_{33}^u|}\right| \epsilon^4\} v / \sqrt{2},$$

$$\{m_b, m_s, m_d\} \simeq \{|y_{33}^d| \epsilon, \left|y_{22}^d - \frac{y_{23}^d y_{32}^d}{|y_{33}^d|}\right| \epsilon^3, \quad (7)$$

$$\left|y_{11}^d - \frac{y_{12}^d y_{21}^d}{|y_{22}^d - y_{23}^d y_{32}^d / y_{33}^d|} - \frac{y_{13}^d |y_{31}^d y_{22}^d - y_{21}^d y_{32}^d| - y_{31}^d y_{12}^d y_{23}^d}{|y_{22}^d - y_{23}^d y_{32}^d / y_{33}^d| |y_{33}^d|}\right| \epsilon^5\} v / \sqrt{2},$$

$$\{m_\tau, m_\mu, m_e\} \simeq \{|y_{33}^\ell| \epsilon, \left|y_{22}^\ell - \frac{y_{23}^\ell y_{32}^\ell}{|y_{33}^\ell|}\right| \epsilon^3, \quad (8)$$

$$\left|y_{11}^\ell - \frac{y_{12}^\ell y_{21}^\ell}{|y_{22}^\ell - y_{23}^\ell y_{32}^\ell / y_{33}^\ell|} - \frac{y_{13}^\ell |y_{31}^\ell y_{22}^\ell - y_{21}^\ell y_{32}^\ell| - y_{31}^\ell y_{12}^\ell y_{23}^\ell}{|y_{22}^\ell - y_{23}^\ell y_{32}^\ell / y_{33}^\ell| |y_{33}^\ell|}\right| \epsilon^5\} v / \sqrt{2}. \quad (9)$$

The quark mixing angles are [49],

$$\begin{aligned} \sin \theta_{12} \simeq |V_{us}| &\simeq \left| \frac{y_{12}^d}{y_{22}^d} - \frac{y_{12}^u}{y_{22}^u} \right| \epsilon^2, \sin \theta_{23} \simeq |V_{cb}| \simeq \left| \frac{y_{23}^d}{y_{33}^d} - \frac{y_{23}^u}{y_{33}^u} \right| \epsilon^2, \\ \sin \theta_{13} \simeq |V_{ub}| &\simeq \left| \frac{y_{13}^d}{y_{33}^d} - \frac{y_{12}^u y_{23}^d}{y_{22}^u y_{33}^d} - \frac{y_{13}^u}{y_{33}^u} \right| \epsilon^4. \end{aligned} \quad (10)$$

2.2 $\mathcal{Z}_2 \times \mathcal{Z}_9$ flavor symmetry

A non-minimal realization of the $\mathcal{Z}_N \times \mathcal{Z}_M$ flavor symmetry is the $\mathcal{Z}_2 \times \mathcal{Z}_9$ flavor symmetry. The scalar and fermionic fields transform under this symmetry, as given in table 2.

Fields	\mathcal{Z}_2	\mathcal{Z}_9
u_R, t_R	+	1
c_R	+	ω^4
$d_R, s_R, b_R, e_R, \mu_R, \tau_R$	-	ω^3
$\psi_{L_1}^q$	+	ω
$\psi_{L_2}^q$	+	ω^8
$\psi_{L_3}^q$	+	1
$\psi_{L_1}^\ell$	+	ω
$\psi_{L_2}^\ell$	+	ω^8
$\psi_{L_3}^\ell$	+	ω^6
χ	-	ω
φ	+	1

Table 2: The charges of left and right-handed fermions of three families of the SM, right-handed neutrinos, Higgs, and singlet scalar field under \mathcal{Z}_2 and \mathcal{Z}_9 symmetries, where ω is the ninth root of unity.

After imposing the $\mathcal{Z}_2 \times \mathcal{Z}_9$ flavor symmetry on the SM, the mass Lagrangian for charged fermions reads as,

$$\begin{aligned}
-\mathcal{L}_{\text{Yukawa}} = & \left(\frac{\chi^\dagger}{\Lambda}\right)^8 y_{11}^u \bar{\psi}_{L_1}^q \tilde{\varphi} u_R + \left(\frac{\chi}{\Lambda}\right)^6 y_{12}^u \bar{\psi}_{L_1}^q \tilde{\varphi} c_R + \left(\frac{\chi^\dagger}{\Lambda}\right)^8 y_{13}^u \bar{\psi}_{L_1}^q \tilde{\varphi} t_R + \left(\frac{\chi}{\Lambda}\right)^8 y_{21}^u \bar{\psi}_{L_2}^q \tilde{\varphi} u_R \\
& + \left(\frac{\chi}{\Lambda}\right)^4 y_{22}^u \bar{\psi}_{L_2}^q \tilde{\varphi} c_R + \left(\frac{\chi}{\Lambda}\right)^8 y_{23}^u \bar{\psi}_{L_2}^q \tilde{\varphi} t_R + y_{31}^u \bar{\psi}_{L_3}^q \tilde{\varphi} u_R + \left(\frac{\chi^\dagger}{\Lambda}\right)^4 y_{32}^u \bar{\psi}_{L_3}^q \tilde{\varphi} c_R + y_{33}^u \bar{\psi}_{L_3}^q \tilde{\varphi} t_R \\
& + \left(\frac{\chi}{\Lambda}\right)^7 y_{11}^d \bar{\psi}_{L_1}^q \varphi d_R + \left(\frac{\chi}{\Lambda}\right)^7 y_{12}^d \bar{\psi}_{L_1}^q \varphi s_R + \left(\frac{\chi}{\Lambda}\right)^7 y_{13}^d \bar{\psi}_{L_1}^q \varphi b_R + \left(\frac{\chi}{\Lambda}\right)^5 y_{21}^d \bar{\psi}_{L_2}^q \varphi d_R \\
& + \left(\frac{\chi}{\Lambda}\right)^5 y_{22}^d \bar{\psi}_{L_2}^q \varphi s_R + \left(\frac{\chi}{\Lambda}\right)^5 y_{23}^d \bar{\psi}_{L_2}^q \varphi b_R + \left(\frac{\chi^\dagger}{\Lambda}\right)^3 y_{31}^d \bar{\psi}_{L_3}^q \varphi d_R + \left(\frac{\chi^\dagger}{\Lambda}\right)^3 y_{32}^d \bar{\psi}_{L_3}^q \varphi s_R \\
& + \left(\frac{\chi^\dagger}{\Lambda}\right)^3 y_{33}^d \bar{\psi}_{L_3}^q \varphi b_R + \left(\frac{\chi}{\Lambda}\right)^7 y_{11}^\ell \bar{\psi}_{L_1}^\ell \varphi e_R + \left(\frac{\chi}{\Lambda}\right)^7 y_{12}^\ell \bar{\psi}_{L_1}^\ell \varphi \mu_R + \left(\frac{\chi}{\Lambda}\right)^7 y_{13}^\ell \bar{\psi}_{L_1}^\ell \varphi \tau_R \\
& + \left(\frac{\chi}{\Lambda}\right)^5 y_{21}^\ell \bar{\psi}_{L_2}^\ell \varphi e_R + \left(\frac{\chi}{\Lambda}\right)^5 y_{22}^\ell \bar{\psi}_{L_2}^\ell \varphi \mu_R + \left(\frac{\chi}{\Lambda}\right)^5 y_{23}^\ell \bar{\psi}_{L_2}^\ell \varphi \tau_R + \left(\frac{\chi}{\Lambda}\right)^3 y_{31}^\ell \bar{\psi}_{L_3}^\ell \varphi e_R \\
& + \left(\frac{\chi}{\Lambda}\right)^3 y_{32}^\ell \bar{\psi}_{L_3}^\ell \varphi \mu_R + \left(\frac{\chi}{\Lambda}\right)^3 y_{33}^\ell \bar{\psi}_{L_3}^\ell \varphi \tau_R + \text{H.c.}
\end{aligned}$$

The mass matrices for up and down-type quarks and charged leptons read,

$$\mathcal{M}_u = \frac{v}{\sqrt{2}} \begin{pmatrix} y_{11}^u \epsilon^8 & y_{12}^u \epsilon^6 & y_{13}^u \epsilon^8 \\ y_{21}^u \epsilon^8 & y_{22}^u \epsilon^4 & y_{23}^u \epsilon^8 \\ y_{31}^u & y_{32}^u \epsilon^4 & y_{33}^u \end{pmatrix}, \mathcal{M}_d = \frac{v}{\sqrt{2}} \begin{pmatrix} y_{11}^d \epsilon^7 & y_{12}^d \epsilon^7 & y_{13}^d \epsilon^7 \\ y_{21}^d \epsilon^5 & y_{22}^d \epsilon^5 & y_{23}^d \epsilon^5 \\ y_{31}^d \epsilon^3 & y_{32}^d \epsilon^3 & y_{33}^d \epsilon^3 \end{pmatrix}, \mathcal{M}_\ell = \frac{v}{\sqrt{2}} \begin{pmatrix} y_{11}^\ell \epsilon^7 & y_{12}^\ell \epsilon^7 & y_{13}^\ell \epsilon^7 \\ y_{21}^\ell \epsilon^5 & y_{22}^\ell \epsilon^5 & y_{23}^\ell \epsilon^5 \\ y_{31}^\ell \epsilon^3 & y_{32}^\ell \epsilon^3 & y_{33}^\ell \epsilon^3 \end{pmatrix}. \quad (11)$$

where $\epsilon = 0.225$ is chosen to produce the masses of fermions.

The masses of charged fermions are approximately [48],

$$\{m_t, m_c, m_u\} \simeq \{|y_{33}^u|, \left|y_{22}^u \epsilon^4 - \frac{y_{23}^u y_{32}^u}{|y_{33}^u|} \epsilon^{12}\right|, \quad (12)$$

$$\left|y_{11}^u \epsilon^8 - \frac{y_{12}^u y_{21}^u}{|y_{22}^u|} \epsilon^{10} - \frac{y_{13}^u |y_{31}^u y_{22}^u - y_{21}^u y_{32}^u|}{|y_{22}^u| |y_{33}^u|} \epsilon^8\right\} v / \sqrt{2}, \\
\{m_b, m_s, m_d\} \simeq \{|y_{33}^d| \epsilon^3, \left|y_{22}^d - \frac{y_{23}^d y_{32}^d}{|y_{33}^d|}\right| \epsilon^5, \quad (13)$$

$$\left|y_{11}^d - \frac{y_{12}^d y_{21}^d}{|y_{22}^d - y_{23}^d y_{32}^d / y_{33}^d|} - \frac{y_{13}^d |y_{31}^d y_{22}^d - y_{21}^d y_{32}^d| - y_{31}^d y_{12}^d y_{23}^d}{|y_{22}^d - y_{23}^d y_{32}^d / y_{33}^d| |y_{33}^d|}\right| \epsilon^7\} v / \sqrt{2}, \\
\{m_\tau, m_\mu, m_e\} \simeq \{|y_{33}^l| \epsilon^3, \left|y_{22}^l - \frac{y_{23}^l y_{32}^l}{|y_{33}^l|}\right| \epsilon^5, \quad (14)$$

$$\left|y_{11}^l - \frac{y_{12}^l y_{21}^l}{|y_{22}^l - y_{23}^l y_{32}^l / y_{33}^l|} - \frac{y_{13}^l |y_{31}^l y_{22}^l - y_{21}^l y_{32}^l| - y_{31}^l y_{12}^l y_{23}^l}{|y_{22}^l - y_{23}^l y_{32}^l / y_{33}^l| |y_{33}^l|}\right| \epsilon^7\} v / \sqrt{2}. \quad (15)$$

The quark mixing angles are identical to that of the minimal $\mathcal{Z}_2 \times \mathcal{Z}_5$ flavor symmetry.

2.3 $\mathcal{Z}_2 \times \mathcal{Z}_{11}$ flavor symmetry

The next non-minimal realization of the $\mathcal{Z}_N \times \mathcal{Z}_M$ flavor symmetry is the $\mathcal{Z}_2 \times \mathcal{Z}_{11}$ flavor symmetry. The $\mathcal{Z}_2 \times \mathcal{Z}_{11}$ flavor symmetry, in this work, is chosen to probe a relatively large value of the parameter ϵ , which is 0.28. The scalar and fermionic fields transform under this symmetry, as shown in table 3.

The mass Lagrangian for charged fermions after imposing $\mathcal{Z}_2 \times \mathcal{Z}_{11}$ flavor symmetry on the SM reads,

$$-\mathcal{L}_{\text{Yukawa}} = \left(\frac{\chi}{\Lambda}\right)^{10} y_{11}^u \bar{\psi}_{L_1}^q \tilde{\varphi} u_R + \left(\frac{\chi}{\Lambda}\right)^{10} y_{12}^u \bar{\psi}_{L_1}^q \tilde{\varphi} c_R + \left(\frac{\chi}{\Lambda}\right)^{12} y_{13}^u \bar{\psi}_{L_1}^q \tilde{\varphi} t_R + \left(\frac{\chi^\dagger}{\Lambda}\right)^6 y_{21}^u \bar{\psi}_{L_2}^q \tilde{\varphi} u_R$$

Fields	\mathcal{Z}_2	\mathcal{Z}_{11}
u_R, c_R	+	ω^2
t_R	+	1
$d_R, s_R, b_R, e_R, \mu_R, \tau_R$	-	ω^3
ψ_L^1	+	ω
ψ_L^2	+	ω^7
ψ_L^3	+	1
χ	-	ω
φ	+	1
σ	+	ω^4

Table 3: The charges of left and right-handed fermions of three families of the SM, right-handed neutrinos, Higgs, and singlet scalar fields under \mathcal{Z}_2 and \mathcal{Z}_{11} symmetries, where ω is the eleventh root of unity.

$$\begin{aligned}
& + \left(\frac{\chi^\dagger}{\Lambda}\right)^6 y_{22}^u \bar{\psi}_{L_2}^q \tilde{\varphi} c_R + \left(\frac{\chi^\dagger}{\Lambda}\right)^4 y_{23}^u \bar{\psi}_{L_2}^q \tilde{\varphi} t_R + \left(\frac{\chi^\dagger}{\Lambda}\right)^2 y_{31}^u \bar{\psi}_{L_3}^q \tilde{\varphi} u_R + \left(\frac{\chi^\dagger}{\Lambda}\right)^2 y_{32}^u \bar{\psi}_{L_3}^q \tilde{\varphi} c_R \\
& + y_{33}^u \bar{\psi}_{L_3}^q \tilde{\varphi} t_R + \left(\frac{\chi}{\Lambda}\right)^9 y_{11}^d \bar{\psi}_{L_1}^q \varphi d_R + \left(\frac{\chi}{\Lambda}\right)^9 y_{12}^d \bar{\psi}_{L_1}^q \varphi s_R + \left(\frac{\chi}{\Lambda}\right)^9 y_{13}^d \bar{\psi}_{L_1}^q \varphi b_R + \left(\frac{\chi^\dagger}{\Lambda}\right)^7 y_{21}^d \bar{\psi}_{L_2}^q \varphi d_R \\
& + \left(\frac{\chi^\dagger}{\Lambda}\right)^7 y_{22}^d \bar{\psi}_{L_2}^q \varphi s_R + \left(\frac{\chi^\dagger}{\Lambda}\right)^7 y_{23}^d \bar{\psi}_{L_2}^q \varphi b_R + \left(\frac{\chi^\dagger}{\Lambda}\right)^3 y_{31}^d \bar{\psi}_{L_3}^q \varphi d_R + \left(\frac{\chi^\dagger}{\Lambda}\right)^3 y_{32}^d \bar{\psi}_{L_3}^q \varphi s_R \\
& + \left(\frac{\chi^\dagger}{\Lambda}\right)^3 y_{33}^d \bar{\psi}_{L_3}^q \varphi b_R + \left(\frac{\chi}{\Lambda}\right)^9 y_{11}^\ell \bar{\psi}_{L_1}^\ell \varphi e_R + \left(\frac{\chi}{\Lambda}\right)^9 y_{12}^\ell \bar{\psi}_{L_1}^\ell \varphi \mu_R + \left(\frac{\chi}{\Lambda}\right)^9 y_{13}^\ell \bar{\psi}_{L_1}^\ell \varphi \tau_R \\
& + \left(\frac{\chi^\dagger}{\Lambda}\right)^7 y_{21}^\ell \bar{\psi}_{L_2}^\ell \varphi e_R + \left(\frac{\chi^\dagger}{\Lambda}\right)^7 y_{22}^\ell \bar{\psi}_{L_2}^\ell \varphi \mu_R + \left(\frac{\chi^\dagger}{\Lambda}\right)^7 y_{23}^\ell \bar{\psi}_{L_2}^\ell \varphi \tau_R + \left(\frac{\chi^\dagger}{\Lambda}\right)^3 y_{31}^\ell \bar{\psi}_{L_3}^\ell \varphi e_R \\
& + \left(\frac{\chi^\dagger}{\Lambda}\right)^3 y_{32}^\ell \bar{\psi}_{L_3}^\ell \varphi \mu_R + \left(\frac{\chi^\dagger}{\Lambda}\right)^3 y_{33}^\ell \bar{\psi}_{L_3}^\ell \varphi \tau_R + \text{H.c.}
\end{aligned}$$

The mass matrices for up- and down-type quarks and charged leptons turn out to be,

$$\mathcal{M}_u = \frac{v}{\sqrt{2}} \begin{pmatrix} y_{11}^u \epsilon^{10} & y_{12}^u \epsilon^{10} & y_{13}^u \epsilon^{12} \\ y_{21}^u \epsilon^6 & y_{22}^u \epsilon^6 & y_{23}^u \epsilon^4 \\ y_{31}^u \epsilon^2 & y_{32}^u \epsilon^2 & y_{33}^u \end{pmatrix}, \mathcal{M}_d = \frac{v}{\sqrt{2}} \begin{pmatrix} y_{11}^d \epsilon^9 & y_{12}^d \epsilon^9 & y_{13}^d \epsilon^9 \\ y_{21}^d \epsilon^7 & y_{22}^d \epsilon^7 & y_{23}^d \epsilon^7 \\ y_{31}^d \epsilon^3 & y_{32}^d \epsilon^3 & y_{33}^d \epsilon^3 \end{pmatrix}, \mathcal{M}_\ell = \frac{v}{\sqrt{2}} \begin{pmatrix} y_{11}^\ell \epsilon^9 & y_{12}^\ell \epsilon^9 & y_{13}^\ell \epsilon^9 \\ y_{21}^\ell \epsilon^7 & y_{22}^\ell \epsilon^7 & y_{23}^\ell \epsilon^7 \\ y_{31}^\ell \epsilon^3 & y_{32}^\ell \epsilon^3 & y_{33}^\ell \epsilon^3 \end{pmatrix}. \quad (16)$$

The masses of quarks and charged leptons are approximately [48],

$$\{m_t, m_c, m_u\} \simeq \{|y_{33}^u|, \left|y_{22}^u - \frac{y_{23}^u y_{32}^u}{|y_{33}^u|}\right| \epsilon^6, \quad (17)$$

$$\left|y_{11}^u - \frac{y_{12}^u y_{21}^u}{|y_{22}^u - y_{23}^u y_{32}^u / y_{33}^u|} - \frac{y_{13}^u |y_{31}^u y_{22}^u - y_{21}^u y_{32}^u| - y_{31}^u y_{12}^u y_{23}^u}{|y_{22}^u - y_{23}^u y_{32}^u / y_{33}^u| |y_{33}^u|}\right| \epsilon^{10} \} v / \sqrt{2},$$

$$\{m_b, m_s, m_d\} \simeq \{|y_{33}^d| \epsilon^3, \left|y_{22}^d - \frac{y_{23}^d y_{32}^d}{|y_{33}^d|}\right| \epsilon^7, \quad (18)$$

$$\left|y_{11}^d - \frac{y_{12}^d y_{21}^d}{|y_{22}^d - y_{23}^d y_{32}^d / y_{33}^d|} - \frac{y_{13}^d |y_{31}^d y_{22}^d - y_{21}^d y_{32}^d| - y_{31}^d y_{12}^d y_{23}^d}{|y_{22}^d - y_{23}^d y_{32}^d / y_{33}^d| |y_{33}^d|}\right| \epsilon^9 \} v / \sqrt{2},$$

$$\{m_\tau, m_\mu, m_e\} \simeq \{|y_{33}^\ell| \epsilon^3, \left|y_{22}^\ell - \frac{y_{23}^\ell y_{32}^\ell}{|y_{33}^\ell|}\right| \epsilon^7, \quad (19)$$

$$\left|y_{11}^\ell - \frac{y_{12}^\ell y_{21}^\ell}{|y_{22}^\ell - y_{23}^\ell y_{32}^\ell / y_{33}^\ell|} - \frac{y_{13}^\ell |y_{31}^\ell y_{22}^\ell - y_{21}^\ell y_{32}^\ell| - y_{31}^\ell y_{12}^\ell y_{23}^\ell}{|y_{22}^\ell - y_{23}^\ell y_{32}^\ell / y_{33}^\ell| |y_{33}^\ell|}\right| \epsilon^9 \} v / \sqrt{2}. \quad (20)$$

The mixing angles of quarks are found to be [49],

$$\begin{aligned}\sin \theta_{12} \simeq |V_{us}| &\simeq \left| \frac{y_{12}^d}{y_{22}^d} \epsilon^2 - \frac{y_{12}^u}{y_{22}^u} \epsilon^4 \right|, \sin \theta_{23} \simeq |V_{cb}| \simeq \left| \frac{y_{23}^d}{y_{33}^d} - \frac{y_{23}^u}{y_{33}^u} \right| \epsilon^4, \\ \sin \theta_{13} \simeq |V_{ub}| &\simeq \left| \frac{y_{13}^d}{y_{33}^d} \epsilon^6 - \frac{y_{12}^u y_{23}^d}{y_{22}^u y_{33}^d} \epsilon^8 \right|.\end{aligned}\quad (21)$$

The mixing angles in this have a consistent hierarchical pattern of the order $(\epsilon^2, \epsilon^4, \epsilon^6)$. However, to produce the observed values of the fermionic masses and mixing angles, we need a relatively large value of the parameter ϵ .

2.4 The $\mathcal{Z}_8 \times \mathcal{Z}_{22}$ flavor symmetry

This symmetry can provide the so-called flavonic dark matter [50], and is inspired by the hierarchical VEVs model[3, 4], where the mass of the top quark originates from the dimension-5 operator. The transformations of fermionic and scalar fields under this symmetry are given in table 4.

Fields	\mathcal{Z}_8	\mathcal{Z}_{22}	Fields	\mathcal{Z}_8	\mathcal{Z}_{22}	Fields	\mathcal{Z}_8	\mathcal{Z}_{22}	Fields	\mathcal{Z}_8	\mathcal{Z}_{22}	Fields	\mathcal{Z}_8	\mathcal{Z}_{22}
u_R	ω^2	ω^2	c_R	ω^5	ω^5	t_R	ω^6	ω^6	d_R	ω^3	ω^3	s_R	ω^4	ω^4
b_R	ω^4	ω^4	$\psi_{L,1}^q$	ω^2	ω^{10}	$\psi_{L,2}^q$	ω	ω^9	$\psi_{L,3}^q$	ω^7	ω^7	$\psi_{L,1}^\ell$	ω^3	ω^3
$\psi_{L,2}^\ell$	ω^2	ω^2	$\psi_{L,3}^\ell$	ω^2	ω^2	e_R	ω^2	ω^{16}	μ_R	ω^5	ω^{19}	τ_R	ω^7	ω^{21}
ν_{eR}	ω^2	1	$\nu_{\mu R}$	ω^5	ω^3	$\nu_{\tau R}$	ω^6	ω^4	χ	ω	ω	φ	1	1

Table 4: The charges of the SM and the flavon fields under the $\mathcal{Z}_8 \times \mathcal{Z}_{22}$ symmetry, where ω is the 8th and 22nd root of unity.

The $\mathcal{Z}_8 \times \mathcal{Z}_{22}$ symmetry allows us to write mass Lagrangian for the charged fermions as,

$$\begin{aligned}-\mathcal{L}_{\text{Yukawa}} &= \left(\frac{\chi}{\Lambda}\right)^8 y_{11}^u \bar{\psi}_{L1}^q \tilde{\varphi} u_R + \left(\frac{\chi}{\Lambda}\right)^5 y_{12}^u \bar{\psi}_{L1}^q \tilde{\varphi} c_R + \left(\frac{\chi}{\Lambda}\right)^4 y_{13}^u \bar{\psi}_{L1}^q \tilde{\varphi} t_R + \left(\frac{\chi}{\Lambda}\right)^7 y_{21}^u \bar{\psi}_{L2}^q \tilde{\varphi} u_R \\ &+ \left(\frac{\chi}{\Lambda}\right)^4 y_{22}^u \bar{\psi}_{L2}^q \tilde{\varphi} c_R + \left(\frac{\chi}{\Lambda}\right)^3 y_{23}^u \bar{\psi}_{L2}^q \tilde{\varphi} t_R + \left(\frac{\chi}{\Lambda}\right)^5 y_{31}^u \bar{\psi}_{L3}^q \tilde{\varphi} u_R + \left(\frac{\chi}{\Lambda}\right)^2 y_{32}^u \bar{\psi}_{L3}^q \tilde{\varphi} c_R \\ &+ \left(\frac{\chi}{\Lambda}\right) y_{33}^u \bar{\psi}_{L3}^q \tilde{\varphi} t_R + \left(\frac{\chi}{\Lambda}\right)^7 y_{11}^d \bar{\psi}_{L1}^q \varphi d_R + \left(\frac{\chi}{\Lambda}\right)^6 y_{12}^d \bar{\psi}_{L1}^q \varphi s_R + \left(\frac{\chi}{\Lambda}\right)^6 y_{13}^d \bar{\psi}_{L1}^q \varphi b_R + \left(\frac{\chi}{\Lambda}\right)^6 y_{21}^d \bar{\psi}_{L2}^q \varphi d_R \\ &+ \left(\frac{\chi}{\Lambda}\right)^5 y_{22}^d \bar{\psi}_{L2}^q \varphi s_R + \left(\frac{\chi}{\Lambda}\right)^5 y_{23}^d \bar{\psi}_{L2}^q \varphi b_R + \left(\frac{\chi}{\Lambda}\right)^4 y_{31}^d \bar{\psi}_{L3}^q \varphi d_R + \left(\frac{\chi}{\Lambda}\right)^3 y_{32}^d \bar{\psi}_{L3}^q \varphi s_R \\ &+ \left(\frac{\chi}{\Lambda}\right)^3 y_{33}^d \bar{\psi}_{L3}^q \varphi b_R + \left(\frac{\chi}{\Lambda}\right)^9 y_{11}^\ell \bar{\psi}_{L1}^\ell \varphi e_R + \left(\frac{\chi}{\Lambda}\right)^6 y_{12}^\ell \bar{\psi}_{L1}^\ell \varphi \mu_R + \left(\frac{\chi}{\Lambda}\right)^4 y_{13}^\ell \bar{\psi}_{L1}^\ell \varphi \tau_R \\ &+ \left(\frac{\chi}{\Lambda}\right)^8 y_{21}^\ell \bar{\psi}_{L2}^\ell \varphi e_R + \left(\frac{\chi}{\Lambda}\right)^5 y_{22}^\ell \bar{\psi}_{L2}^\ell \varphi \mu_R + \left(\frac{\chi}{\Lambda}\right)^3 y_{23}^\ell \bar{\psi}_{L2}^\ell \varphi \tau_R + \left(\frac{\chi}{\Lambda}\right)^8 y_{31}^\ell \bar{\psi}_{L3}^\ell \varphi e_R \\ &+ \left(\frac{\chi}{\Lambda}\right)^5 y_{32}^\ell \bar{\psi}_{L3}^\ell \varphi \mu_R + \left(\frac{\chi}{\Lambda}\right)^3 y_{33}^\ell \bar{\psi}_{L3}^\ell \varphi \tau_R + \text{H.c.}\end{aligned}$$

The mass matrices of the up and down-type quarks and charged leptons take the forms,

$$\mathcal{M}_u = \frac{v}{\sqrt{2}} \begin{pmatrix} y_{11}^u \epsilon^8 & y_{12}^u \epsilon^5 & y_{13}^u \epsilon^4 \\ y_{21}^u \epsilon^7 & y_{22}^u \epsilon^4 & y_{23}^u \epsilon^3 \\ y_{31}^u \epsilon^5 & y_{32}^u \epsilon^2 & y_{33}^u \epsilon \end{pmatrix}, \mathcal{M}_d = \frac{v}{\sqrt{2}} \begin{pmatrix} y_{11}^d \epsilon^7 & y_{12}^d \epsilon^6 & y_{13}^d \epsilon^6 \\ y_{21}^d \epsilon^6 & y_{22}^d \epsilon^5 & y_{23}^d \epsilon^5 \\ y_{31}^d \epsilon^4 & y_{32}^d \epsilon^3 & y_{33}^d \epsilon^3 \end{pmatrix}, \mathcal{M}_\ell = \frac{v}{\sqrt{2}} \begin{pmatrix} y_{11}^\ell \epsilon^9 & y_{12}^\ell \epsilon^6 & y_{13}^\ell \epsilon^4 \\ y_{21}^\ell \epsilon^8 & y_{22}^\ell \epsilon^5 & y_{23}^\ell \epsilon^3 \\ y_{31}^\ell \epsilon^8 & y_{32}^\ell \epsilon^5 & y_{33}^\ell \epsilon^3 \end{pmatrix}, \quad (22)$$

where $\epsilon = 0.225$ produces the masses and mixing of fermions.

The masses of charged fermions are given by [48],

$$\{m_t, m_c, m_u\} \simeq \{|y_{33}^u| \epsilon, \left| y_{22}^u - \frac{y_{23}^u y_{32}^u}{y_{33}^u} \right| \epsilon^4, \quad (23)$$

$$\left\{m_b, m_s, m_d\right\} \simeq \left\{|y_{33}^d|\epsilon^3, \left|y_{22}^d - \frac{y_{23}^d y_{32}^d}{y_{33}^d}\right|\epsilon^5, \left|y_{11}^u - \frac{y_{12}^u y_{21}^u}{y_{22}^u - y_{23}^u y_{32}^u/y_{33}^u} - \frac{y_{13}^u (y_{31}^u y_{22}^u - y_{21}^u y_{32}^u) - y_{31}^u y_{12}^u y_{23}^u}{(y_{22}^u - y_{23}^u y_{32}^u/y_{33}^u) y_{33}^u}\right|\epsilon^8\right\} v/\sqrt{2}, \quad (24)$$

$$\left\{m_\tau, m_\mu, m_e\right\} \simeq \left\{|y_{33}^l|\epsilon^3, \left|y_{22}^l - \frac{y_{23}^l y_{32}^l}{y_{33}^l}\right|\epsilon^5, \left|y_{11}^d - \frac{y_{12}^d y_{21}^d}{y_{22}^d - y_{23}^d y_{32}^d/y_{33}^d} - \frac{y_{13}^d (y_{31}^d y_{22}^d - y_{21}^d y_{32}^d) - y_{31}^d y_{12}^d y_{23}^d}{(y_{22}^d - y_{23}^d y_{32}^d/y_{33}^d) y_{33}^d}\right|\epsilon^7\right\} v/\sqrt{2}, \quad (25)$$

The mixing angles of quarks can be written as[48],

$$\begin{aligned} \sin \theta_{12} \simeq |V_{us}| &\simeq \left| \frac{y_{12}^d}{y_{22}^d} - \frac{y_{12}^u}{y_{22}^u} \right| \epsilon, \quad \sin \theta_{23} \simeq |V_{cb}| \simeq \left| \frac{y_{23}^d}{y_{33}^d} - \frac{y_{23}^u}{y_{33}^u} \right| \epsilon^2, \\ \sin \theta_{13} \simeq |V_{ub}| &\simeq \left| \frac{y_{13}^d}{y_{33}^d} - \frac{y_{12}^u y_{23}^d}{y_{22}^u y_{33}^d} - \frac{y_{13}^u}{y_{33}^u} \right| \epsilon^3. \end{aligned} \quad (26)$$

We show, in table 5, the values of the parameter ϵ , and the minimum values of the Yukawa couplings $|y_{ij}|_{\min}$ for all four $\mathcal{Z}_N \times \mathcal{Z}_M$ flavor symmetries, we discussed. We notice that the models based on the symmetries $\mathcal{Z}_2 \times \mathcal{Z}_9$ and $\mathcal{Z}_8 \times \mathcal{Z}_{22}$ are described by ideally an order-one couplings providing the best description of fermion masses and mixings.

Model	ϵ	$ y_{ij} _{\min}$
$\mathcal{Z}_2 \times \mathcal{Z}_5$	0.1	≈ 0.1
$\mathcal{Z}_2 \times \mathcal{Z}_9$	0.23	≈ 1
$\mathcal{Z}_2 \times \mathcal{Z}_{11}$	0.28	≈ 0.7
$\mathcal{Z}_8 \times \mathcal{Z}_{22}$	0.23	≈ 1

Table 5: Values of ϵ and $|y_{ij}|_{\min}$ for each $\mathcal{Z}_N \times \mathcal{Z}_M$ flavor symmetry.

3 The scalar potential

The scalar potential of the model acquires the following form,

$$-\mathcal{L}_{\text{potential}} = -\mu^2 \varphi^\dagger \varphi + \lambda (\varphi^\dagger \varphi)^2 - \mu_\chi^2 \chi^* \chi + \lambda_\chi (\chi^* \chi)^2 + \lambda_{\varphi\chi} (\chi^* \chi) (\varphi^\dagger \varphi). \quad (27)$$

In the phenomenological investigation, we assume $\lambda_{\varphi\chi} = 0$, i.e., no Higgs-flavon mixing. The effects of this coupling are explored in reference [38]. We parametrize the scalar fields as,

$$\chi = \frac{f + s + i a}{\sqrt{2}}, \quad \varphi = \begin{pmatrix} G^+ \\ \frac{v+h+iG^0}{\sqrt{2}} \end{pmatrix}. \quad (28)$$

We have the SM VEV given by $\langle \phi \rangle = v (\equiv v_{SM}) \simeq 246$ GeV and $\langle \chi \rangle = f$. Here, G^+, G^0 are the Goldstone modes, which become the longitudinal components of the gauge bosons and give them mass after the electroweak symmetry is spontaneously broken.

3.1 Softly broken scalar potential

In the conventional approach [22, 32, 33, 35, 36], we can provide mass to the pseudoscalar component of the flavon field by adding the following term to the scalar potential, which breaks the $\mathcal{Z}_N \times \mathcal{Z}_M$ flavor symmetry softly,

$$V_\rho = \rho \chi^2 + \text{H.c.} \quad (29)$$

The parameter ρ is complex, and its phase can be rotated away by redefining the flavon field χ resulting in a real value of the VEV of the field χ .

The minimization conditions produce the masses of scalar and pseudoscalar flavons,

$$m_s = \sqrt{\lambda_\chi} f \quad \text{and} \quad m_a = \sqrt{2\rho}. \quad (30)$$

The mass of the pseudoscalar flavon depends on the soft-breaking parameter ρ , and is a free parameter of the model. The flavor and collider phenomenology of flavon based on the softly broken scalar potential can be found in references [22, 32, 33, 35, 36].

3.2 Symmetry-conserving scalar potential

The $\mathcal{Z}_N \times \mathcal{Z}_M$ flavor symmetry presents a novel scenario that simultaneously addresses the flavor problem and dark matter within a unified and generic framework [50]. This is achieved by formulating the flavon potential as,

$$V_\lambda = -\lambda \frac{\chi^{\tilde{N}}}{\Lambda^{\tilde{N}-4}} + \text{H.c.}, \quad (31)$$

where \tilde{N} is the least common multiple of N and M .

Upon the $\mathcal{Z}_N \times \mathcal{Z}_M$ flavor symmetry breaking by the VEV $\langle \chi \rangle$, the flavonic Goldstone boson (a) receives the potential,

$$V_{\tilde{N}} = -\frac{1}{4} |\lambda| \epsilon^{\tilde{N}-4} f^4 \cos \left(\tilde{N} \frac{a}{f} + \alpha \right), \quad (32)$$

where $\lambda = |\lambda| e^{i\alpha}$.

The axial flavon mass now turns out to be,

$$m_a^2 = \frac{1}{8} |\lambda| \tilde{N}^2 \epsilon^{\tilde{N}-4} f^2, \quad (33)$$

which depends on the symmetry breaking scale and is no longer an arbitrary free parameter of the model. We notice that for a large value of the \tilde{N} , the axial flavon can be the so-called flavonic dark matter, a new class of dark matter particles [50].

3.3 Couplings of flavon to fermions

Now, using equation 28, we can write

$$\frac{\chi}{\Lambda} = \epsilon \left[1 + \frac{s + ia}{f} \right]. \quad (34)$$

For obtaining the couplings of the scalar and pseudoscalar couplings to fermionic pair, we write the effective Yukawa couplings in the following form,

$$Y_{ij}^f \left(\frac{v+h}{\sqrt{2}} \right) = y_{ij}^f \left(\frac{\chi}{\Lambda} \right)^{n_{ij}^f} \left(\frac{v+h}{\sqrt{2}} \right) \cong y_{ij}^f \epsilon^{n_{ij}^f} \frac{v}{\sqrt{2}} \left[1 + \frac{n_{ij}^f (s + ia)}{f} + \frac{h}{v} \right] = \mathcal{M}_f \left[1 + \frac{n_{ij}^f (s + ia)}{f} + \frac{h}{v} \right], \quad (35)$$

where $f = u, d, \ell$, and n_{ij}^f denote the power of the ϵ , which appears in the mass matrices \mathcal{M}_f .

We keep only the linear terms of the flavon field components s and a in equation 35 in our phenomenological analysis. The higher-order terms are not relevant for the analysis given in this work. The couplings of the scalar and pseudoscalar components s and a of the flavon field to the fermionic pair are derived from the matrix $n_{ij}^f \mathcal{M}_f$, which cannot be diagonalized. This results in the non-diagonal flavor-changing and CP -violating interactions of the flavon field.

The couplings of the scalar component of the flavon field are obtained as,

$$y_{ij} = y_{s f_{iL} f_{jR}} = -i y_{a f_{iL} f_{jR}}. \quad (36)$$

4 Quark flavor physics constraints on the flavon of the $\mathcal{Z}_N \times \mathcal{Z}_M$ flavor symmetries

In this section, we thoroughly investigate the bounds on the parameter space of the $\mathcal{Z}_N \times \mathcal{Z}_M$ flavor symmetries using the quark-flavor physics data. We shall present the bounds on the flavon VEV f and mass of the pseudoscalar field m_a in both soft symmetry-breaking as well as symmetry-preserving scenarios.

We note that the bounds on the parameter space of flavons of different $\mathcal{Z}_N \times \mathcal{Z}_M$ flavor symmetries from quark and leptonic flavor observables, in general, can be understood in terms of a generic behavior of the corresponding Wilson coefficients. The Wilson coefficients, in general, behave as $y_{ij} \epsilon^{n_{ij}} y_{ji} \epsilon^{n_{ji}} / f^2$, where y_{ij} are the dimensionless couplings of flavons with a fermionic pair. Thus, a small contribution of the Wilson coefficient from the flavon to the corresponding observable, such as kaon mixing, can be accommodated by either increasing the value of the VEV f , or changing the values of the coupling y_{ij} and the order parameter ϵ while keeping a low value of the flavon VEV f . We shall analyze the constraints arising from quark and lepton flavor physics by employing the above observation.

4.1 Neutral meson mixing

The neutral meson-antimeson mixing receives a contribution from the FCNC interactions occurring at the tree-level due to the non-diagonal couplings of the flavon to fermions. This contribution can be incorporated by writing the following $\Delta F = 2$ effective Hamiltonian,

$$\begin{aligned} \mathcal{H}_{\text{NP}}^{\Delta F=2} = & C_1^{ij} (\bar{q}_L^i \gamma_\mu q_L^j)^2 + \tilde{C}_1^{ij} (\bar{q}_R^i \gamma_\mu q_R^j)^2 + C_2^{ij} (\bar{q}_R^i q_L^j)^2 + \tilde{C}_2^{ij} (\bar{q}_L^i q_R^j)^2 \\ & + C_4^{ij} (\bar{q}_R^i q_L^j) (\bar{q}_L^i q_R^j) + C_5^{ij} (\bar{q}_L^i \gamma_\mu q_L^j) (\bar{q}_R^i \gamma^\mu q_R^j) + \text{H.c.}, \end{aligned} \quad (37)$$

where $q_{R,L} = \frac{1 \pm \gamma_5}{2} q$, and we do not show the colour indices for simplicity.

The Wilson coefficients corresponding to the tree-level contribution to neutral meson mixing due to the flavon exchange read as [60, 61],

$$\begin{aligned} C_2^{ij} &= -(y_{ji}^*)^2 \left(\frac{1}{m_s^2} - \frac{1}{m_a^2} \right) \\ \tilde{C}_2^{ij} &= -y_{ij}^2 \left(\frac{1}{m_s^2} - \frac{1}{m_a^2} \right) \\ C_4^{ij} &= -\frac{y_{ij} y_{ji}}{2} \left(\frac{1}{m_s^2} + \frac{1}{m_a^2} \right), \end{aligned} \quad (38)$$

where m_s and m_a represent the masses of scalar and pseudoscalar degrees of the flavon field.

We evolve down the Wilson coefficients C_i from a scale Λ to the hadronic scales, used in the lattice computations of the corresponding matrix elements [53, 57, 58], 4.6 GeV for bottom mesons, 2.8 GeV for charmed mesons, and 2 GeV for kaons. The renormalization group running of the matrix elements is performed using the procedure discussed in reference [58], and matrix elements are adopted from reference [53, 57]. Thus, the

G_F	1.166×10^{-5} GeV [51]	v	246.22 GeV [51]
$\alpha_s[M_Z]$	0.1184 [52]	m_u	$(2.16^{+0.49}_{-0.26}) \times 10^{-3}$ GeV [51]
M_W	80.387 ± 0.016 GeV [51]	m_d	$(4.67^{+0.48}_{-0.17}) \times 10^{-3}$ GeV [51]
f_K	159.8 MeV [53]	m_c	1.27 ± 0.02 GeV [51]
m_K	497.611 ± 0.013 MeV [51]	m_s	$93.4^{+8.6}_{-3.4}$ GeV [51]
\hat{B}_K	0.7625 [52]	m_t	172.69 ± 0.30 GeV [51]
B_1^K	0.60(6) [53]	m_b	$4.18^{+0.03}_{-0.02}$ GeV [51]
B_2^K	0.66(4) [53]	$m_c(m_c)$	1.275 GeV
B_3^K	1.05(12) [53]	$m_b(m_b)$	4.18 GeV
B_4^K	1.03(6) [53]	$m_t(m_t)$	162.883 GeV
B_5^K	0.73(10) [53]	α	1/137.035 [51]
η_1	1.87 ± 0.76 [54]	e	0.302862 GeV
η_2	0.574 [55]	m_e	0.51099 MeV [51]
η_3	0.496 ± 0.047 [56]	m_μ	105.65837 MeV [51]
f_{B_s}	230.3 MeV [52]	m_τ	1776.86 ± 0.12 MeV [51]
m_{B_s}	5366.88 MeV [51]	τ_μ	2.196811×10^{-6} sec [51]
\hat{B}_{B_s}	1.232[52]	τ_τ	$(290.3 \pm 0.5) \times 10^{-15}$ sec [51]
$B_1^{B_s}$	0.86(2)($^{+5}_{-4}$) [57]	m_p	938.272 MeV [51]
$B_2^{B_s}$	0.83(2)(4) [57]	m_n	939.565 MeV [51]
$B_3^{B_s}$	1.03(4)(9) [57]	m_D	1864.83 MeV [51]
$B_4^{B_s}$	1.17(2)($^{+5}_{-7}$) [57]	f_D	212 MeV[52]
$B_5^{B_s}$	1.94(3)($^{+23}_{-7}$) [57]	B_1^D	0.861 [58]
η_{2B}	0.551 [55]	B_2^D	0.82 [58]
f_{B_d}	190.0 MeV [52]	B_3^D	1.07 [58]
m_{B_d}	5279.65 MeV [51]	B_4^D	1.08 [58]
\hat{B}_{B_d}	1.222[52]	B_5^D	1.455 [58]
$B_1^{B_d}$	0.87(4)($^{+5}_{-4}$) [57]	τ_{B_d}	$(1.520 \pm 0.004) \times 10^{-12}$ sec [59]
$B_2^{B_d}$	0.82(3)(4) [57]	τ_{B_s}	$(1.505 \pm 0.005) \times 10^{-12}$ sec [59]
$B_3^{B_d}$	1.02(6)(9) [57]	τ_{K_L}	$(5.116 \pm 0.021) \times 10^{-8}$ sec [51]
$B_4^{B_d}$	1.16(3)($^{+5}_{-7}$) [57]	τ_D	$(410.1 \pm 1.5) \times 10^{-15}$ sec [51]
$B_5^{B_d}$	1.91(4)($^{+22}_{-7}$) [57]		

Table 6: The numerical values of the used input parameters in this work.

$B_q - \bar{B}_q$ mixing amplitudes beyond the SM can be written as [58],

$$\langle \bar{B}_q | \mathcal{H}_{\text{eff}}^{\Delta B=2} | B_q \rangle_i = \sum_{j=1}^5 \sum_{r=1}^5 \left(b_j^{(r,i)} + \eta c_j^{(r,i)} \right) \eta^{a_j} C_i(\Lambda) \langle \bar{B}_q | Q_r^{bq} | B_q \rangle, \quad (39)$$

where $q = d, s$, $\eta = \alpha_s(\Lambda)/\alpha_s(m_t)$, a_j , $b_j^{(r,i)}$, $c_j^{(r,i)}$ denote the so-called magic numbers taken from reference [62], and α_s is the strong coupling constant. A similar expression can be written for the $D^0 - \bar{D}^0$ for which the magic numbers are present in reference [58]. The corresponding expression for the $K^0 - \bar{K}^0$ mixing reads as [58],

$$\langle \bar{K}^0 | \mathcal{H}_{\text{eff}}^{\Delta S=2} | K^0 \rangle_i = \sum_{j=1}^5 \sum_{r=1}^5 \left(b_j^{(r,i)} + \eta c_j^{(r,i)} \right) \eta^{a_j} C_i(\Lambda) R_r \langle \bar{K}^0 | Q_1^{sd} | K^0 \rangle, \quad (40)$$

where R_r denotes the ratio of the matrix elements of NP operators over that of the SM [63]. The numerical values of R_r can be found in reference [58]. For the $K^0 - \bar{K}^0$ mixing, the magic numbers are used from reference [53].

Observables	Phase I	Phase II	Ref.
h_d	$0 - 0.04$	$0 - 0.028$	[64]
h_s	$0 - 0.036$	$0 - 0.025$	[64]
h_K	$0 - 0.3$	—	[65]

Table 7: The future projected sensitivities of the neutral meson mixing.

For constraining the flavon mass and the VEV, we use the experimental measurements of the mixing observables of the $K^0 - \bar{K}^0$ mixing, which is given as [58],

$$C_{\epsilon_K} = \frac{\text{Im}\langle K^0 | \mathcal{H}_{\text{eff}}^{\Delta F=2} | \bar{K}^0 \rangle}{\text{Im}\langle K^0 | \mathcal{H}_{\text{SM}}^{\Delta F=2} | \bar{K}^0 \rangle} = 1.12_{-0.25}^{+0.27}, C_{\Delta m_K} = \frac{\text{Re}\langle K^0 | \mathcal{H}_{\text{eff}}^{\Delta F=2} | \bar{K}^0 \rangle}{\text{Re}\langle K^0 | \mathcal{H}_{\text{SM}}^{\Delta F=2} | \bar{K}^0 \rangle} = 0.93_{-0.42}^{+1.14}, \quad (41)$$

where $\mathcal{H}_{\text{eff}}^{\Delta F=2}$ represents the SM and flavon contributions, and $\mathcal{H}_{\text{SM}}^{\Delta F=2}$ denotes only the SM contribution.

The $B_q - \bar{B}_q$ mixing observables are,

$$C_{B_q} e^{2i\phi_{B_q}} = \frac{\langle B_q^0 | \mathcal{H}^{\Delta F=2} | \bar{B}_q^0 \rangle}{\langle B_q^0 | \mathcal{H}_{\text{SM}}^{\Delta F=2} | \bar{B}_q^0 \rangle},$$

where $q = s, d$ for the B_s and B_d mixing, respectively. We use the following measurements at 95 % CL limits in this work [58],

$$C_{B_s} = 1.110 \pm 0.090 [0.942, 1.288], \quad \phi_{B_s}^o = 0.42 \pm 0.89 [-1.35, 2.21] \\ C_{B_d} = 1.05 \pm 0.11 [0.83, 1.29], \quad \phi_{B_d}^o = -2.0 \pm 1.8 [-6.0, 1.5].$$

We write the new physics contributions to neutral meson mixing in the following form,

$$M_{12}^{d,s,K} = (M_{12}^{d,s,K})_{\text{SM}} (1 + h_{d,s,K} e^{2i\sigma_{d,s,K}}). \quad (42)$$

The following future sensitivity phases are adopted in this work [64]:

1. Phase I which corresponds to $50fb^{-1}$ LHCb and $50ab^{-1}$ Belle II (late 2020s);
2. Phase II which corresponds to $300fb^{-1}$ LHCb and $250ab^{-1}$ Belle II (late 2030s).

In table 7, we show the expected sensitivities to the observables $C_{\Delta m_K}$ and C_{B_q} in the future phase I and II of the LHCb and the Belle II.

Now, we discuss the bounds on the parameter space of the flavon of the $\mathcal{Z}_N \times \mathcal{Z}_M$ flavor symmetries arising from the neutral meson mixing. We discuss these bounds simultaneously for the soft symmetry-breaking as well as the symmetry-conserving scenarios. In figure 1, we show the bounds on the parameter space of the flavon corresponding to different $\mathcal{Z}_N \times \mathcal{Z}_M$ flavor symmetries from neutral kaon mixing observable $C_{\Delta m_K}$ on the left, and that from the observable C_{ϵ_K} on the right for the quartic coupling $\lambda_\chi = 2$. The region above the continuous curves show the allowed parameter space in the soft symmetry-breaking scenario for different $\mathcal{Z}_N \times \mathcal{Z}_M$ flavor symmetries. On the other side, the dashed curves represent symmetry-conserving scenario defined by equation 31. In the case of the soft symmetry-breaking scenario, the shaded region of the parameter space below the continuous curves is excluded by the corresponding observables. The symmetry-conserving scenario turns out to be extremely predictive in the sense that the allowed flavon parameter space is only along the dashed straight lines, and the rest of the region is excluded by the corresponding observables.

We observe that the bounds from the observable $C_{\Delta m_K}$ are most stringent for the flavor symmetry $\mathcal{Z}_2 \times \mathcal{Z}_9$, shown by the region above yellow-coloured continuous curve in figure 1a. This is followed by the $\mathcal{Z}_2 \times \mathcal{Z}_{11}$ and $\mathcal{Z}_8 \times \mathcal{Z}_{22}$ flavor symmetries for which the allowed parameter space is almost similar, shown in figure 1a by the region above the violet and green coloured continuous curves, respectively. The bounds become more stringent when the observable C_{ϵ_K} is used as shown in figure 1b. The most stringent bounds continue to be for the $\mathcal{Z}_2 \times \mathcal{Z}_9$ flavor symmetry even from the observable C_{ϵ_K} . The bounds from the observable C_{ϵ_K} on the flavor symmetries $\mathcal{Z}_2 \times \mathcal{Z}_5$ and $\mathcal{Z}_8 \times \mathcal{Z}_{22}$ are very close and are more stringent than that of the $\mathcal{Z}_2 \times \mathcal{Z}_{11}$ flavor

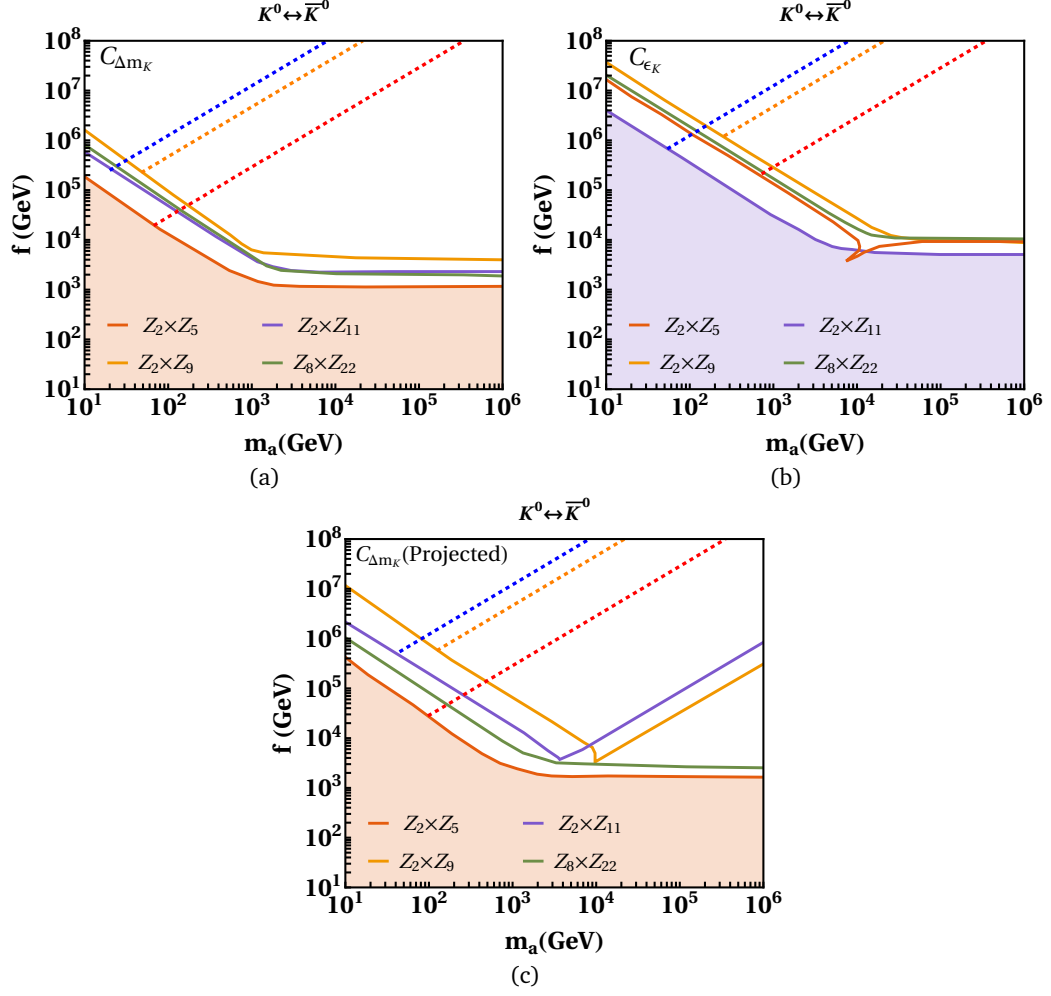


Figure 1: Bounds on the parameter space of the flavon of different $\mathcal{Z}_N \times \mathcal{Z}_M$ flavor symmetries in $f - m_a$ plane from the neutral-kaon oscillations. On the top left, we show the constraints arising from the observable $C_{\Delta m_K}$, and on the top right, the bounds from the observable C_{ϵ_K} are shown for the value $\lambda_\chi = 2$. The figure 1c depicts the allowed parameter space for projected sensitivities of $C_{\Delta m_K}$ in the LHCb Phase-I. The blank region above the continuous curves in figures shows the allowed $f - m_a$ parameter space in the soft symmetry-breaking framework, while the dashed curves are allowed for the symmetry-preserving scenario as defined by equation 31. The colored region below the continuous curves indicates the $f - m_a$ parameter space excluded by all four $\mathcal{Z}_N \times \mathcal{Z}_M$ models in the soft symmetry-breaking scenario.

symmetry, shown by the blue continuous curve. In figure 1c, we show the bounds on the parameter space of the flavon of different $\mathcal{Z}_N \times \mathcal{Z}_M$ flavor symmetries for the projected future sensitivities of the neutral meson mixing given in table 7 for the soft symmetry-breaking and symmetry-conserving scenario again by the solid continuous curves.

In figures 1a and 1c, the bounds corresponding to the $\mathcal{Z}_2 \times \mathcal{Z}_5$ flavor symmetry are relatively loose from the observable $C_{\Delta m_K}$. The reason for this is a low value of the order parameter $\epsilon = 0.1$, which dominates the behavior of the Wilson coefficients, in general, and allows a low value of the flavon VEV f . The symmetries $\mathcal{Z}_{2,8} \times \mathcal{Z}_{9,11,22}$ are showing a similar behavior since the order parameter ϵ is very close for them. On the other side, in figure 1b the contribution from the imaginary part of the product $y_{ij}y_{ij}$ is very large for the $\mathcal{Z}_2 \times \mathcal{Z}_5$ flavor symmetry, making it closer to the predictions of $\mathcal{Z}_{2,8} \times \mathcal{Z}_{9,22}$ symmetries. The symmetry-conserving scenario is dominated by the values of the parameter ϵ , leading to the strongest bounds for the $\mathcal{Z}_2 \times \mathcal{Z}_{9,11}$ flavor

symmetries. This is a generic observation in the sense that it will continue to show up even for leptonic flavor observables except for the D^0 mixing. Therefore, we shall discuss it only for the D^0 mixing later.

For the symmetry-conserving scenario, the most stringent bounds from the observable $C_{\Delta m_K}$ again appear for the $\mathcal{Z}_2 \times \mathcal{Z}_9$ flavor symmetry denoted by the orange dashed line in figure 1a. We must note that for the symmetry-conserving case, the dashed straight lines are the only allowed parameter space, and the rest of the region is excluded by the corresponding mixing observables. The bounds for the projected future sensitivities of the neutral meson mixing given in table 7 in the case of the symmetry-conserving scenario are shown by the dashed straight lines in figure 1c for different $\mathcal{Z}_N \times \mathcal{Z}_M$ flavor symmetries.

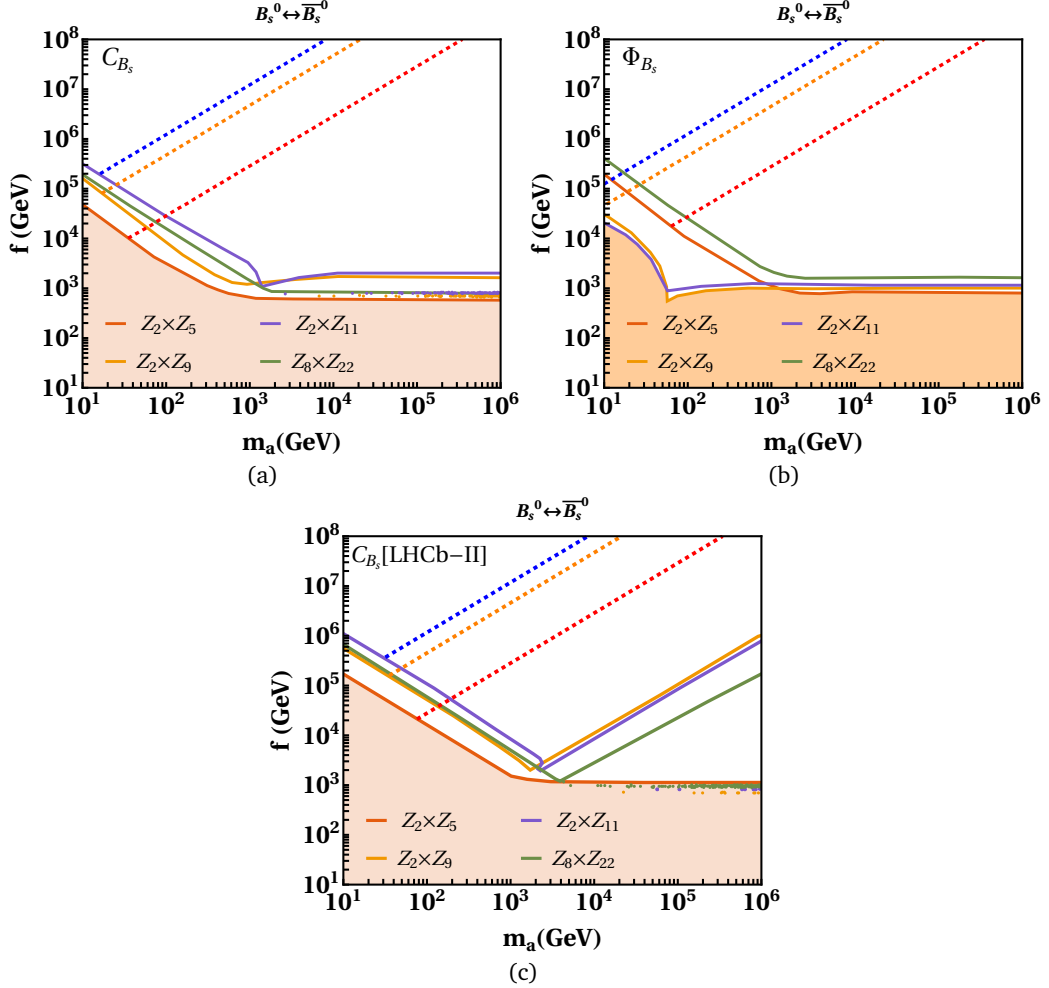


Figure 2: Bounds on the parameter space of the flavon of different $\mathcal{Z}_N \times \mathcal{Z}_M$ flavor symmetries in $f - m_a$ plane from the neutral B_s -meson mixing. On the top left, we show the constraints arising from the observable C_{B_s} , and on the top right, the bounds from the observable Φ_{B_s} are shown for the value $\lambda_\chi = 2$. The figure 2c depicts the allowed parameter space for projected sensitivities of C_{B_s} in the LHCb Phase-II. Moreover, the region above the continuous curves represent the allowed $f - m_a$ parameter space in the soft symmetry-breaking framework, and dashed curves are for the symmetry-preserving scenario defined by equation 31. The colored region below the continuous curves indicates the $f - m_a$ parameter space excluded by all four $\mathcal{Z}_N \times \mathcal{Z}_M$ models in the soft symmetry-breaking scenario.

The bounds on the parameter space of the flavon of the $\mathcal{Z}_N \times \mathcal{Z}_M$ flavor symmetries arising from the neutral B_s -meson mixing are represented in figure 2. On the left in figure 2a, we show the constraints on the parameter space of the flavon derived from the observable C_{B_s} . For the soft symmetry-breaking case, the

bounds are depicted by the solid continuous curves, and the region below these curves is excluded by the experimental measurement of the observable C_{B_s} . We notice that the observable C_{B_s} , unlike the neutral-kaon mixing, which was more constraining to the $\mathcal{Z}_2 \times \mathcal{Z}_9$ flavor symmetry, place stronger bounds on the $\mathcal{Z}_2 \times \mathcal{Z}_{11}$ flavor symmetry for the flavon mass approximately below 1 TeV. Above the flavon mass 1 TeV, the bounds are similar for the $\mathcal{Z}_2 \times \mathcal{Z}_{11}$ and $\mathcal{Z}_2 \times \mathcal{Z}_9$ flavor symmetries. The observable Φ_{B_s} is more suitable to constrain the parameter space corresponding to the $\mathcal{Z}_8 \times \mathcal{Z}_{22}$ flavor symmetry, as observed in figure 2b. The future projected sensitivity of the observable C_{B_s} in the LHCb phases-I, II further constrains the parameter space corresponding to the $\mathcal{Z}_2 \times \mathcal{Z}_{11}$ flavor symmetry for the flavon mass approximately up to 1 TeV. The constraints for the future projected sensitivity of the observable C_{B_s} in the LHCb phase-I are almost similar to that of phase-II. Therefore, we show them only for phase-II in this work. Above the flavon mass 1 TeV, the bounds are further stronger and again similar for the $\mathcal{Z}_2 \times \mathcal{Z}_{11}$ and $\mathcal{Z}_2 \times \mathcal{Z}_9$ flavor symmetries.

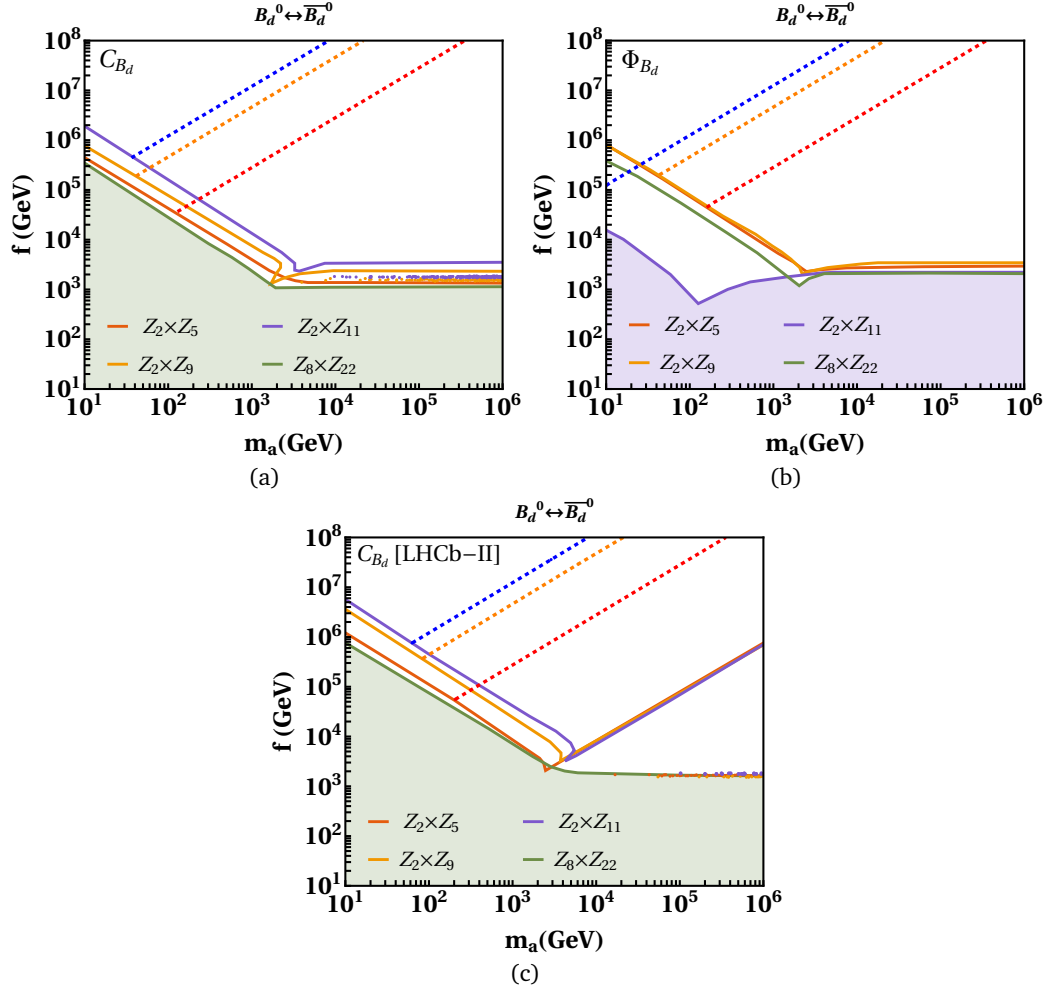


Figure 3: Bounds on the parameter space of the flavon of different $\mathcal{Z}_N \times \mathcal{Z}_M$ flavor symmetries in $f - m_a$ plane from the neutral B_d -meson mixing. On the top left, we show the constraints arising from the observable C_{B_d} , and on the right, the bounds from the observable Φ_{B_d} are shown for the value $\lambda_\chi = 2$. The figure 3c depicts the allowed parameter space for projected sensitivities of C_{B_d} in the LHCb Phase-II. Moreover, the region above the continuous curves represent the allowed $f - m_a$ parameter space in the soft symmetry-breaking framework, and dashed curves are for the symmetry-preserving scenario defined by equation 31.

For the symmetry-conserving scenario, the most stringent constraints are derived for the symmetry $\mathcal{Z}_2 \times \mathcal{Z}_{11}$ from both the observables C_{B_s} and Φ_{B_s} , as shown by the dashed blue straight lines in figures 2a, 2b, and

in 2c for the future projected sensitivity of the observable C_{B_s} in the LHCb phase-II. After the $\mathcal{Z}_2 \times \mathcal{Z}_{11}$ flavor symmetry, the parameter space corresponding to the flavon of the $\mathcal{Z}_2 \times \mathcal{Z}_9$ flavor symmetry receives the stronger bounds denoted by the orange dashed straight lines in figure 2.

We notice that the bounds from the observable C_{B_s} depend on the value $|y_{ij}y_{ij}|$, which is small for the $\mathcal{Z}_2 \times \mathcal{Z}_5$ flavor symmetry allowing a large parameter space for the order parameter $\epsilon = 0.1$. The parameter ϵ is largest for the $\mathcal{Z}_2 \times \mathcal{Z}_{11}$ flavor symmetry resulting in the most stringent bounds. The bounds for the rest of the symmetries are closer to that of the $\mathcal{Z}_2 \times \mathcal{Z}_{11}$ flavor symmetry due to the closer value of the ϵ parameter. The observable Φ_{B_s} is sensitive to the $\arg(y_{ij}y_{ij})$, which is large for the $\mathcal{Z}_2 \times \mathcal{Z}_5$ flavor symmetry leading to a more constrained parameter space, which is close to that of the $\mathcal{Z}_8 \times \mathcal{Z}_{22}$ flavor symmetry. The value of the $\arg(y_{ij}y_{ij})$ is small and close for the $\mathcal{Z}_2 \times \mathcal{Z}_{9,11}$ flavor symmetries producing similar bounds.

For the B_d -meson mixing, we can make observations similar to that of the B_s -meson mixing discussed earlier. The absolute values of the product $|y_{ij}y_{ij}|$ together with the value of the parameter ϵ determines the bounds from the observable C_{B_d} . On the other side, the $\arg(y_{ij}y_{ij})$ together with the value of the parameter ϵ determines the bounds from the observable Φ_{B_d} .

Thus, the observable C_{B_d} places the most stringent bounds on the parameter space of the flavon of the $\mathcal{Z}_2 \times \mathcal{Z}_{11}$ flavor symmetry for the soft symmetry-breaking scenario, as shown in figure 3a. This observation is similar to that obtained from the neutral B_s -meson mixing in figure 2. This feature continues to be seen even in the future projected sensitivity of the observable C_{B_d} in the LHCb phase-II, as shown in figure 3c. The bounds for the future projected sensitivity of the observable C_{B_d} in the LHCb phase-I are very similar to that of phase-II. Therefore, we do not show them in this work. On the other side, the observable Φ_{B_d} provides more stringent bounds on the parameter space of the flavon of the $\mathcal{Z}_2 \times \mathcal{Z}_{5,9}$ flavor symmetries for the soft symmetry-breaking scenario as shown in figure 3b.

In the symmetry-conserving scenario, the B_d -meson mixing places bounds on the parameter space of the flavon of $\mathcal{Z}_N \times \mathcal{Z}_M$ flavor symmetries similar to that of the B_s -meson mixing, as can be observed from figure 3a-3c, where the allowed parameter space is shown by dashed straight lines. The strongest bounds in this case turn out to be for the flavon of the $\mathcal{Z}_2 \times \mathcal{Z}_{11}$ flavor symmetry, followed by the flavon of the $\mathcal{Z}_2 \times \mathcal{Z}_9$ flavor symmetry.

Large hadronic uncertainties exist in the SM contribution of the $D^0 - \bar{D}^0$ mixing. For this reason, the flavon contribution to the $D^0 - \bar{D}^0$ mixing is chosen to lie within the 2σ experimental bound [66], that is,

$$|M_{12}^D| = |\langle D^0 | \mathcal{H}^{\Delta F=2} | \bar{D}^0 \rangle| < 7.5 \times 10^{-3} ps^{-1} \quad (43)$$

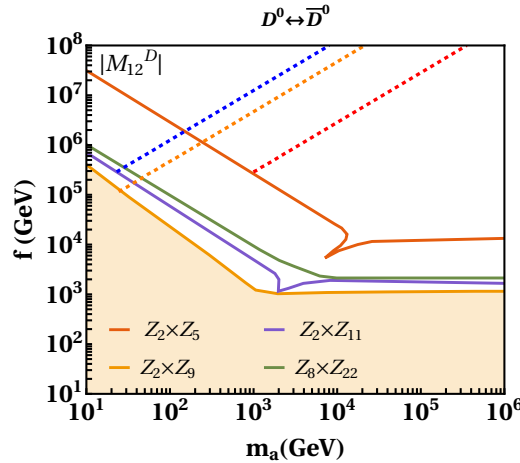


Figure 4: Bounds on the parameter space of the flavon of different $\mathcal{Z}_N \times \mathcal{Z}_M$ flavor symmetries in $f - m_a$ plane from the neutral $D^0 - \bar{D}^0$ meson mixing for the soft symmetry-breaking as well as for the symmetry-conserving scenarios for $\lambda_\chi = 2$.

In figure 4, we show the bounds arising from the D -meson mixing. In this case, the absolute values of the product $|y_{ij}y_{ij}|$ dictate the behavior of bounds from the observable $|M_{12}^D|$. For instance, the absolute values of the product $|y_{ij}y_{ij}|$ is very large for the $\mathcal{Z}_2 \times \mathcal{Z}_5$ flavor symmetry, leading to more stringent bounds for the soft symmetry-breaking, as well as for the symmetry-conserving scenarios.

4.2 Two body leptonic decays of pseudoscalar mesons

The two-body leptonic decays of a pseudoscalar meson into charged leptons can be described by the following effective Hamiltonian,

$$\mathcal{H}_{\text{eff}} = -\frac{G_F^2 m_W^2}{\pi^2} \left(C_S^{ij} (\bar{q}_i P_L q_j) \bar{\ell} \ell + \tilde{C}_S^{ij} (\bar{q}_i P_R q_j) \bar{\ell} \ell + C_P^{ij} (\bar{q}_i P_L q_j) \bar{\ell} \gamma_5 \ell + \tilde{C}_P^{ij} (\bar{q}_i P_R q_j) \bar{\ell} \gamma_5 \ell \right) + \text{H.c.} \quad (44)$$

The branching ratio for such a leptonic decay of meson can be written as,

$$\text{BR}(M \rightarrow \ell^+ \ell^-) = \frac{G_F^4 m_W^4}{8\pi^5} \beta m_M f_M^2 m_\ell^2 \tau_M \left(\left| \frac{m_M^2 (C_P^{ij} - \tilde{C}_P^{ij})}{2m_\ell(m_i + m_j)} - C_A^{\text{SM}} \right|^2 + \left| \frac{m_M^2 (C_S^{ij} - \tilde{C}_S^{ij})}{2m_\ell(m_i + m_j)} \right|^2 \beta^2 \right), \quad (45)$$

where $\beta(x) = \sqrt{1 - 4x^2}$ with $x = m_\ell/m_M$.

The tree-level contribution of the flavon to the corresponding Wilson coefficients reads as [60, 61],

$$\begin{aligned} C_S^{ij} &= \frac{\pi^2}{2G_F^2 m_W^2} \frac{2y_{\ell\ell} y_{ji}}{m_s^2} \\ \tilde{C}_S^{ij} &= \frac{\pi^2}{2G_F^2 m_W^2} \frac{2y_{\ell\ell} y_{ij}}{m_s^2} \\ C_P^{ij} &= \frac{\pi^2}{2G_F^2 m_W^2} \frac{2y_{\ell\ell} y_{ji}}{m_a^2} \\ \tilde{C}_P^{ij} &= \frac{\pi^2}{2G_F^2 m_W^2} \frac{2y_{\ell\ell} y_{ij}}{m_a^2}. \end{aligned} \quad (46)$$

In the SM, the two-body leptonic decays of a pseudoscalar meson into two charged leptons occur at one-loop, and their contribution is given by [61],

$$C_A^{\text{SM}} = -V_{tb}^* V_{ts} Y \left(\frac{m_t^2}{m_W^2} \right) - V_{cb}^* V_{cs} Y \left(\frac{m_c^2}{m_W^2} \right), \quad (47)$$

where $Y(x)$ is the Inami-Lim function, given by [67],

$$Y(x) = \eta_{\text{QCD}} \frac{x}{8} \left[\frac{4-x}{1-x} + \frac{3x}{(1-x)^2} \log x \right], \quad (48)$$

where $\eta_{\text{QCD}} = 1.0113$ shows the NLO QCD effects [68]. For B_d meson, the SM predictions can be obtained by replacing the indices in equation 47.

4.2.1 The $B_{s,d}$ meson decays

The HFLAV group provides the branching fraction of $B_s \rightarrow \mu^+ \mu^-$ to be [69],

$$\text{BR}(B_s \rightarrow \mu^+ \mu^-) = (3.45 \pm 0.29) \times 10^{-9}. \quad (49)$$

The branching ratio of the $B_d \rightarrow \mu^+ \mu^-$ decay is [70, 71],

$$\text{BR}(B_d \rightarrow \mu^+ \mu^-) < 2.6 \times 10^{-10}. \quad (50)$$

To convert the theoretical branching ratio of the B_s meson to the experimental branching ratio, we multiply by the factor $(1 - y_s)^{-1}$ [72], where $y_s = 0.088 \pm 0.014$ [73]. This is done due to the sizeable width difference of the B_s meson, and this correction can be ignored in the case of the B_d meson.

Observables	Current	LHCb-I	LHCb-II	CMS	ATLAS
$\text{BR}(B_s \rightarrow \mu^+ \mu^-)(\times 10^9)$	± 0.38	± 0.30	± 0.16	—	± 0.50
$\mathcal{R}_{\mu\mu}$	$\sim 70\%$	$\sim 34\%$	$\sim 10\%$	$\sim 21\%$	—
$\tau_{\mu\mu}$	$\sim 12\%$	± 0.16 ps	± 0.04 ps	—	—

Table 8: The values of the rare B decays observables for the current and expected experimental precision. The LHCb-I corresponds to $23fb^{-1}$, LHCb-II corresponds to $300fb^{-1}$, and the CMS and the ATLAS correspond to $3ab^{-1}$ [74, 75].

We note that the LHCb collaboration has also measured the ratio of the $\text{BR}(B_d \rightarrow \mu^+ \mu^-)$ and $\text{BR}(B_s \rightarrow \mu^+ \mu^-)$ branching fractions, $\mathcal{R}_{\mu\mu}$ [70, 71]. This observable can also be used to constrain the parameter space of flavon of different $\mathcal{Z}_N \times \mathcal{Z}_M$ flavor symmetries, and we shall show later that it provides the striking bounds of the parameter space of flavon of different $\mathcal{Z}_N \times \mathcal{Z}_M$ flavor symmetries. It should be noted that the ratio $\mathcal{R}_{\mu\mu}$ turns out to be an excellent observable to probe the minimal flavor violation [75]. Moreover, the effective lifetime, $\tau_{\mu\mu}$, of the $B_s \rightarrow \mu^+ \mu^-$ decay is also measured by the CMS [74]. The effective lifetime, $\tau_{\mu\mu}$, is capable of distinguishing between the contributions due to any possible new scalar and pseudoscalar mediators [75].

The ratio of branching fractions, $\mathcal{R}_{\mu\mu}$ is [70, 71],

$$\mathcal{R}_{\mu\mu} = \frac{\text{BR}(B_d \rightarrow \mu^+ \mu^-)}{\text{BR}(B_s \rightarrow \mu^+ \mu^-)} = 0.039^{+0.030+0.006}_{-0.024-0.004}. \quad (51)$$

The CMS has measured the effective lifetime $\tau_{\mu\mu}$ and the branching fraction of $B_s \rightarrow \mu^+ \mu^-$, which are [74],

$$\tau_{\mu\mu} = 1.83^{+0.23+0.04}_{-0.20-0.04} \text{ ps}, \quad (52)$$

$$\text{BR}(B_s \rightarrow \mu^+ \mu^-) = 3.83^{+0.38+0.19+0.14}_{-0.36-0.16-0.13} \times 10^{-9}. \quad (53)$$

The HFLAV measurement average of the effective lifetime $\tau_{\mu\mu}$ is [69],

$$\tau_{\mu\mu} = 2.00^{+0.27}_{-0.26} \text{ ps}, \quad (54)$$

with $\text{BR}(B_s \rightarrow \mu^+ \mu^-)$ given in equation 49.

We summarize the current and future sensitivities of these observables in table 8. The effective lifetime can be expressed as [76],

$$\tau_{\mu\mu} = \tau_{B_s} \frac{(B_s \rightarrow \mu^+ \mu^-)^{\text{experiment}}}{(B_s \rightarrow \mu^+ \mu^-)^{\text{theory}}}, \quad (55)$$

where the SM value of the final state dependent observable is $\mathcal{A}_{\Delta\Gamma}^f = 1$ [73].

4.2.2 The K_L meson decays

The short-distance (SD) part of $K_L \rightarrow \mu^+ \mu^-$ decay can be estimated in a reliable manner [60]. Its SM prediction is given in reference [60], and reads as,

$$C_A^{\text{SM}} = -V_{ts}^* V_{td} Y \left(\frac{m_t^2}{m_W^2} \right) - V_{cs}^* V_{cd} Y_{\text{NNL}}, \quad (56)$$

where at NNLO $Y_{\text{NNL}} = \lambda^4 P_c(Y)$, $\lambda = |V_{us}|$ and $P_c(Y) = 0.113 \pm 0.017$ [77]. The short-distance contribution is extracted from the experimental measurement, and its upper limit is [61],

$$\text{BR}(K_L \rightarrow \mu^+ \mu^-)_{\text{SD}} < 2.5 \times 10^{-9}. \quad (57)$$

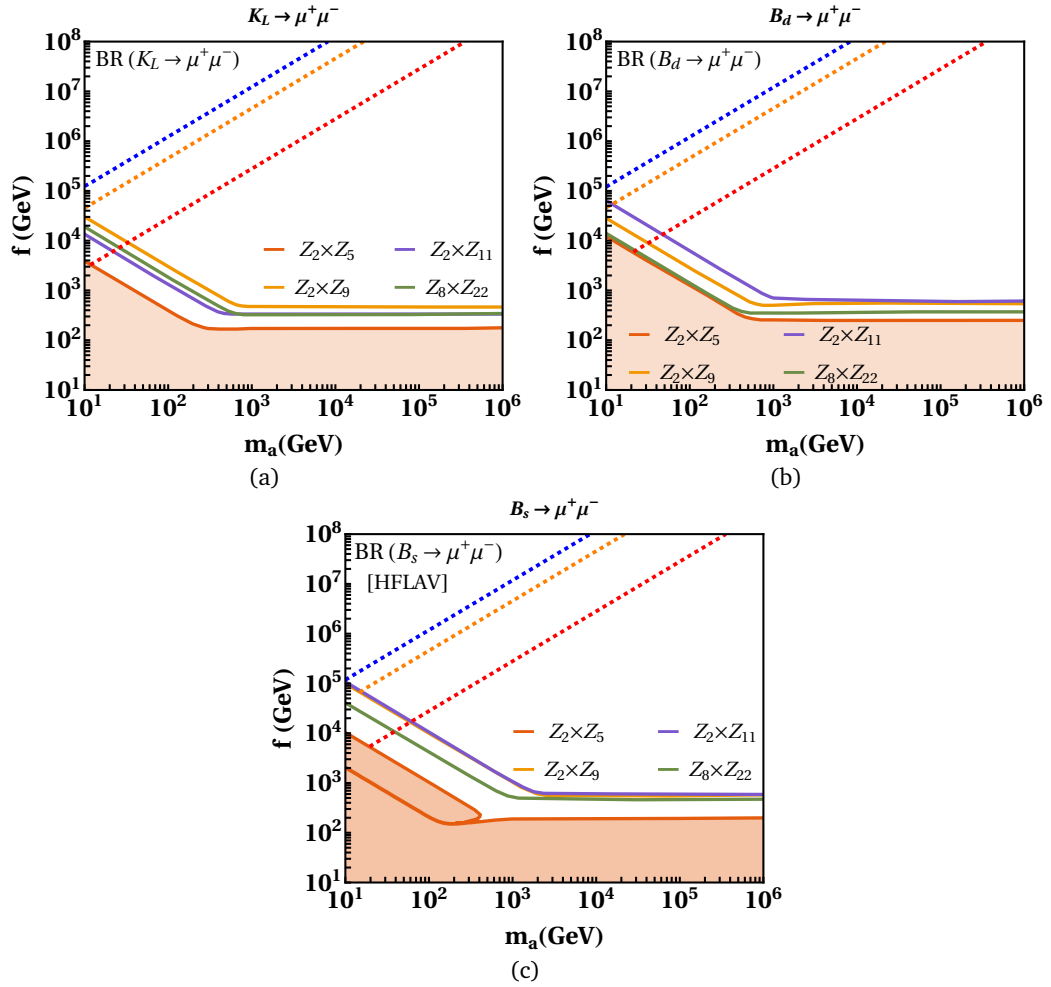


Figure 5: The coloured region represents the excluded parameter space for the flavon of all four $\mathcal{Z}_N \times \mathcal{Z}_M$ flavor symmetries by the limits on branching ratios $\text{BR}(K_L \rightarrow \mu^+ \mu^-)_{\text{SD}}$, $\text{BR}(B_d \rightarrow \mu^+ \mu^-)$ and the $\text{BR}(B_s \rightarrow \mu^+ \mu^-)$ for the soft symmetry-breaking scenario. The dashed line represents the allowed parameter space by the same observables for symmetry-conserving scenario, with $\lambda_\chi = 2$ for both the scenarios.

4.2.3 The D meson decays

The SM contribution of the $D \rightarrow \mu^+ \mu^-$ decay is marred by the large non-perturbative effects. Therefore, we assume that the flavon contribution to this decay rate lies within the experimental upper bound on the branching

ratio, given at 90% C.L.[78],

$$\text{BR}(D \rightarrow \mu^+ \mu^-) < 6.2 \times 10^{-9}. \quad (58)$$

We note that the bounds from the two-body leptonic decays of a pseudoscalar meson depend on the product $|y_{ij}^q y_{ij}^\ell|$. This quantity is very small for the $\mathcal{Z}_2 \times \mathcal{Z}_5$ flavor symmetry, and closer for the rest of the flavor symmetries for the two-body leptonic decays of a pseudoscalar meson.

In figure 5, we show the bounds on the parameter space of flavon of different $\mathcal{Z}_N \times \mathcal{Z}_M$ flavor symmetries arising from the branching ratio of the $K_L \rightarrow \mu^+ \mu^-$ decay. In the case of the soft symmetry-breaking scenario, the branching ratio of the $K_L \rightarrow \mu^+ \mu^-$ decay imposes stronger bounds on the $\mathcal{Z}_2 \times \mathcal{Z}_9$ flavor symmetry. After this, the constraints are stronger for the $\mathcal{Z}_2 \times \mathcal{Z}_{11}$ flavor symmetry. The decay $B_d \rightarrow \mu^+ \mu^-$ constrains more parameter space of flavon of the $\mathcal{Z}_2 \times \mathcal{Z}_{11}$ flavor symmetry, followed by the $\mathcal{Z}_2 \times \mathcal{Z}_9$ flavor symmetry. On the other hand, the branching ratio of the decay $B_s \rightarrow \mu^+ \mu^-$ bounds both the $\mathcal{Z}_2 \times \mathcal{Z}_9$ and $\mathcal{Z}_2 \times \mathcal{Z}_{11}$ flavor symmetries together with similar strength, while the bounds are comparatively weak in the case of $\mathcal{Z}_8 \times \mathcal{Z}_{22}$ flavor symmetry. In the symmetry-preserving scenario, all three decays place the stronger bounds on the $\mathcal{Z}_2 \times \mathcal{Z}_{11}$ flavor symmetry. This is followed by the $\mathcal{Z}_2 \times \mathcal{Z}_9$ flavor symmetry, and $\mathcal{Z}_2 \times \mathcal{Z}_5$ flavor symmetry. We do not show the bounds from $\text{BR}(D \rightarrow \mu^+ \mu^-)$ as it imposes extremely weak constraint on the parameter space of all four $\mathcal{Z}_N \times \mathcal{Z}_M$ flavor symmetries.

The observable $\tau_{\mu\mu}$ places the strongest bounds on the parameter space of flavon of the $\mathcal{Z}_2 \times \mathcal{Z}_5$ flavor symmetry in the soft symmetry-breaking scenario, as observed in figure 6. This is expected since the lifetime is inverse of the decay-width, and the branching ratio of the decay $B_s \rightarrow \mu^+ \mu^-$ places the most relaxed constraints on the flavon of the $\mathcal{Z}_2 \times \mathcal{Z}_5$ flavor symmetry. This is followed by the flavon of the $\mathcal{Z}_2 \times \mathcal{Z}_{11}$ flavor symmetry. For the symmetry-conserving scenario, the most stringent constraints arise for the flavon of the $\mathcal{Z}_2 \times \mathcal{Z}_{11}$ flavor symmetry, followed by the flavon of the $\mathcal{Z}_2 \times \mathcal{Z}_9$ flavor symmetry. There is no substantial improvement over these bounds in the future projected sensitivities of the LHCb. Therefore, we do not show them in this work.

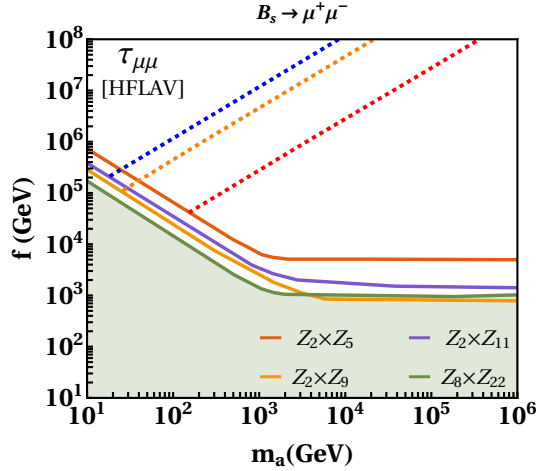


Figure 6: The allowed parameter space by the observable $\tau_{\mu\mu}$ for the flavon of different $\mathcal{Z}_N \times \mathcal{Z}_M$ flavor symmetries for the recent measurement.

The ratio $\mathcal{R}_{\mu\mu}$ is one of the most important observables to test the $\mathcal{Z}_N \times \mathcal{Z}_M$ flavor symmetries. Its future projected sensitivity will play a decisive role in constraining the parameter space of flavon of $\mathcal{Z}_N \times \mathcal{Z}_M$ flavor symmetries. The predictions from this observable are shown in figure 7. The bounds from the ratio $\mathcal{R}_{\mu\mu}$ are minimally sensitive to the product $y_{ij}\epsilon^{n_{ij}}y_{ji}\epsilon^{n_{ji}}$ since it appears in the numerator as well as denominator of the ratio $\mathcal{R}_{\mu\mu}$. Therefore, all the $\mathcal{Z}_N \times \mathcal{Z}_M$ flavor symmetries exhibit a close behavior providing relatively relaxed bounds from the current measurements.

In the case of soft symmetry-breaking scenario, the strongest bounds turn out to be for the $\mathcal{Z}_2 \times \mathcal{Z}_9$ and $\mathcal{Z}_2 \times \mathcal{Z}_{11}$ flavor symmetries for the current measurement of the observable $\mathcal{R}_{\mu\mu}$, as observed in figure 7a. This

feature continues to grow stronger further in the future high luminosity phase-I of the LHCb, as can be seen in figure 7b. In the symmetry-conserving scenario, the parameter space of the flavon of the $\mathcal{Z}_2 \times \mathcal{Z}_{11}$ is more constrained than any other flavor symmetry for the current measurement as well as for the high luminosity phase-I of the LHCb, as can be seen in figure 7a and 7b. This is followed by the $\mathcal{Z}_2 \times \mathcal{Z}_9$ flavor symmetry.

We obtain very stringent bounds on the parameter space of the flavon of different $\mathcal{Z}_N \times \mathcal{Z}_M$ flavor symmetries from the future high luminosity phase-II of the LHCb, as can be seen in figure 7c. We emphasize to note that the colored stripes in this figure are allowed parameter space for the soft symmetry-breaking scenario, and the blank region is the excluded parameter space. We observe from 7c that the allowed parameter space is very narrow and different for $\mathcal{Z}_N \times \mathcal{Z}_M$ flavor symmetries for $m_a < 1$ TeV. The stripe corresponding to the $\mathcal{Z}_2 \times \mathcal{Z}_9$ flavor symmetry resides inside the stripe corresponding to the $\mathcal{Z}_2 \times \mathcal{Z}_5$ flavor symmetry in this case. Above $m_a > 1$ TeV, the stripes corresponding to the $\mathcal{Z}_2 \times \mathcal{Z}_9$ and $\mathcal{Z}_2 \times \mathcal{Z}_{11}$ flavor symmetries overlap around 10^4 TeV.

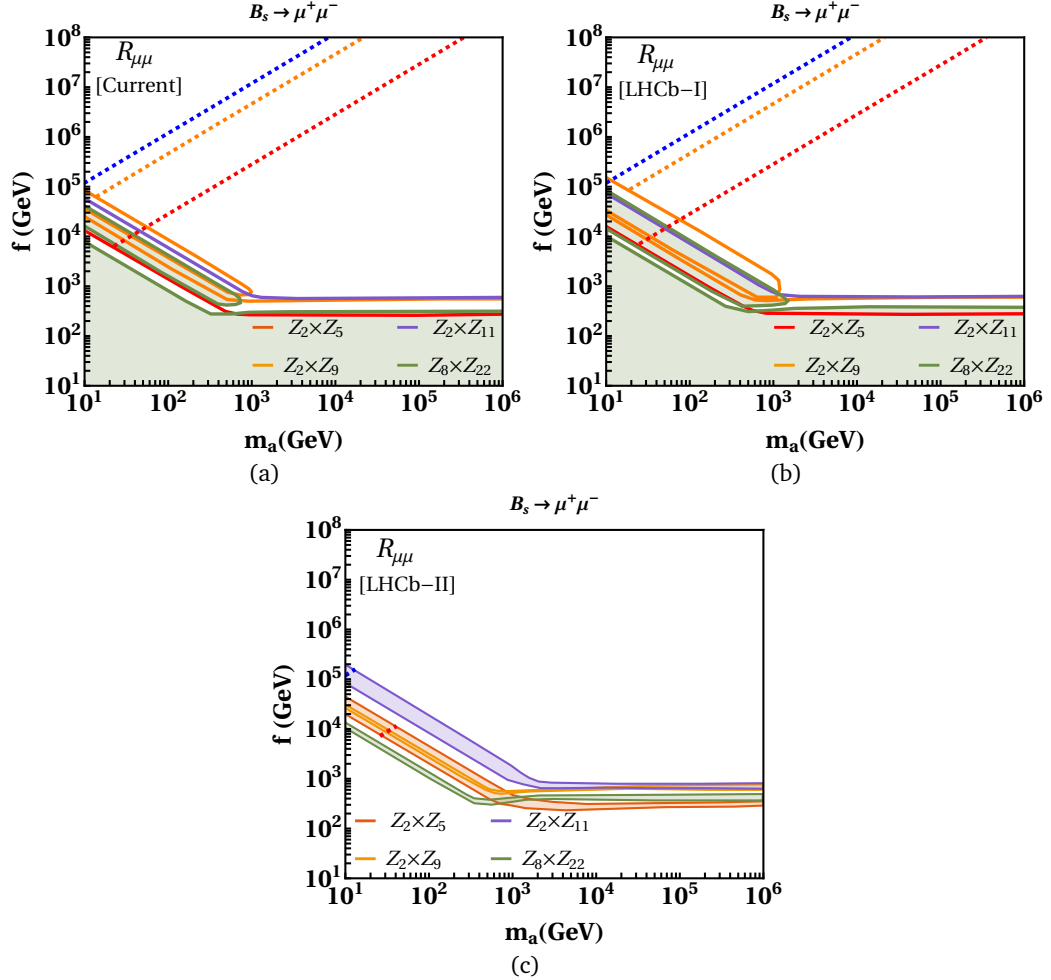


Figure 7: The blank region above the continuous curves in figure 7a and 7b shows the allowed $f - m_a$ parameter space of the flavon of different $\mathcal{Z}_N \times \mathcal{Z}_M$ models by current measurement as well as the future projected sensitivities in the LHCb Phase-I for the observable $\mathcal{R}_{\mu\mu}$, with $\lambda_\chi = 2$, in the soft symmetry-breaking scenario. The coloured region in figure 7c depicts the same allowed parameter space for projected sensitivities of $\mathcal{R}_{\mu\mu}$ in the LHCb Phase-II, while the dashed lines represent the allowed parameter space in the symmetry-conserving scenario.

The remarkable predictions are obtained in the case of the symmetry-conserving scenario. As evident from figure 7c, there is a very small allowed parameter space for symmetries $\mathcal{Z}_2 \times \mathcal{Z}_5$ and $\mathcal{Z}_2 \times \mathcal{Z}_{11}$, shown by the

dashed-red and dashed-blue lines within the stripes, respectively. There is no allowed parameter space for other symmetries for the symmetry-conserving scenario. Thus, the future high luminosity phase-II of the LHCb will be crucial in ruling out the symmetry-conserving scenario discussed in this work.

4.3 Constraints from $b \rightarrow s\mu^+\mu^-$ transition

In this section, we explore constraints arising from a plethora of observables in diverse decay channels triggered by the quark-level transition $b \rightarrow s\mu^+\mu^-$. This also encompasses the branching ratio of $B_s \rightarrow \mu^+\mu^-$, which was addressed in the preceding sub-section. The effective Hamiltonian for $b \rightarrow s\mu^+\mu^-$ transition can be written as follows:

$$\mathcal{H}_{\text{eff}} = -\frac{4G_F}{\sqrt{2}} \frac{e^2}{16\pi^2} m_b V_{ts}^* V_{tb} \left[\mathcal{C}_S^{\mu\mu} (\bar{s}_L b_R) (\bar{\mu}\mu) + \mathcal{C}_S^{\prime\mu\mu} (\bar{s}_R b_L) (\bar{\mu}\mu) + \mathcal{C}_P^{\mu\mu} (\bar{s}_L b_R) (\bar{\mu}\gamma_5\mu) + \mathcal{C}_P^{\prime\mu\mu} (\bar{s}_R b_L) (\bar{\mu}\gamma_5\mu) \right]. \quad (59)$$

Here, $\mathcal{C}_S^{\mu\mu}$, $\mathcal{C}_P^{\mu\mu}$, $\mathcal{C}_S^{\prime\mu\mu}$, and $\mathcal{C}_P^{\prime\mu\mu}$ represent the new physics scalar/pseudoscalar Wilson coefficients (WCs). In the model under consideration, these WCs are generated at the tree level and are expressed in terms of model parameters. For various flavor symmetries, these WCs are given in Table 9.

WCs	$\mathcal{Z}_2 \times \mathcal{Z}_5$	$\mathcal{Z}_2 \times \mathcal{Z}_9$	$\mathcal{Z}_2 \times \mathcal{Z}_{11}$	$\mathcal{Z}_8 \times \mathcal{Z}_{22}$
$\mathcal{C}_S^{\mu\mu}$	$\mathcal{N}(9\epsilon^6/m_s^2)y_{23}^d y_{22}^{\ell*}$	$\mathcal{N}(25\epsilon^{10}/m_s^2)y_{23}^d y_{22}^{\ell*}$	$\mathcal{N}(49\epsilon^{14}/m_s^2)y_{23}^d y_{22}^{\ell*}$	$\mathcal{N}(25\epsilon^{10}/m_s^2)y_{23}^d y_{22}^{\ell*}$
$\mathcal{C}_S^{\prime\mu\mu}$	$\mathcal{N}(3\epsilon^4/m_s^2)y_{32}^{d*} y_{22}^{\ell*}$	$\mathcal{N}(15\epsilon^8/m_s^2)y_{32}^{d*} y_{22}^{\ell*}$	$\mathcal{N}(21\epsilon^{10}/m_s^2)y_{32}^{d*} y_{22}^{\ell*}$	$\mathcal{N}(15\epsilon^8/m_s^2)y_{32}^{d*} y_{22}^{\ell*}$
$\mathcal{C}_P^{\mu\mu}$	$\mathcal{N}(9\epsilon^6/m_a^2)y_{23}^d y_{22}^{\ell*}$	$\mathcal{N}(25\epsilon^{10}/m_a^2)y_{23}^d y_{22}^{\ell*}$	$\mathcal{N}(49\epsilon^{14}/m_a^2)y_{23}^d y_{22}^{\ell*}$	$\mathcal{N}(25\epsilon^{10}/m_a^2)y_{23}^d y_{22}^{\ell*}$
$\mathcal{C}_P^{\prime\mu\mu}$	$\mathcal{N}(3\epsilon^4/m_a^2)y_{32}^{d*} y_{22}^{\ell*}$	$\mathcal{N}(15\epsilon^8/m_a^2)y_{32}^{d*} y_{22}^{\ell*}$	$\mathcal{N}(21\epsilon^{10}/m_a^2)y_{32}^{d*} y_{22}^{\ell*}$	$\mathcal{N}(15\epsilon^8/m_a^2)y_{32}^{d*} y_{22}^{\ell*}$

Table 9: Scalar and pseudoscalar WCs for $b \rightarrow s\mu^+\mu^-$ decay in terms of model parameters for various flavor symmetries. Here $\mathcal{N} = -\frac{2\sqrt{2}\pi^2 v^2}{G_F m_b V_{tb} V_{ts}^* e^2 f^2}$ whereas the benchmark values of y_{23}^d (y_{32}^d), and y_{22}^{ℓ} couplings are given in the appendix for all four $\mathcal{Z}_N \times \mathcal{Z}_M$ flavor symmetries.

These new physics WCs, which are complex, are subject to constraints imposed by a multitude of $b \rightarrow s\mu^+\mu^-$ observables (158 observables), which include:

1. The branching ratio of $B_s \rightarrow \mu^+\mu^-$ [69, 79] and $B \rightarrow X_s \mu^+\mu^-$ in both low and high- q^2 bins [80]. Here, we consider the modified world average of the branching ratio of $B_s \rightarrow \mu^+\mu^-$ [79] obtained after the recent CMS update, which is based on the full Run 2 dataset [74]. The updated world average now aligns with the predictions of the SM.
2. The differential branching ratios of $B^0 \rightarrow K^{*0} \mu^+\mu^-$ [81, 82, 83], $B^+ \rightarrow K^{*+} \mu^+\mu^-$, $B^0 \rightarrow K^0 \mu^+\mu^-$, $B^+ \rightarrow K^+ \mu^+\mu^-$ [84, 82] and $B_s \rightarrow \phi \mu^+\mu^-$ [85] in various q^2 intervals. It should be noted that for all of these observables, as well as for other $b \rightarrow s\mu^+\mu^-$ observables utilized in our analysis, we have excluded measurements within the $6 \text{ GeV}^2 \leq q^2 \leq 14.0 \text{ GeV}^2$ bin.
3. In addition to branching fractions, our analysis incorporates various angular observables as constraints within the fit. These observables encompass the longitudinal polarization fraction f_L , forward-backward asymmetry A_{FB} , and $S_{3,4,5,7,8,9}$ observables measured in the $B^0 \rightarrow K^{*0} \mu^+\mu^-$ decay across multiple q^2 bins, as reported by the LHCb collaboration [86]. Furthermore, we include the observables f_L , P_1 , P_4' , P_5' , P_6' , and P_8' measured in $B^0 \rightarrow K^{*0} \mu^+\mu^-$ decay by ATLAS [87], along with P_1 and P_5' measurements from CMS [88]. Additionally, measurements of f_L and A_{FB} by the CDF and CMS collaborations [82, 83] are also integrated into our fit.
4. The f_L and $P_1 - P_8'$ angular observables in $B^+ \rightarrow K^{*+} \mu^+\mu^-$ decay mode are also included [89] in the fit.
5. The fit also incorporates f_L , S_3 , S_4 , and S_7 observables obtained from the measurements of the $B_s \rightarrow \phi \mu^+\mu^-$ decay by the LHCb collaboration, as reported in [90].

The constraints on new physics couplings are obtained by performing a χ^2 fit using the CERN minimization code MINUIT [91]. The available experimental correlations [86, 89, 90], as well as theoretical correlations, are included in the analysis. The theoretical correlations, along with the expressions for various observables, are computed using `flavio` [92]. The observables in `flavio` are pre-implemented on the basis of refs. [93, 94]. For the fit, we closely follow the methodology adopted in [95, 96, 97].

The value of χ^2_{SM} is 164.80, whereas the χ^2 at the best-fit point is 164.26, indicating that the addition of new physics in the form of scalar and pseudoscalar interactions only provides an extremely marginal improvement over the SM (Pull = 0.54). The fit results are (1σ allowed range of real and complex components of the WCs)

$$\begin{aligned} C_S^{\mu\mu} &= [(-0.13, 0.13), (-0.13, 0.13)] \\ C_P^{\mu\mu} &= [(-0.07, 0.13), (-0.12, 0.12)] \\ C_S^{\prime\mu\mu} &= [(-0.11, 0.10), (-0.12, 0.12)] \\ C_P^{\prime\mu\mu} &= [(-0.07, 0.13), (-0.11, 0.11)]. \end{aligned} \quad (60)$$

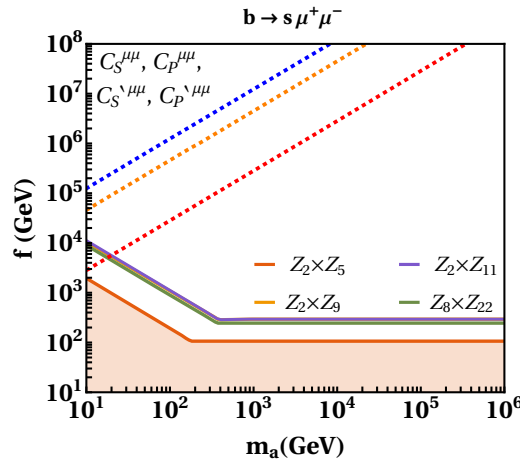


Figure 8: Bounds on the $f - m_a$ parameter space of the flavon of different $\mathcal{Z}_N \times \mathcal{Z}_M$ models by obtained limits on $C_S^{\mu\mu}$, $C_P^{\mu\mu}$, $C_S^{\prime\mu\mu}$ and $C_P^{\prime\mu\mu}$ as in equation 60 for the soft symmetry-breaking as well as symmetry-conserving scenario.

The model-independent fit results for the Wilson coefficients of $b \rightarrow s\mu^+\mu^-$ obtained in equation 60 can be utilized to constrain free parameters for the different $\mathcal{Z}_N \times \mathcal{Z}_M$ symmetries, as shown in figure 8. In the case of soft symmetry-breaking, the region above the continuous curves represents the allowed parameter space, and it is evident that the bounds are weakest for the minimal $\mathcal{Z}_2 \times \mathcal{Z}_5$ flavor symmetry, while the $\mathcal{Z}_2 \times \mathcal{Z}_9$, $\mathcal{Z}_2 \times \mathcal{Z}_{11}$, and $\mathcal{Z}_8 \times \mathcal{Z}_{22}$ impose almost similar constraints on the free parameters. In the symmetry-conserving scenario, the corresponding allowed parameter space for $\mathcal{Z}_2 \times \mathcal{Z}_{5,9,11}$ models are represented by the dashed straight lines, among which, the parameter space for the flavon of $\mathcal{Z}_2 \times \mathcal{Z}_{11}$ is most constrained.

4.4 Muon forward-backward asymmetry in $B \rightarrow K\mu^+\mu^-$

Within the framework of the SM, the muon forward-backward asymmetry in the context of $B \rightarrow K\mu^+\mu^-$ decay is inherently predicted to have a value of approximately zero. This prediction holds even when considering the effects of new physics scenarios involving vector-axial vector interactions. However, it's noteworthy that if new physics manifests in the form of scalar or pseudoscalar interactions, it has the potential to introduce a non-zero value to A_{FB} [98, 99]. Given this intriguing possibility, it is prudent to investigate this observable within the framework of flavons. Such an exploration could yield valuable insights into whether the new physics parameter space allowed in the context of this model has the potential to enhance A_{FB} to a value that can be measured experimentally.

The muon forward-backward asymmetry in $B \rightarrow K\mu^+\mu^-$ is given by [98]

$$A_{FB} = \frac{\int_{q_{\min}^2}^{q_{\max}^2} b_\mu(q^2) dq^2}{\int_{q_{\min}^2}^{q_{\max}^2} (2a_\mu(q^2) + \frac{2}{3}c_\mu(q^2)) dq^2}, \quad (61)$$

where

$$a_\mu(q^2) = N(q^2) \left[q^2 |F_P|^2 + \frac{\lambda}{4} (|F_V|^2 + |F_A|^2) + 2m_\mu (m_B^2 - m_K^2 + q^2) \text{Re}(F_P F_A^*) + 4m_\mu^2 m_B^2 |F_A|^2 \right], \quad (62)$$

$$b_\mu(q^2) = 2N(q^2) \left[m_\mu \beta_\mu \sqrt{\lambda_K} \text{Re}(F_S F_V^*) \right], \quad (63)$$

$$c_\mu(q^2) = -\frac{\lambda}{4} \beta_\mu^2 N(q^2) (|F_V|^2 + |F_A|^2), \quad (64)$$

with

$$N(q^2) = \frac{G_F^2 \alpha |V_{tb} V_{ts}^*|^2}{512 \pi^5 m_B^3} \beta_\mu \lambda_K f_+(q^2). \quad (65)$$

Here $\lambda = m_B^4 + m_K^4 + q^4 - 2(m_B^2 m_K^2 + m_B^2 q^2 + m_K^2 q^2)$ and $\beta_\mu = \sqrt{1 - 4m_\mu^2/q^2}$. The F functions are written in terms of WCs and form-factors as

$$F_A = C_{10}, \quad (66)$$

$$F_V = C_9 + \frac{2m_B}{M_B} \frac{T_P(q^2)}{f_+(q^2)}, \quad (67)$$

$$F_S = \frac{M_B^2 - M_K^2}{2(m_b - m_s)} \frac{f_0(q^2)}{f_+(q^2)} m_b (C_S^{\mu\mu} + C_S^{\prime\mu\mu}), \quad (68)$$

$$F_P = \frac{M_B^2 - M_K^2}{2(m_b - m_s)} \frac{f_0(q^2)}{f_+(q^2)} m_b (C_P^{\mu\mu} + C_P^{\prime\mu\mu}) + m_\mu C_{10} \left[\frac{M_B^2 - M_K^2}{q^2} \left(\frac{f_0(q^2)}{f_+(q^2)} - 1 \right) - 1 \right] \quad (69)$$

Here $f_0(q^2)$ and $f_+(q^2)$ are $B \rightarrow K$ form-factors whereas $C_{9,10}$ are SM WCs. The function $T_P(q^2)$ in the expression of F_V incorporates contributions from virtual one-photon exchange between the hadrons and the lepton pair, in addition to the hard scattering contributions [98]. At low- q^2 values, all form factors simplify to a single soft form factor [100, 101]. It is evident that in the absence of new physics scalar and pseudoscalar couplings, the muon-forward backward asymmetry remains zero. Consequently, in the current scenario, we anticipate a non-zero value for A_{FB} . Nonetheless, it would be intriguing to determine whether the constraints imposed by the new physics scalar and pseudoscalar couplings, as derived from the existing $b \rightarrow s\mu^+\mu^-$ data, permit any meaningful enhancements or not.

Utilizing the model-independent constraints on the new physics scalar and pseudoscalar couplings as derived in the previous sub-section, the FB asymmetry in both the low and high- q^2 regions is illustrated in Fig. 9. The figure clearly demonstrates that the existing $b \rightarrow s\mu^+\mu^-$ data permits an enhancement in A_{FB} , reaching up to a percent level.

We now explore the prediction of A_{FB} within the flavon model, considering both symmetry-conserving and symmetry-breaking scenarios. In the symmetry-conserving scenario, the flavon masses, as discussed in equation 33, are dependent on its VEV (f). Therefore, for all these symmetries, f serves as the sole free parameter. It is observed that, in order to satisfy the model-independent constraints on scalar as well as pseudoscalar couplings derived in eq. 60, the values of f need to be large. This holds true for all four flavor symmetries. However, such large values of f result in exceedingly small values of $C_S^{\mu\mu}$ and $C_S^{\prime\mu\mu}$ couplings, leading to predicted values of A_{FB} that are too negligible to be observed.

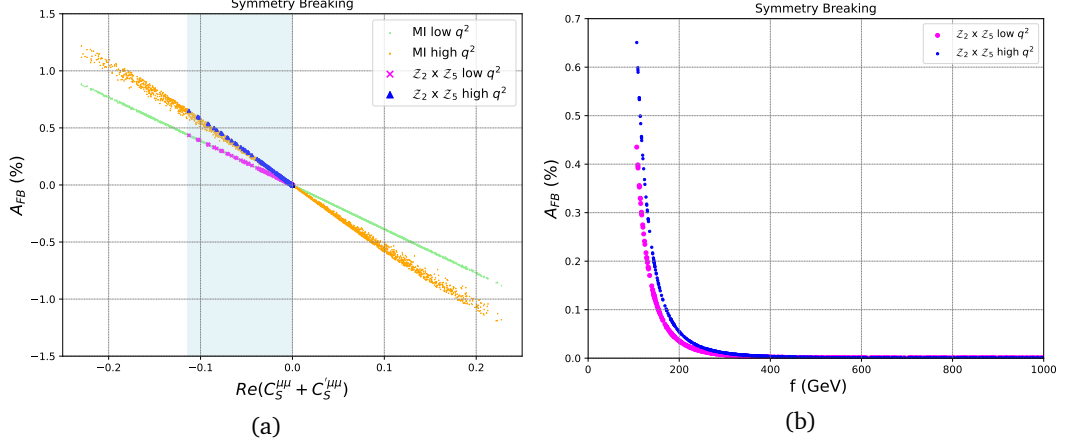


Figure 9: Predictions for the muon FB asymmetry in the $B^+ \rightarrow K^+ \mu^+ \mu^-$ decay.

In the scenario of symmetry breaking, both f and m_a serve as free parameters. The parameter space of $(m_a - f)$ is constrained by eq. 60. For all flavor symmetries except $Z_2 \times Z_5$, the constraints derived from eq. 60 limits the $(m_a - f)$ parameter space to such an extent that any significant enhancement in A_{FB} is precluded. The prediction of A_{FB} for the $Z_2 \times Z_5$ flavor symmetry is illustrated in Fig. 9. As depicted in the left panel of the figure, A_{FB} can be enhanced by up to half a percent level, both in the low and high- q^2 regions. This enhancement is smaller as compared to the model independent results because the allowed $(C_S^{\mu\mu} + C_S^{\prime\mu\mu})$ values (indicated by the light blue band), which are pertinent to A_{FB} , are more restrictive compared to the model-independent bounds. The right panel displays A_{FB} as a function of the parameter f . It is apparent from the plot that a meaningful enhancement of A_{FB} is achievable only for smaller values of f , specifically $f < 200$ GeV.

5 Leptonic flavor physics of the flavon of the $Z_N \times Z_M$ flavor symmetries

The current and future experiments on the charged lepton flavor violation (CLFV) processes have a great potential to place stringent bounds on the parameter space of the flavon of the $Z_N \times Z_M$ flavor symmetries, and even may provide an improvement over the constraints arising from the quark flavor physics. The sensitivities of the CLFV processes for the current as well as future projected experiments are shown in table 10.

The bounds from the leptonic flavor physics are sensitive to the $|y_{ij}^\ell \epsilon^{n_{ij}} y_{ji}^\ell \epsilon^{n_{ji}}|$, which is minimum for the $Z_2 \times Z_5$ flavor symmetry, providing the most relaxed constraints on the flavon corresponding to this symmetry. For other flavor symmetries, the value of the $|y_{ij}^\ell \epsilon^{n_{ij}} y_{ji}^\ell \epsilon^{n_{ji}}|$ is close, resulting in bounds, that are close in magnitude. This is a generic observation about the leptonic flavor physics.

5.1 Radiative leptonic decays

We write the following effective Lagrangian for the radiative leptonic decays,

$$\mathcal{L}_{\text{eff}} = m_{\ell'} C_T^L \bar{\ell} \sigma^{\rho\lambda} P_L \ell' F_{\rho\lambda} + m_{\ell'} C_T^R \bar{\ell} \sigma^{\rho\lambda} P_R \ell' F_{\rho\lambda}. \quad (70)$$

The branching ratio of the radiative leptonic decays is given by,

$$\text{BR}(\ell' \rightarrow \ell \gamma) = \frac{m_{\ell'}^5}{4\pi\Gamma_{\ell'}} (|C_T^L|^2 + |C_T^R|^2). \quad (71)$$

Observables	Current sensitivity	Ref.	Future projection	Ref.
$\text{BR}(\mu \rightarrow e \gamma)$	$< 4.2 \times 10^{-13}$	MEG [102]	6×10^{-14}	MEGII [103]
$\text{BR}(\tau \rightarrow e \gamma)$	$< 3.3 \times 10^{-8}$	Babar [104]	$\sim 10^{-9}$	Belle II [105]
$\text{BR}(\tau \rightarrow \mu \gamma)$	$< 4.4 \times 10^{-8}$	Babar [104]	$\sim 10^{-9}$	Belle II [105]
$\text{BR}(\mu \rightarrow e)^{\text{Au}}$	$< 7 \times 10^{-13}$	SINDRUM II [106]	—	—
$\text{BR}(\mu \rightarrow e)^{\text{Al}}$	—	—	3×10^{-15}	COMET Phase-I [107, 108]
$\text{BR}(\mu \rightarrow e)^{\text{Al}}$	—	—	6×10^{-17}	COMET Phase-II [107]
$\text{BR}(\mu \rightarrow e)^{\text{Al}}$	—	—	6×10^{-17}	Mu2e [109]
$\text{BR}(\mu \rightarrow e)^{\text{Al}}$	—	—	3×10^{-18}	Mu2e II [108]
$\text{BR}(\mu \rightarrow e)^{\text{Si}}$	—	—	2×10^{-14}	DeeMe [110]
$\text{BR}(\mu \rightarrow e)^{\text{Ti}}$	—	—	$\sim 10^{-20} - 10^{-18}$	PRISM/PRIME [111, 112]
$\text{BR}(\mu \rightarrow e \bar{e} e)$	$< 1.0 \times 10^{-12}$	SINDRUM [113]	$\sim 10^{-16}$	Mu3e [114]
$\text{BR}(\tau \rightarrow 3\mu)$	$< 2.1 \times 10^{-8}$	Belle [115]	$\sim 10^{-9}$	Belle II [105]
$\text{BR}(\tau \rightarrow 3e)$	$< 2.7 \times 10^{-8}$	Belle [115]	$\sim 10^{-9}$	Belle II [105]

Table 10: Experimental upper limits on various Leptonic flavor violation (LFV) processes.

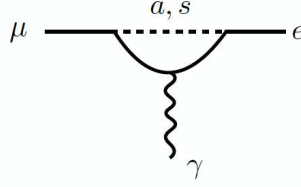


Figure 10: Feynman diagram representing $\mu \rightarrow e \gamma$ decay.

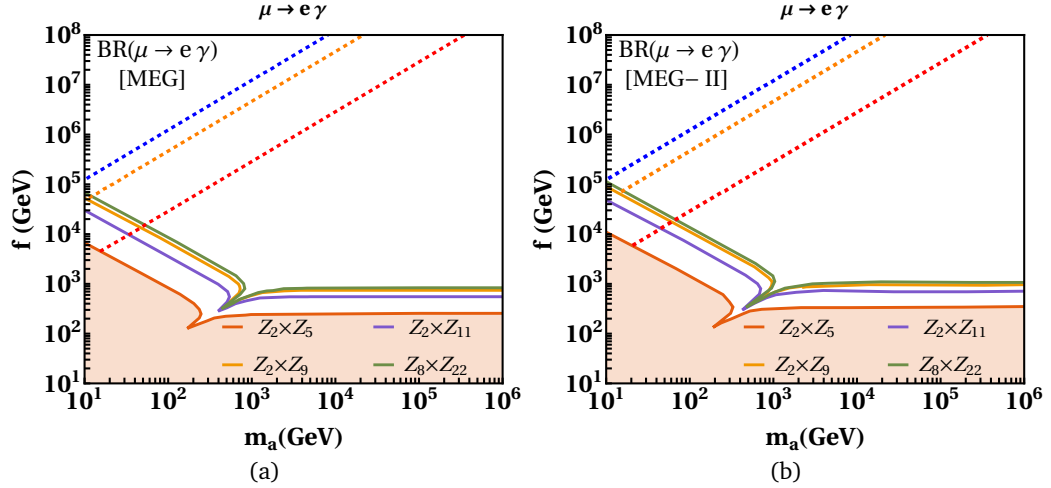


Figure 11: Bounds on the $f - m_a$ parameter space of the flavon of different $\mathcal{Z}_N \times \mathcal{Z}_M$ models by $\text{BR}(\mu \rightarrow e \gamma)$ for current as well as projected measurements from MEG and MEG-II experiments. The region above continuous curves represents the allowed parameter space for the corresponding $\mathcal{Z}_N \times \mathcal{Z}_M$ flavor symmetries in the soft symmetry-breaking scenario. The dashed lines show the allowed parameter space in the symmetry-conserving scenario. For both the scenario, $\lambda_\chi = 2$.

The radiative leptonic decays receive the one-loop contribution, as shown in figure 10. The Wilson coeffi-

cients corresponding to the one-loop contribution read as [33],

$$C_T^L = (C_T^R)^* = \frac{e}{32\pi^2} \sum_{k=e,\mu,\tau} \left\{ \frac{1}{6} \left(y_{\ell k}^* y_{\ell' k} + \frac{m_\ell}{m_k} y_{k\ell}^* y_{k\ell'} \right) \left(\frac{1}{m_s^2} - \frac{1}{m_a^2} \right) - y_{\ell k} y_{k\ell'} \frac{m_k}{m_{\ell'}} \left[\frac{1}{m_s^2} \left(\frac{3}{2} + \log \frac{m_{\ell'}^2}{m_s^2} \right) - \frac{1}{m_a^2} \left(\frac{3}{2} + \log \frac{m_{\ell'}^2}{m_a^2} \right) \right] \right\}. \quad (72)$$

The $\mu \rightarrow e\gamma$ decay impose the most stringent constraints on the parameter space of flavon of the $\mathcal{Z}_8 \times \mathcal{Z}_{22}$ and $\mathcal{Z}_2 \times \mathcal{Z}_9$ flavor symmetries in the soft symmetry-breaking scenario, as observed in figure 11a and 11b for the MEG and MEG-II experiments. This is followed by the $\mathcal{Z}_2 \times \mathcal{Z}_{11}$ flavor symmetry. For the symmetry-conserving case, the strongest bounds arise for the flavon of the $\mathcal{Z}_2 \times \mathcal{Z}_{11}$ flavor symmetry, followed by the flavon of the $\mathcal{Z}_2 \times \mathcal{Z}_9$ flavor symmetry.

5.2 $A \mu \rightarrow A e$ conversion

We write the following effective Lagrangian describing $A \mu \rightarrow A e$ conversion,

$$\mathcal{L}_{\text{eff}} = C_{qq}^{VL} \bar{e} \gamma^\nu P_L \mu \bar{q} \gamma_\nu q + m_\mu m_q C_{qq}^{SL} \bar{e} P_R \mu \bar{q} q + m_\mu \alpha_s C_{gg}^L \bar{e} P_R \mu G_{\rho\nu} G^{\rho\nu} + (R \leftrightarrow L), \quad (73)$$

Moreover, the dipole operators given in equation (70) provide additional contribution to $A \mu \rightarrow A e$ conversion. We show the Feynman diagram for $A \mu \rightarrow A e$ conversion in figure 12. The Wilson coefficients for the diagram on the left in figure 12 are given by [33],

$$C_{qq}^{SL} = \left(\frac{1}{m_s^2} + \frac{1}{m_a^2} \right) y_{\mu e}^* \text{Re}(y_{qq}),$$

$$C_{qq}^{SR} = \left(\frac{1}{m_s^2} - \frac{1}{m_a^2} \right) y_{e\mu} \text{Re}(y_{qq}). \quad (74)$$

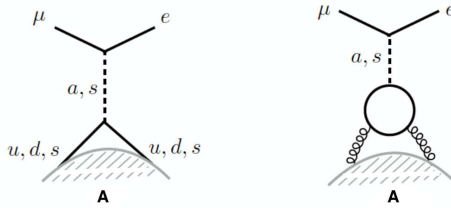


Figure 12: Feynman diagram showing $A \mu \rightarrow A e$ conversion.

The nucleon-level Wilson coefficients which include the nuclear effects of quarks inside the nucleons as well as the contribution of the Feynman diagram on the right side of figure 12 can be written as,

$$\tilde{C}_p^{VL} = \sum_{q=u,d} C_{qq}^{VL} f_{V_q}^p, \quad (75)$$

$$\tilde{C}_p^{SL} = \sum_{q=u,d,s} C_{qq}^{SL} f_q^p - \sum_{Q=c,b,t} C_{QQ}^{SL} f_{\text{heavy}}^p,$$

where the proton quark content is parameterized by the vector and scalar couplings $f_{V_q}^p, f_q^p$, and $f_{\text{heavy}}^p = 2/27(1 - f_u^p - f_d^p - f_s^p)$ [116]. For right-handed operators, analogous expressions can be obtained by replacing L with R , and for the neutron p is replaced by n . The contribution of the vector operators is much less than that of the scalar operators. Therefore, it can be ignored [33]. We use the numerical values of vector and scalar couplings given in references [117, 118], which are obtained after using the lattice average given in reference [119],

$$f_u^p = 0.0191, \quad f_u^n = 0.0171, \quad f_d^p = 0.0363, \quad f_d^n = 0.0404, \quad f_s^p = f_s^n = 0.043. \quad (76)$$

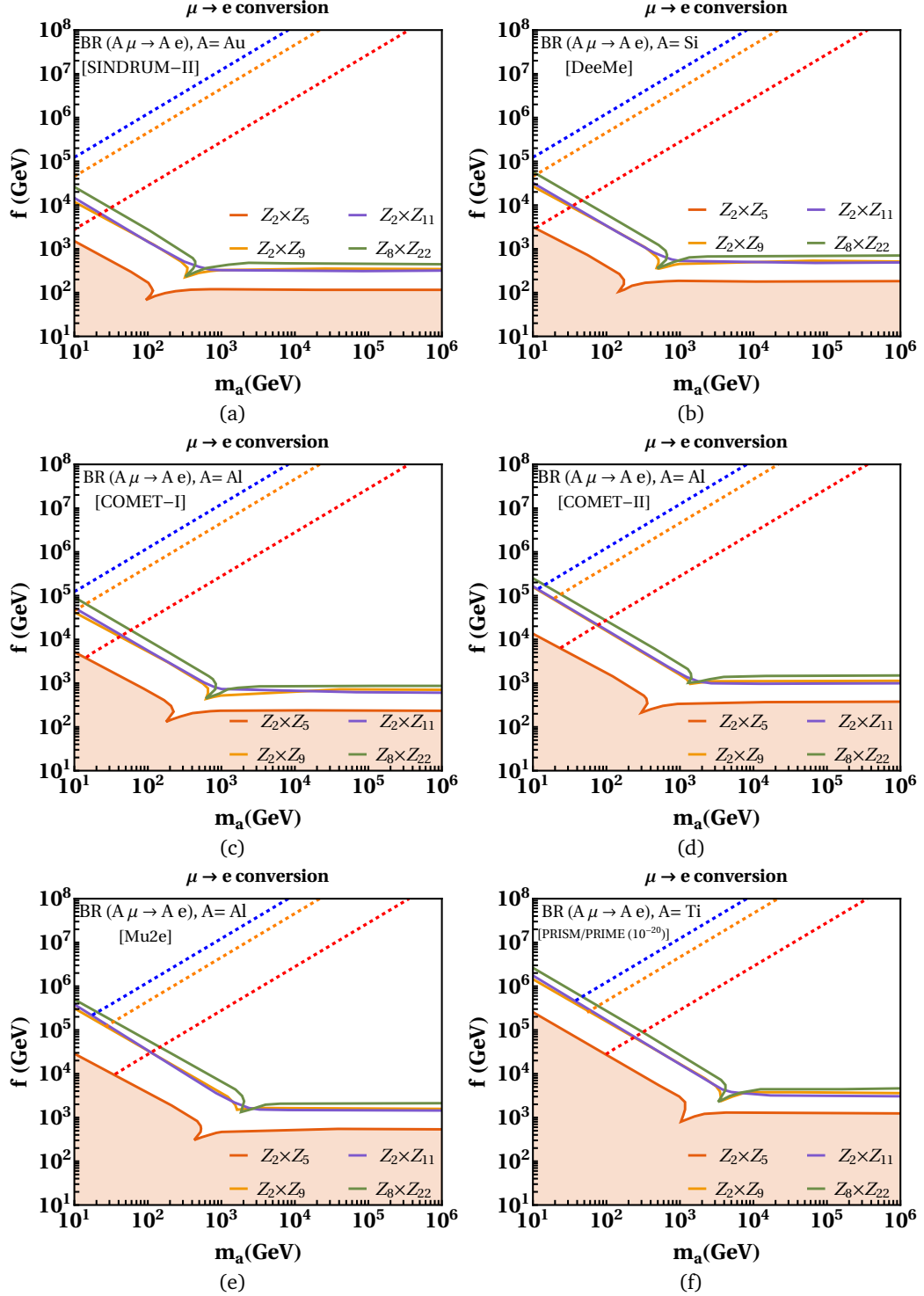


Figure 13: Bounds on the $f - m_a$ parameter space of the flavon of different $Z_N \times Z_M$ symmetries by $\text{BR}(A\mu \rightarrow Ae)$ for the current as well as projected sensitivities of the experiments given in table 10. The coloured region represents the excluded parameter space by all four $Z_N \times Z_M$ symmetries in the soft symmetry-breaking scenario, while the dashed lines represent the allowed parameter space in the symmetry-conserving scenario.

After including nuclear effects, the $A \mu \rightarrow A e$ conversion rate reads as [33],

$$\Gamma_{A \mu \rightarrow A e} = \frac{m_\mu^5}{4} \left| C_T^L D + 4 \left[m_\mu m_p \tilde{C}_p^{SL} + \tilde{C}_p^{VL} V^p + (p \rightarrow n) \right] \right|^2 + L \rightarrow R, \quad (77)$$

where the dimensionless coefficients D , $S^{p,n}$, and $V^{p,n}$ are functions of the overlap integrals of the initial state muon and the final-state electron wave functions with the target nucleus. We use their numerical values given in table 11 [120].

Target	D	S^p	S^n	V^p	V^n	$\Gamma_{\text{capt}} [10^6 \text{s}^{-1}]$
Au	0.189	0.0614	0.0918	0.0974	0.146	13.06
Al	0.0362	0.0155	0.0167	0.0161	0.0173	0.705
Si	0.0419	0.0179	0.0179	0.0187	0.0187	0.871
Ti	0.0864	0.0368	0.0435	0.0396	0.0468	2.59

Table 11: Numerical values of the dimensionless coefficients D , $S^{p,n}$, $V^{p,n}$ and the muon capture rate for different nuclei where Γ_{capt} denotes the muon capture rate.

The most stringent constraints from the $A \mu \rightarrow A e$ conversion rate on the parameter space of flavon of $\mathcal{Z}_N \times \mathcal{Z}_M$ flavor symmetries arise for the $\mathcal{Z}_8 \times \mathcal{Z}_{22}$ and $\mathcal{Z}_2 \times \mathcal{Z}_{9,11}$ flavor symmetries. The bounds from the future experiments are remarkably stronger than the existing limits. This can be seen in figure 13 for different ongoing and future experiments. This is followed by the $\mathcal{Z}_2 \times \mathcal{Z}_5$ flavor symmetries. In the symmetry-conserving scenario, the most stringent bounds are for the $\mathcal{Z}_2 \times \mathcal{Z}_{11}$ flavor symmetry, followed by the $\mathcal{Z}_2 \times \mathcal{Z}_{9,5}$ flavor symmetries.

5.3 $\mu \rightarrow 3e$ and $\tau \rightarrow 3\mu$ decays

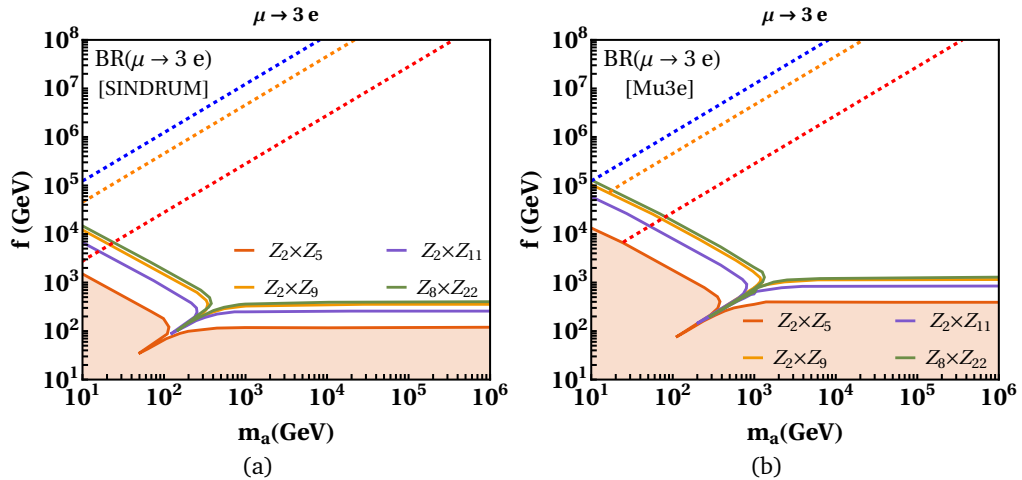


Figure 14: Bounds on the $f - m_a$ parameter space of the flavon of different $\mathcal{Z}_N \times \mathcal{Z}_M$ symmetries by $\text{BR}(\mu \rightarrow 3e)$ for sensitivities of the SINDRUM and Mu3e experiments. The coloured region represents the excluded parameter space by all four $\mathcal{Z}_N \times \mathcal{Z}_M$ symmetries in the soft symmetry-breaking scenario, while the dashed lines represent the allowed parameter space in the symmetry-conserving scenario.

The additional probes of the dipole operators given in equation (70) can emerge from the three body flavor violating leptonic decays $\mu \rightarrow 3e$ and $\tau \rightarrow 3\mu$ where $\ell = e, \mu$. The decay width of these decays is given by [33],

$$\Gamma(\ell' \rightarrow 3\ell) = \frac{\alpha m_\ell'^5}{12\pi^2} \left| \log \frac{m_\ell'^2}{m_\ell^2} - \frac{11}{4} \right| (|C_T^L|^2 + |C_T^R|^2). \quad (78)$$

where the tree-level contribution is negligible due to the strong chiral-suppression caused by the logarithmic enhancement of the dipole operators[33]. We ignore other contributions, such as Z -mediated penguin, due to their strong suppression [121].

The $\mu \rightarrow 3e$ decays places the most stringent bounds on the parameter space of flavon of the $\mathcal{Z}_8 \times \mathcal{Z}_{22}$ flavor symmetry for the soft symmetry-breaking case as shown in figure 14 for the SINDRUM and Mu3e experiments. The bounds on the flavor symmetry $\mathcal{Z}_2 \times \mathcal{Z}_9$ are almost similar to that of the $\mathcal{Z}_8 \times \mathcal{Z}_{22}$ flavor symmetry. This is followed by the $\mathcal{Z}_2 \times \mathcal{Z}_{11}$ flavor symmetry. For the symmetry-conserving scenario, the strongest bounds are for the $\mathcal{Z}_2 \times \mathcal{Z}_{11}$ flavor symmetry, followed by the $\mathcal{Z}_2 \times \mathcal{Z}_{9,5}$ flavor symmetries.

5.4 Summary of the flavor bounds

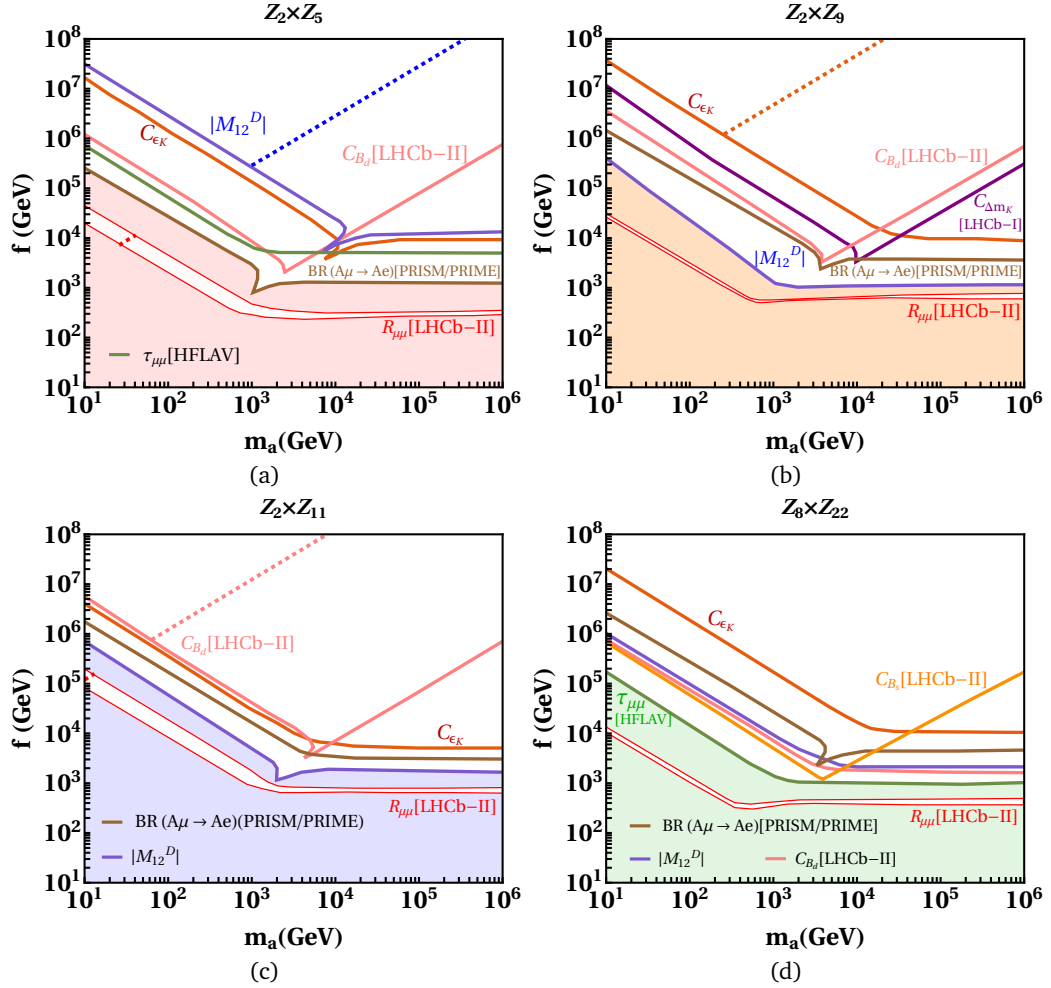


Figure 15: Summary of the excluded parameter space constrained significantly by the quark and leptonic flavor observables for different $\mathcal{Z}_N \times \mathcal{Z}_M$ flavor symmetries are shown with the coloured region in the soft symmetry-breaking scenario. The dashed line represents the allowed parameter space, which is most stringently constrained by the corresponding flavor observable in the symmetry-conserving scenario, except for the $\mathcal{Z}_8 \times \mathcal{Z}_{22}$ flavor symmetry.

In figure 15, we present the summary of the most significant bounds on the parameter space of the flavon of different $\mathcal{Z}_N \times \mathcal{Z}_M$ flavor symmetries. We notice that in the soft symmetry-breaking scenario the most stringent bound for the $\mathcal{Z}_2 \times \mathcal{Z}_5$ flavor symmetry arise from the observable $|M_{12}^D|$, while for the $\mathcal{Z}_2 \times \mathcal{Z}_9$ and $\mathcal{Z}_8 \times \mathcal{Z}_{22}$ flavor

symmetries, bounds from the observable C_{ϵ_K} are most stringent, and in the case of the $\mathcal{Z}_2 \times \mathcal{Z}_{11}$ the observable C_{B_d} in the phase-II of the LHCb places the strongest constraint. For the symmetry-conserving scenario, the most significant bounds for every $\mathcal{Z}_N \times \mathcal{Z}_M$ flavor symmetry are shown with the dashed straight-lines in figure 15.

6 Hadron collider physics of the flavon of the $\mathcal{Z}_N \times \mathcal{Z}_M$ flavor symmetries

We now discuss the collider signatures of the flavon of the $\mathcal{Z}_N \times \mathcal{Z}_M$ flavor symmetries through its decays and production processes. We first discuss the decays of flavon to a pair of fermions, as well as decays of top quark involving flavon. After this, we investigate the production mechanisms of the flavon of the $\mathcal{Z}_N \times \mathcal{Z}_M$ flavor symmetries. Our aim is to identify different $\mathcal{Z}_N \times \mathcal{Z}_M$ flavor symmetries as much as possible through the collider signatures. Therefore, we shall finally discuss the sensitivity of signatures of different $\mathcal{Z}_N \times \mathcal{Z}_M$ flavor symmetries to the HL-LHC, the HE-LHC, and a 100 TeV collider. We use the square root of the luminosity to scale the sensitivity of the HL-LHC, HE-LHC, and 100 TeV collider, which is a conservative estimate.

For collider investigation, we employ the parameter space of the flavon of the $\mathcal{Z}_N \times \mathcal{Z}_M$ flavor symmetries provided by the observable $R_{\mu\mu}$ in figure 7c. The observable $R_{\mu\mu}$ is sufficiently capable of differentiating the $\mathcal{Z}_N \times \mathcal{Z}_M$ flavor symmetries investigated in this work. For instance, we use the lower boundary of the allowed region of the parameter space corresponding to the $\mathcal{Z}_2 \times \mathcal{Z}_5$ flavor symmetry, which does not overlap with the parameter space corresponding to the $\mathcal{Z}_2 \times \mathcal{Z}_9$ flavor symmetry.

We notice that in our framework, there is no Higgs-flavon mixing. Therefore, the flavon does not directly couple to the gauge bosons. This fact leads to no constraints on low masses of flavon from the direct LHC searches [122]. Moreover, the WW and ZZ decays of flavon occur at one-loop level, and are much suppressed. The WW and ZZ final states searches set limits on masses above 300 GeV from ATLAS [123] and 200 GeV from CMS [124]. The searches in the di-photon channel place bounds on the masses above 200 GeV from the ATLAS [125], and above 500 GeV from the CMS [126].

6.1 Flavon decays to a pair of fermions

The flavon of the $\mathcal{Z}_N \times \mathcal{Z}_M$ flavor symmetries decays to a pair of fermions at tree-level, while the decays $a \rightarrow gg$ and $a \rightarrow \gamma\gamma$ are loop-induced. This is due to the non-zero off-diagonal couplings of the flavon to fermions. The partial decay width of the decay $a \rightarrow f_i \bar{f}_j$ at the tree-level can be written as,

$$\Gamma(a \rightarrow f_i \bar{f}_j) = \frac{N_c m_a}{16\pi} \left[\frac{(m_a^2 - (m_i + m_j)^2)(m_a^2 - (m_i - m_j)^2)}{m_a^4} \right]^{1/2} \left[(|y_{ij}|^2 + |y_{ji}|^2) \left(1 - \frac{m_i^2 + m_j^2}{m_a^2} \right) - 2(y_{ij}y_{ji} + y_{ij}^*y_{ji}^*) \frac{m_i m_j}{m_a^2} \right], \quad (79)$$

where N_c is the number of colors.

We present the branching ratios of $a \rightarrow f_i \bar{f}_j$, $a \rightarrow gg$ and $a \rightarrow \gamma\gamma$ in figure 16 for $\mathcal{Z}_2 \times \mathcal{Z}_{5,9,11}$ flavor symmetries, and in figure 17 for the $\mathcal{Z}_8 \times \mathcal{Z}_{22}$ flavor symmetry. In the quark sector, the dominant decay mode is $a \rightarrow b\bar{b}$ below the top quark threshold except for the minimal $\mathcal{Z}_2 \times \mathcal{Z}_5$ symmetry. For the minimal $\mathcal{Z}_2 \times \mathcal{Z}_5$ symmetry the mode $cu(c\bar{u}, \bar{c}u)$ prevails over other modes. This is due to the specific flavor structure of models based on the $\mathcal{Z}_N \times \mathcal{Z}_M$ flavor symmetries and the corresponding Yukawa couplings given in the appendix. As m_a approaches m_t , decay modes involving top quark, particularly, $tc(t\bar{c}, \bar{t}c)$, become increasingly significant for both the $\mathcal{Z}_2 \times \mathcal{Z}_{11}$ and $\mathcal{Z}_8 \times \mathcal{Z}_{22}$ models. These top quark related decay modes, however, remain comparatively less prominent than the decay modes of the flavon involving bottom and charm quark, such as, bd, bs, cc, cu , and bb for $\mathcal{Z}_2 \times \mathcal{Z}_5$ as well as $\mathcal{Z}_2 \times \mathcal{Z}_9$ symmetries, even beyond the top-threshold. Among the leptonic decay modes, the decay channels involving at least one τ dominate for all $\mathcal{Z}_N \times \mathcal{Z}_M$ flavor symmetries.

At $m_a > m_t$, in contrast to the other three $\mathcal{Z}_N \times \mathcal{Z}_M$ flavor symmetries, the $\mathcal{Z}_8 \times \mathcal{Z}_{22}$ model exhibits a dominant decay of the flavon into top quark pairs ($t\bar{t}$), as shown by the dashed-blue line in figure 17a. This striking feature arises from the construction of the $\mathcal{Z}_8 \times \mathcal{Z}_{22}$ model, where the top quark couples to the flavon

with a suppression factor of order ϵ . Notably, this feature is absent in the remaining three $\mathcal{Z}_N \times \mathcal{Z}_M$ symmetry-based models under investigation. This feature keeps apart the $\mathcal{Z}_8 \times \mathcal{Z}_{22}$ based model from the other models in terms of collider signatures, which are discussed in the later part of this work.

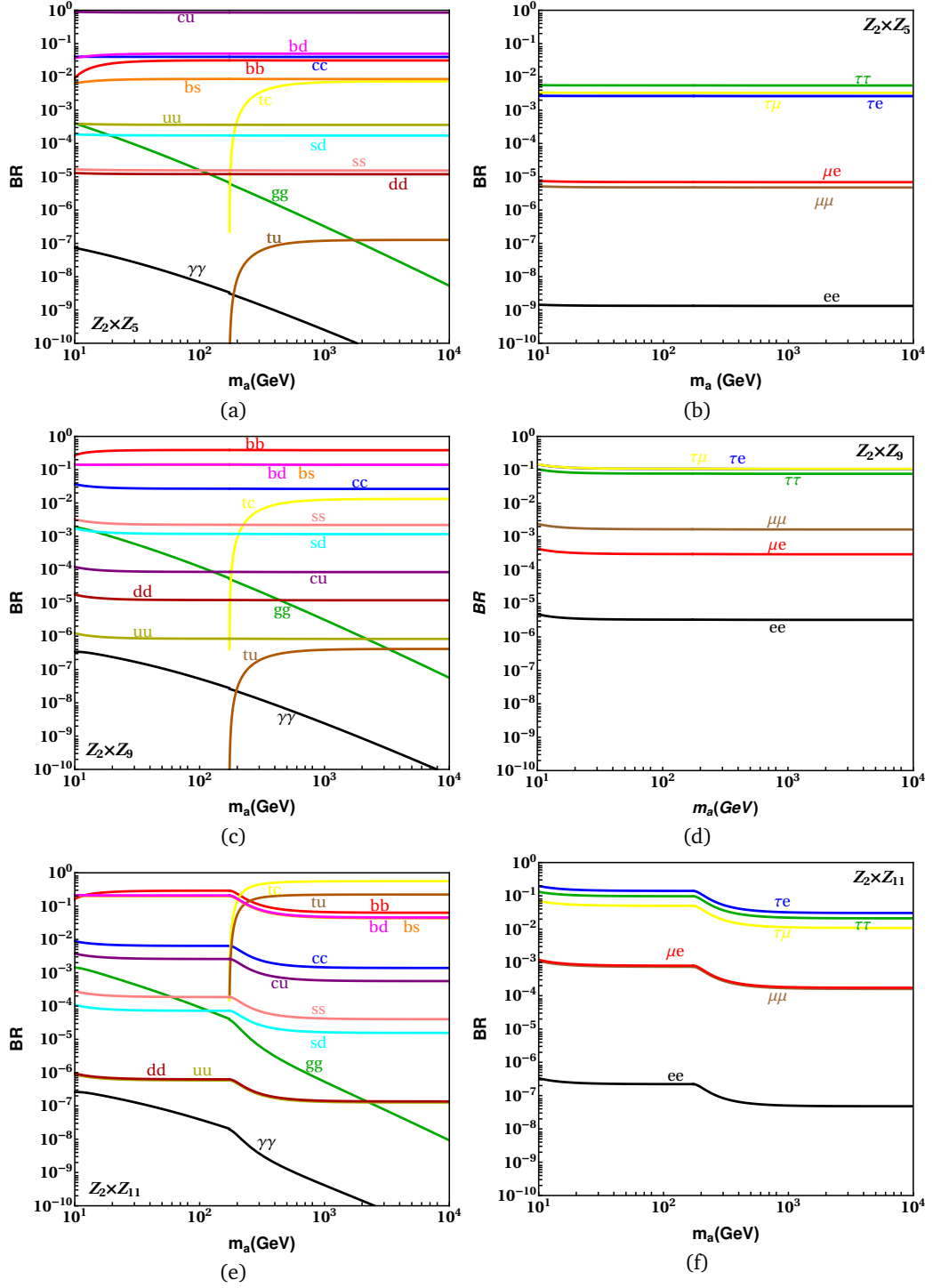


Figure 16: Branching ratios of the various possible decay modes of the flavon into quark and lepton pairs for $\mathcal{Z}_2 \times \mathcal{Z}_5$, $\mathcal{Z}_2 \times \mathcal{Z}_9$, and $\mathcal{Z}_2 \times \mathcal{Z}_{11}$ flavor symmetries.

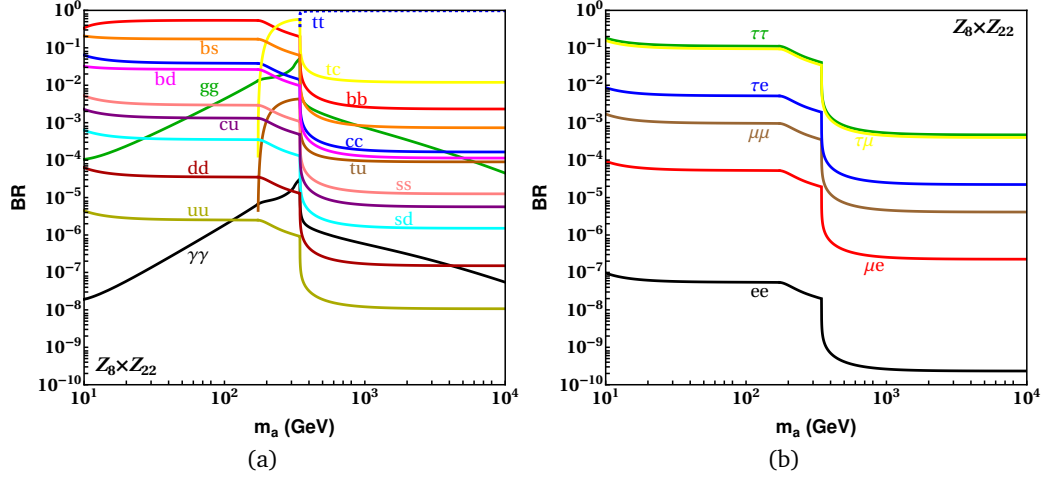


Figure 17: Branching ratios of the various possible decay modes of the flavon into quark and lepton pairs for $\mathcal{Z}_8 \times \mathcal{Z}_{22}$ flavor symmetry.

6.2 Top quark decays to flavon

The top quark decays to flavon play an important role in constraining a low-mass flavon. For the flavon mass, which is less than the mass of the top quark, anomalous top decays $t \rightarrow ac(au)$ provide distinguished signatures of flavon at hadron colliders. For Higgs production via such anomalous top-quark decays, the limits for the expected reach of the current 14 TeV LHC, HE-LHC, as well as a future high luminosity 100 TeV hadron collider are known, which can also be utilized for the flavon production. The current and expected limits on such processes at the LHC and a 100 TeV hadron collider are [127, 34],

$$\begin{aligned}
 BR_{8 \text{ TeV}}(t \rightarrow Hc) &< 5.6 \cdot 10^{-3}, \\
 BR_{14 \text{ TeV}, 3 \text{ ab}^{-1}}(t \rightarrow Hc) &< 4.5 \cdot 10^{-5}, \\
 BR_{27 \text{ TeV}, 15 \text{ ab}^{-1}}(t \rightarrow Hc) &< 9.7 \cdot 10^{-6}, \\
 BR_{100 \text{ TeV}, 30 \text{ ab}^{-1}}(t \rightarrow Hc) &< 2.2 \cdot 10^{-6}.
 \end{aligned} \tag{80}$$

In figure 18, we show the predictions of branching ratios for decays $t \rightarrow (c, u)a$ in the framework of different $\mathcal{Z}_N \times \mathcal{Z}_M$ flavor symmetries. We note that in the case of the soft symmetry-breaking scenario, shown by the solid continuous curves, the top decays to the flavon are investigated along the boundaries of parameter space allowed by the observable $R_{\mu\mu}$ in the phase-II of the LHCb, shown in figure 7c. With mass range m_a lying between 10 up to 200 GeV, the corresponding ranges for the VEV of the flavon f varies approximately as $\sim (2 \times 10^3, 4 \times 10^4)$ GeV for $\mathcal{Z}_2 \times \mathcal{Z}_5$, $\sim (10^3, 2 \times 10^4)$ GeV for $\mathcal{Z}_2 \times \mathcal{Z}_9$, $\sim (9 \times 10^3 - 1.4 \times 10^5)$ GeV for $\mathcal{Z}_2 \times \mathcal{Z}_{11}$, and $\sim (4 \times 10^2 - 10^4)$ GeV for $\mathcal{Z}_8 \times \mathcal{Z}_{22}$ flavor symmetry. We observe that only the flavon of the $\mathcal{Z}_8 \times \mathcal{Z}_{22}$ has the potential to reach the sensitivity of the 14 TeV LHC, the HE-LHC, and a 100 TeV future hadron collider. This prediction is very specific to test the $\mathcal{Z}_8 \times \mathcal{Z}_{22}$ flavor symmetry.

For the symmetry-conserving scenario, represented by the dashed curves in figure 18, we analyze $t \rightarrow (c, u)a$ decays along the parameter space allowed by the observable $BR(K_L \rightarrow \mu^+ \mu^-)$, where VEV f ranges approximately as $\sim (3 \times 10^3, 6 \times 10^4)$ GeV for $\mathcal{Z}_2 \times \mathcal{Z}_5$, $\sim (4 \times 10^4, 9 \times 10^5)$ GeV for $\mathcal{Z}_2 \times \mathcal{Z}_9$, and $\sim (1.2 \times 10^5, 2 \times 10^6)$ GeV for $\mathcal{Z}_2 \times \mathcal{Z}_{11}$ flavor symmetry. It turns out that the decays $t \rightarrow ac(au)$ in the case of symmetry-conserving scenario for a light flavon are beyond the reach of the LHC, the HE-LHC, and a future 100 TeV hadron collider.

In figure 19, we show the prediction of branching ratios of decays $t \rightarrow (c, u)a$ for different $\mathcal{Z}_N \times \mathcal{Z}_M$ flavor symmetries for the flavon VEV $f = 500$ GeV in the soft symmetry-breaking case. This is a conventional choice in literature [34]. In this scenario, the branching ratio of the decay $t \rightarrow ca$ is accessible to a future 100 TeV hadron collider in a certain mass range for all $\mathcal{Z}_N \times \mathcal{Z}_M$ flavor symmetries discussed in this work. For the symmetries $\mathcal{Z}_2 \times \mathcal{Z}_{5,9}$, the branching ratio of the decay $t \rightarrow ca$ is of the order $10^{-6} - 10^{-5}$ for $m_a \leq 150$ GeV. The branching

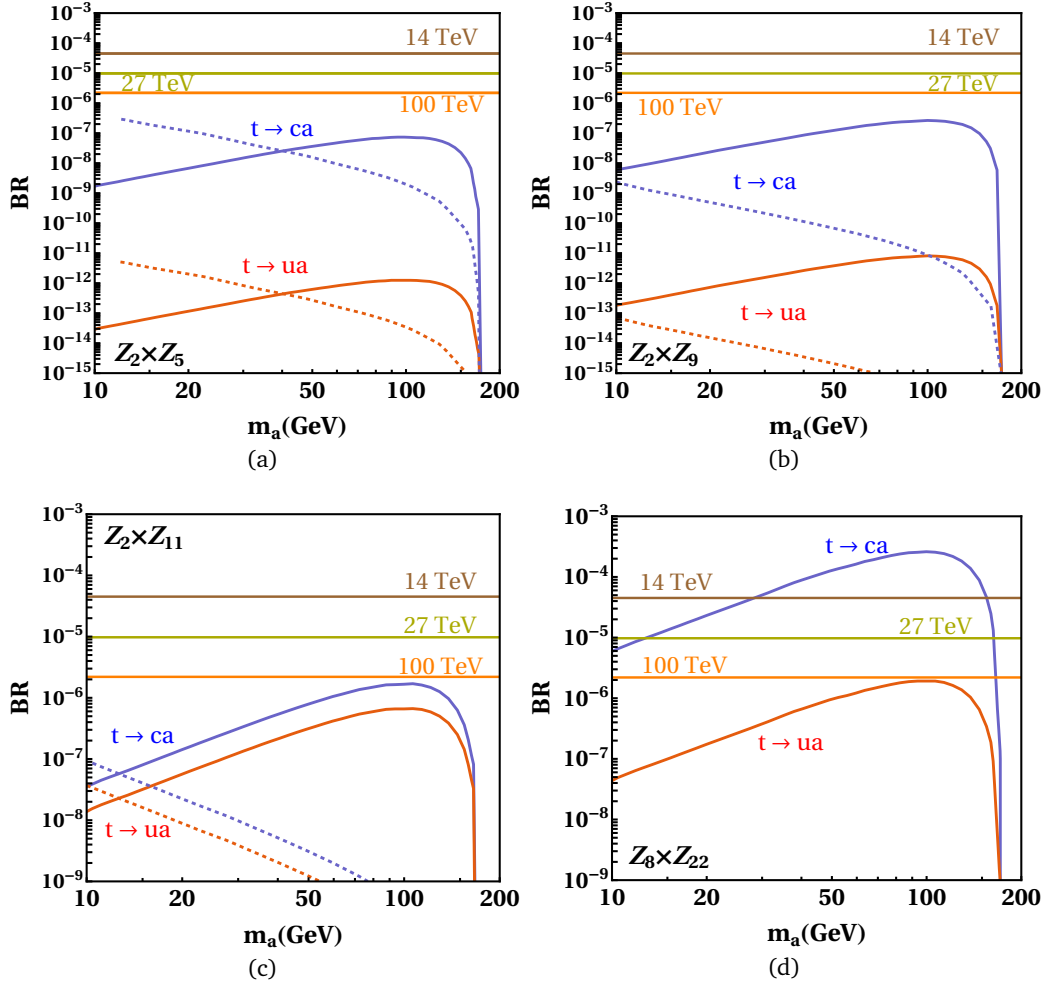


Figure 18: The branching ratios of top quark decays into flavon of $\mathcal{Z}_N \times \mathcal{Z}_M$ flavor symmetries as a function of the flavon mass (m_a) along the parameter space allowed by the observable $R_{\mu\mu}$ in the phase-II of the LHCb for soft-symmetry breaking scenario, and $BR(K_L \rightarrow \mu^+ \mu^-)$ for symmetry-conserving scenario.

ratio of the decay $t \rightarrow ca$ is larger, and is maximally of the order of 10^{-3} for the $\mathcal{Z}_2 \times \mathcal{Z}_{11}$ and $\mathcal{Z}_8 \times \mathcal{Z}_{22}$ flavor symmetries.

The decay $t \rightarrow ca$ can be within the limits of the LHC, HE-LHC and a 100 TeV future hadron collider for the $\mathcal{Z}_2 \times \mathcal{Z}_{11}$ and $\mathcal{Z}_8 \times \mathcal{Z}_{22}$ flavor symmetries. This is a remarkable prediction of this work. The decay $t \rightarrow ca$ is within the reach of the limits of the HE-LHC for the $\mathcal{Z}_2 \times \mathcal{Z}_{5,9}$ flavor symmetries. We notice another important prediction of this work for the branching ratio of the decay $t \rightarrow ua$, which is in the reach of LHC, HE-LHC and a 100 TeV collider only for the $\mathcal{Z}_2 \times \mathcal{Z}_{11}$ flavor symmetry. This decay is accessible to the HE-LHC only for the $\mathcal{Z}_8 \times \mathcal{Z}_{22}$ flavor symmetry. Thus, we conclude that the decays $t \rightarrow (c, u)a$ can be a good test ground for different $\mathcal{Z}_N \times \mathcal{Z}_M$ flavor symmetries for a low mass flavon.

The limits in equation 80 can be used to place bounds on the parameter space of the flavon of the $\mathcal{Z}_N \times \mathcal{Z}_M$ flavor symmetries, as shown in figure 20. We must note that dashed straight lines denote our predictions for the symmetry-conserving scenarios, which are beyond the reach of the sensitivities given in equation 80.

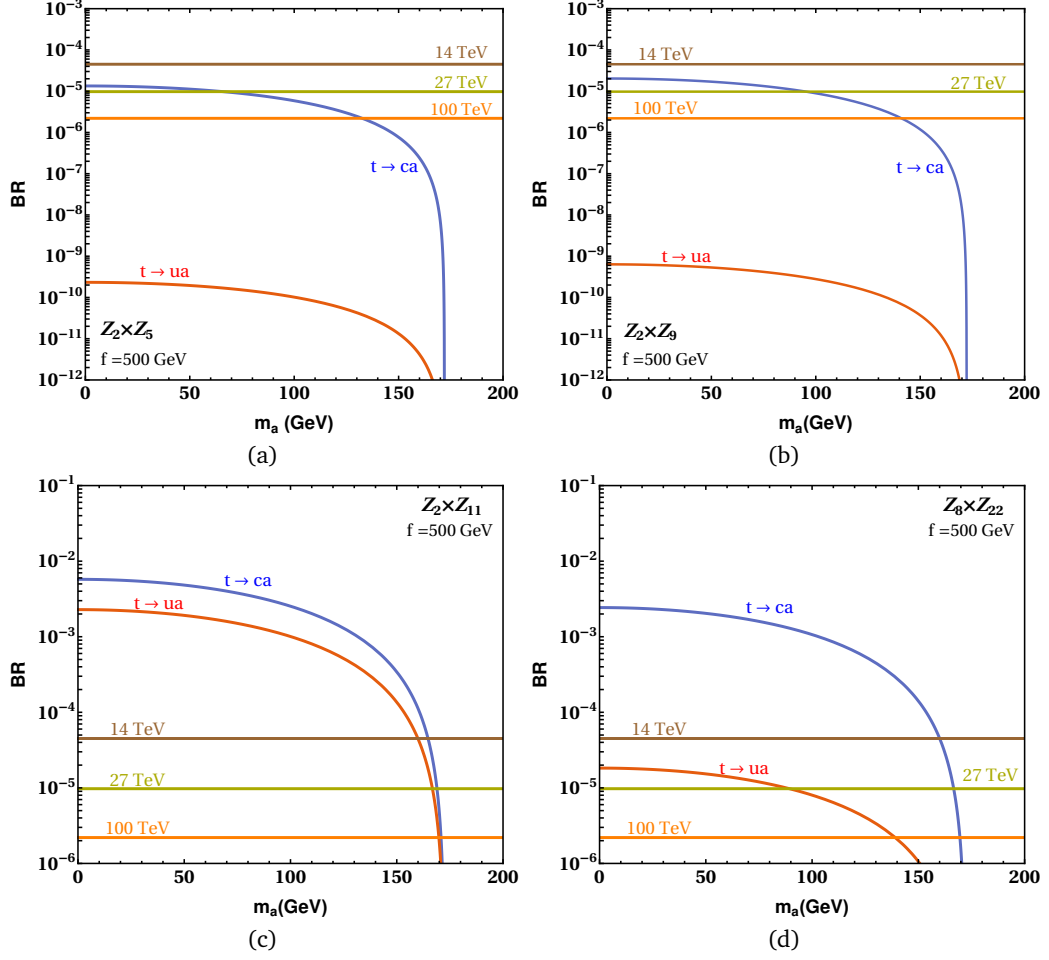


Figure 19: Branching ratios of top quark decays into flavon of $Z_2 \times Z_5$, $Z_2 \times Z_9$, $Z_2 \times Z_{11}$ and $Z_8 \times Z_{22}$ flavor symmetries as a function of m_a , assuming the flavon VEV $f = 500$ GeV.

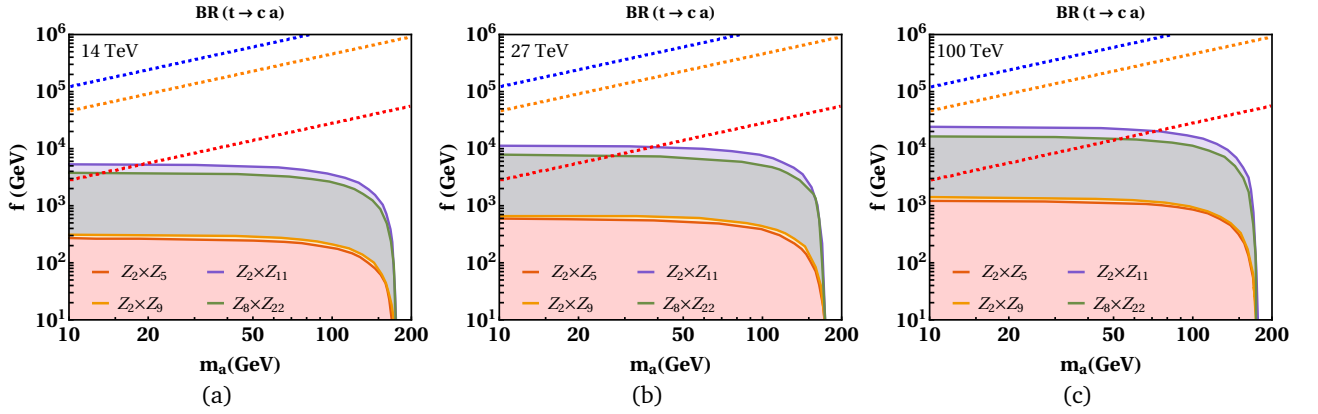


Figure 20: The parameter space excluded by the limits on $BR(t \rightarrow Hc)$ from 14 TeV LHC, 27 TeV HE-LHC, and a 100 TeV collider for $Z_2 \times Z_5$, $Z_2 \times Z_9$, $Z_2 \times Z_{11}$ and $Z_8 \times Z_{22}$ flavor symmetries in the soft symmetry-breaking scenario is shown with the coloured regions. The dashed lines represents the allowed parameter space in the symmetry-conserving scenario.

6.3 Flavon production at the HL-LHC, HE-LHC, and a 100 TeV hadron collider

We now discuss the production of the flavon of the $\mathcal{Z}_N \times \mathcal{Z}_M$ flavor symmetries at the LHC, HE-LHC, and at a 100 TeV future hadron collider. The analytical results for the production cross-sections of the flavon in various channels have been derived using the MSTW2008 PDF [128]. Additionally, FeynRules [129] has been utilized to produce the model UFO files for all four $\mathcal{Z}_N \times \mathcal{Z}_M$ flavor symmetries discussed in this work. We used these files to perform production cross-section calculations with MadGraph [130], and verify our analytical results.

The inclusive production cross-sections of flavon of the $\mathcal{Z}_N \times \mathcal{Z}_M$ flavor symmetries at the LHC, HE-LHC, and at a 100 TeV future hadron collider are shown in figures 21 and 22 for the $\mathcal{Z}_2 \times \mathcal{Z}_{5,9,11}$ and the $\mathcal{Z}_8 \times \mathcal{Z}_{22}$ flavor symmetries. For the soft symmetry-breaking scenario, the boundaries of parameter space allowed by the observable $R_{\mu\mu}$ in the phase-II of the LHCb, shown in figure 7c, are used. The dashed curves are the cross-sections for the symmetry-conserving scenarios using the parameter space allowed by the observable $BR(K_L \rightarrow \mu^+ \mu^-)$.

We use the parameter space allowed by the projected sensitivities of $\mathcal{R}_{\mu\mu}$ in the LHCb Phase-II in figure 7c to show the production cross-sections of a heavy flavon in the different $\mathcal{Z}_N \times \mathcal{Z}_M$ models. Furthermore, the most optimistic scenario is obtained using the flavon VEV $f = 500$ GeV, which is approximately allowed for a heavy flavon by the bounds obtained from the current measurement of the observable $R_{\mu\mu}$ in figure 7a. This choice is also used in previous works, such as references [34, 37]. We continue to use the flavon VEV $f = 500$ GeV even for the production cross-sections of a low mass flavon.

In the soft symmetry-breaking scenario, the projected sensitivities of $\mathcal{R}_{\mu\mu}$ in the LHCb Phase-II allows the mass range m_a lying between 10 up to 10^4 GeV, the corresponding ranges for the VEV of the flavon f vary approximately as $\sim (3 \times 10^2, 4 \times 10^4)$ GeV for $\mathcal{Z}_2 \times \mathcal{Z}_5$, $\sim (6 \times 10^2, 2.6 \times 10^4)$ GeV for $\mathcal{Z}_2 \times \mathcal{Z}_9$, $\sim (7.8 \times 10^2, 1.4 \times 10^5)$ GeV for $\mathcal{Z}_2 \times \mathcal{Z}_{11}$, and $\sim (3.6 \times 10^2, 10^4)$ GeV for $\mathcal{Z}_8 \times \mathcal{Z}_{22}$ flavor symmetry.

For the symmetry-conserving scenario, we analyze flavon production channels with the parameter space allowed the observable $BR(K_L \rightarrow \mu^+ \mu^-)$, where VEV f ranges approximately as $\sim (3 \times 10^3, 3 \times 10^6)$ GeV for $\mathcal{Z}_2 \times \mathcal{Z}_5$, $\sim (4 \times 10^4, 4 \times 10^7)$ GeV for $\mathcal{Z}_2 \times \mathcal{Z}_9$, and $\sim (10^5, 9 \times 10^7)$ GeV for $\mathcal{Z}_2 \times \mathcal{Z}_{11}$ flavor symmetry.

6.3.1 Inclusive production

A flavon can be produced through the inclusive channels,

$$gg, bb \rightarrow a. \quad (81)$$

As it can be noted from figure 21 and 22, the gluon-fusion production cross-sections for the soft symmetry-breaking scenario, is very small for the $\mathcal{Z}_2 \times \mathcal{Z}_{5,9,11}$ flavor symmetries due to the absence of the flavor-diagonal coupling of the flavon to top quarks. However, this observation dramatically changes for the $\mathcal{Z}_8 \times \mathcal{Z}_{22}$ flavor symmetry, where the flavor-diagonal coupling of the flavon to top quarks is allowed. This can be seen in figures 22d-22f. In the case of symmetry-conserving scenario, the gluon-fusion production cross-section turns out to be very small and, as will be shown later, is beyond the reach of the LHC, HE-LHC, and a 100 TeV future collider.

In figures 23 and 24, we show the production cross-sections of the flavon of different $\mathcal{Z}_N \times \mathcal{Z}_M$ flavor symmetries for the VEV $f = 500$ GeV for the soft symmetry-breaking scenario. In this scenario, the production cross-sections can be sufficiently large for the $\mathcal{Z}_2 \times \mathcal{Z}_{5,9,11}$ and $\mathcal{Z}_8 \times \mathcal{Z}_{22}$ flavor symmetries. Therefore, our investigation of the inclusive modes will be performed only for this choice from now on for the heavy mass flavon.

The above results can be used to look for resonance searches of the flavon. For example, a generic search is of the type,

$$pp \rightarrow a \rightarrow b\bar{b}/\ell_i\bar{\ell}_i/\gamma\gamma. \quad (82)$$

On the other side, due to the off-diagonal flavon couplings of flavon to a fermionic pair, searches with a specific signature of the $\mathcal{Z}_N \times \mathcal{Z}_M$ flavor symmetries are,

$$pp \rightarrow a \rightarrow t\bar{c}/t\bar{u}. \quad (83)$$

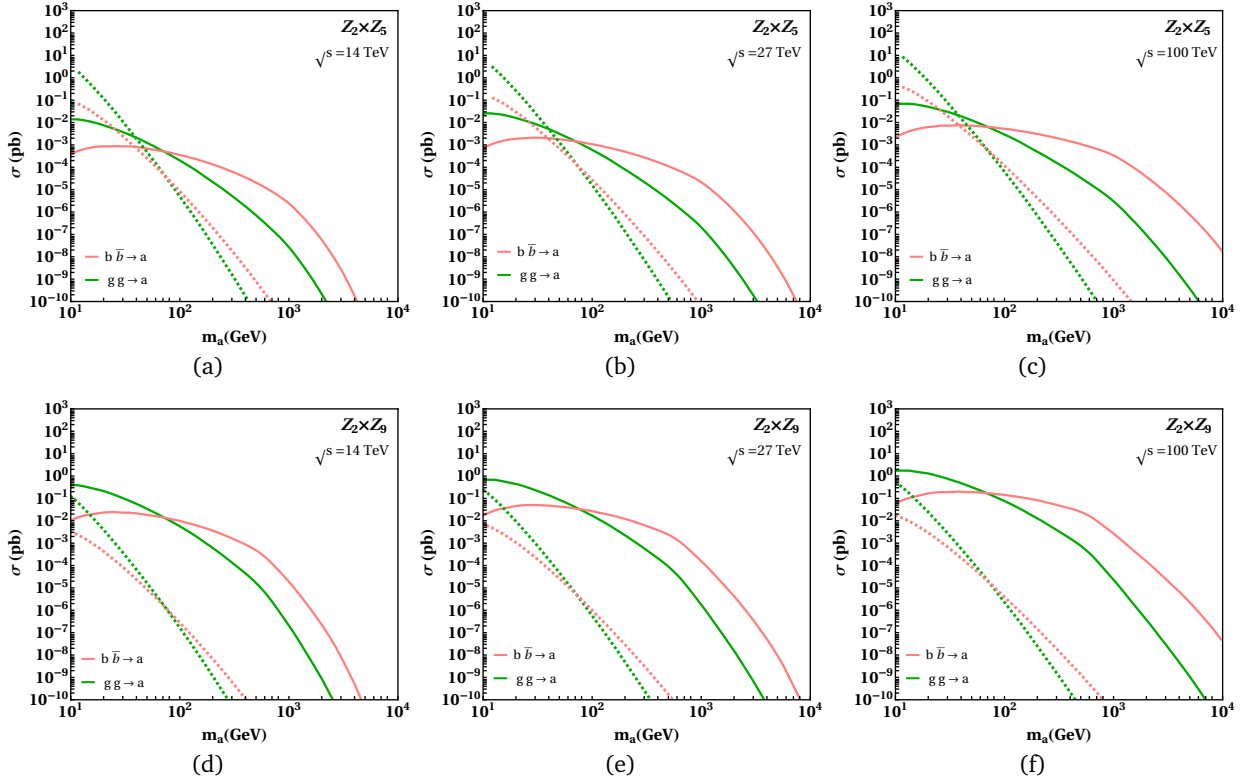


Figure 21: Production cross-sections of the flavon of $Z_2 \times Z_5$, $Z_2 \times Z_9$ flavor symmetries with respect to its mass through different channels for the 14 TeV HL-LHC, 27 TeV HE-LHC, and future 100 TeV hadron collider. The solid lines represents the production cross section along the boundaries of parameter space allowed by the observable $R_{\mu\mu}$ for soft symmetry-breaking scenario, while the dashed lines correspond to that in the symmetry-conserving scenario along the allowed parameter space by the observable $BR(K_L \rightarrow \mu\mu)_{SD}$.

m_a [GeV]	$\mathcal{L}[fb^{-1}]$ [References]		ATLAS 13 TeV		CMS 13 TeV	
	ATLAS	CMS	500	1000	500	1000
jet-jet [pb]	139 [131]	137 [132]		0.1		0.2
$\tau\tau$ [pb]	36.1 [133]	35.9 [134]	$8 \cdot 10^{-2}$	10^{-2}	$6 \cdot 10^{-2}$	10^{-2}
$ee, \mu\mu$ [pb]	139 [135]	140 [136]	$8 \cdot 10^{-4}$	$2 \cdot 10^{-4}$	$2 \cdot 10^{-3}$	$4 \cdot 10^{-4}$
μe [pb]	138 [137]	139 [138]		$3 \cdot 10^{-4}$	$4 \cdot 10^{-3}$	$3 \cdot 10^{-4}$
$\mu\tau$ [pb]	138 [137]	139 [138]		$1 \cdot 10^{-3}$	$7 \cdot 10^{-3}$	$1 \cdot 10^{-3}$
$e\tau$ [pb]	138 [137]	139 [138]		$1 \cdot 10^{-3}$	$5 \cdot 10^{-3}$	$1 \cdot 10^{-3}$
$b\bar{b}$ [pb]	139 [131]	138 [139]		$1 \cdot 10^{-2}$		$4 \cdot 10^{-2}$
$\gamma\gamma$ [pb]	139 [125]	35.9 [126]	$5 \cdot 10^{-4}$	$1 \cdot 10^{-4}$	$4 \cdot 10^{-3}$	$8 \cdot 10^{-4}$
$t\bar{t}$ [pb]	36.1 [140, 141]	35.9 [142]	$2 \cdot 10^2$	2	30	0.4

Table 12: Current limits for production cross section times branching ratio ($\sigma \times BR$) at 13 TeV LHC by ATLAS and CMS in high mass resonance searches for inclusive flavon production channels.

In table 12, we show the present sensitivities of different inclusive flavon production channels at the 14 TeV LHC. These results will be used to estimate the sensitivities of the HL-LHC, HE-LHC, and a 100 TeV collider for a heavy flavon production and decay. We show these sensitivities in table 13. These sensitivities are estimated

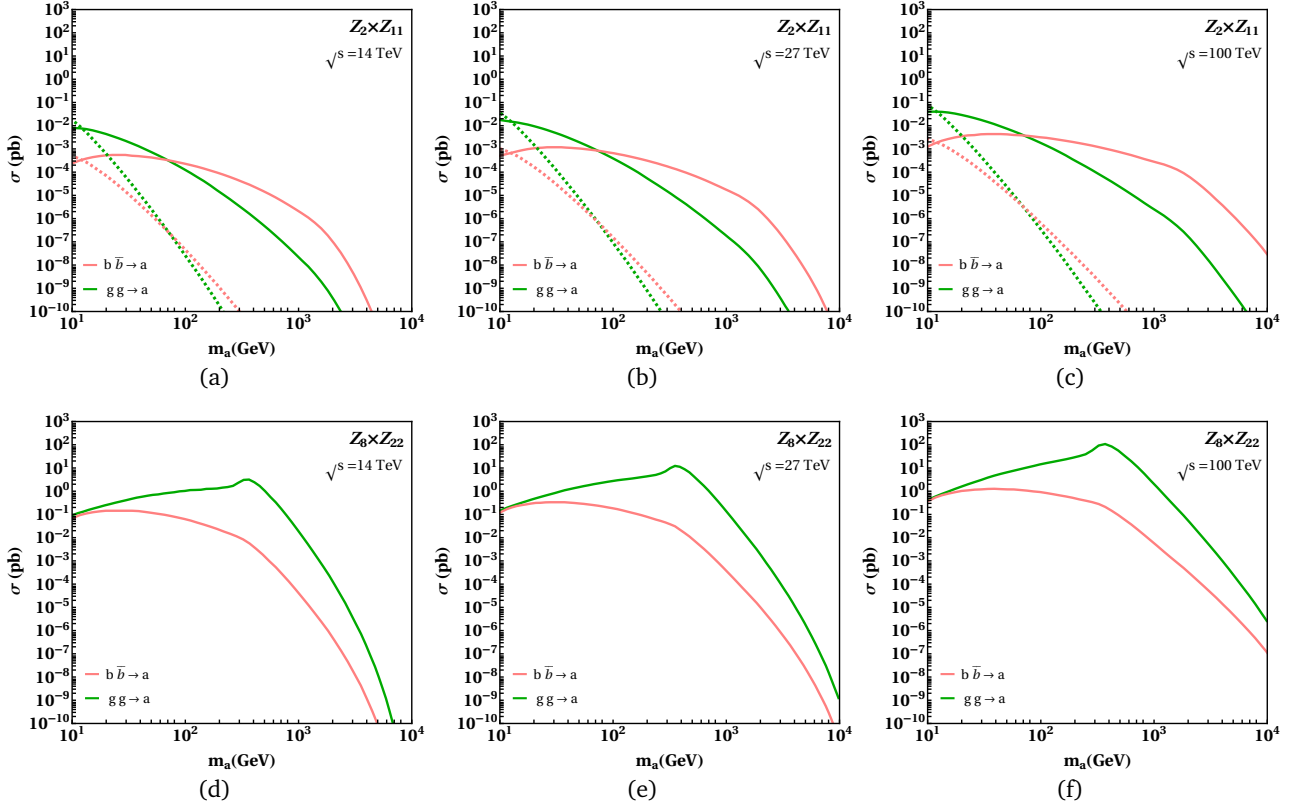


Figure 22: Production cross-sections of the flavon of $Z_2 \times Z_{11}$, and $Z_8 \times Z_{22}$ flavor symmetries with respect to its mass through different channels for the 14 TeV HL-LHC, 27 TeV HE-LHC, and future 100 TeV hadron collider. The solid lines represents the production cross section along the boundaries of parameter space allowed by the observable $R_{\mu\mu}$ for soft symmetry-breaking scenario, while the dashed lines correspond to that in the symmetry-conserving scenario along the allowed parameter space by the observable $BR(K_L \rightarrow \mu\mu)_{SD}$.

using simple square root scaling of the luminosity of the LHC by,

$$S \simeq \frac{S}{\sqrt{B}} \simeq \sqrt{\mathcal{L}} \frac{\sigma_s}{\sqrt{\sigma_B}}, \quad (84)$$

where S is the number of signal events, B denotes the background events, σ_s is the signal cross-section, and σ_B stands for the background cross-section.

We adopt a conservative approach for estimating the sensitivities of the HL-LHC, HE-LHC, and a 100 TeV collider. We make the following assumptions for this purpose.

1. The significance $S \simeq \frac{S}{\sqrt{B}}$ remains constant among the colliders.
2. We assume that there is no appreciable change in the reconstruction efficiencies and background rejection.

We note that similar assumptions are also used in the “Collider Reach” tool, which remarkably provides an estimate of the mass of a BSM physics that can be searched at the LHC and a future collider [143].

Thus, the required sensitive cross-section of any flavon signal at a future collider (FC) is given by

$$\sigma_s^{\text{FC}} = \sqrt{\frac{\mathcal{L}_{\text{LHC}}}{\mathcal{L}_{\text{FC}}}} \sqrt{\frac{\sigma_B^{\text{FC}}}{\sigma_B^{\text{LHC}}}} \sigma_s^{\text{LHC}}, \quad (85)$$

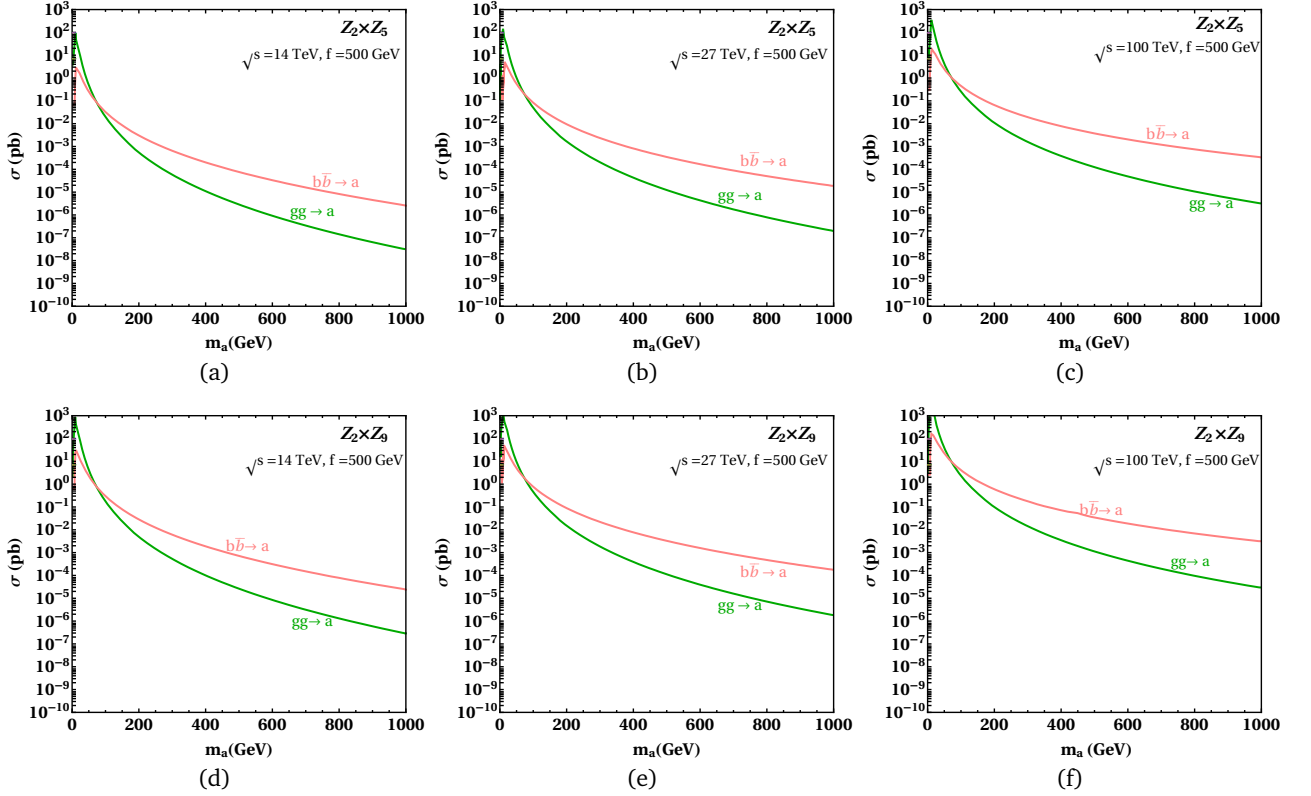


Figure 23: Production cross-sections of the flavon of $\mathcal{Z}_2 \times \mathcal{Z}_5$, and $\mathcal{Z}_2 \times \mathcal{Z}_9$ flavor symmetries with respect to its mass through different channels for 14 TeV HL-LHC, 27 TeV HE-LHC, and future 100 TeV hadron collider, where the flavon VEV $f = 500$ GeV.

where FC= HL-LHC, HE-LHC, and a 100 TeV collider. We have computed σ_B^{FC} and σ_B^{LHC} through MadGraph, and it turns out that $\sigma_B^{HE-LHC} \leq 2\sigma_B^{LHC}$ and $\sigma_B^{100TeV} \leq 10\sigma_B^{LHC}$, and σ_s^{LHC} is given in table 12.

m_a [GeV]	HL-LHC [14 TeV, 3 ab ⁻¹]		HE-LHC [27 TeV, 15 ab ⁻¹]		100 TeV, 30 ab ⁻¹	
	500	1000	500	1000	500	1000
jet-jet [pb]		$4 \cdot 10^{-2}$		$3 \cdot 10^{-2}$		$4 \cdot 10^{-2}$
$\tau\tau$ [pb]	$7 \cdot 10^{-3}$	$1 \cdot 10^{-3}$	$4 \cdot 10^{-3}$	$7 \cdot 10^{-4}$	$5 \cdot 10^{-3}$	$8 \cdot 10^{-4}$
$ee, \mu\mu$ [pb]	$2 \cdot 10^{-4}$	$4 \cdot 10^{-5}$	$1 \cdot 10^{-4}$	$3 \cdot 10^{-5}$	$1 \cdot 10^{-4}$	$3 \cdot 10^{-5}$
μe [pb]	$9 \cdot 10^{-4}$	$7 \cdot 10^{-5}$	$7 \cdot 10^{-4}$	$5 \cdot 10^{-5}$	$1 \cdot 10^{-3}$	$1 \cdot 10^{-4}$
$\mu\tau$ [pb]	$2 \cdot 10^{-3}$	$2 \cdot 10^{-4}$	$1 \cdot 10^{-3}$	$2 \cdot 10^{-4}$	$2 \cdot 10^{-3}$	$3 \cdot 10^{-4}$
$e\tau$ [pb]	$1 \cdot 10^{-3}$	$2 \cdot 10^{-4}$	$8 \cdot 10^{-4}$	$2 \cdot 10^{-4}$	$1 \cdot 10^{-3}$	$3 \cdot 10^{-4}$
$b\bar{b}$ [pb]		$9 \cdot 10^{-3}$		$5 \cdot 10^{-3}$		$7 \cdot 10^{-3}$
$\gamma\gamma$ [pb]	$1 \cdot 10^{-4}$	$2 \cdot 10^{-5}$	$6 \cdot 10^{-5}$	$1 \cdot 10^{-5}$	$7 \cdot 10^{-5}$	$1 \cdot 10^{-5}$
$t\bar{t}$ [pb]	4	$5 \cdot 10^{-2}$	3	$4 \cdot 10^{-2}$	8	0.1

Table 13: Estimated reach ($\sigma \times BR$) of the HL-LHC, HE-LHC and a 100 TeV hadron collider for high flavon mass (m_a) in inclusive flavon production channels.

We show our benchmark predictions for the processes given in table 12, for different $\mathcal{Z}_N \times \mathcal{Z}_M$ flavor symmetries in tables 14- 16 for $f = 500$ GeV and $m_a = 500, 1000$ for the soft symmetry-breaking scenarios. The modes that are accessible to the HL-LHC, HE-LHC, and a 100 TeV collider are marked with a box \square .

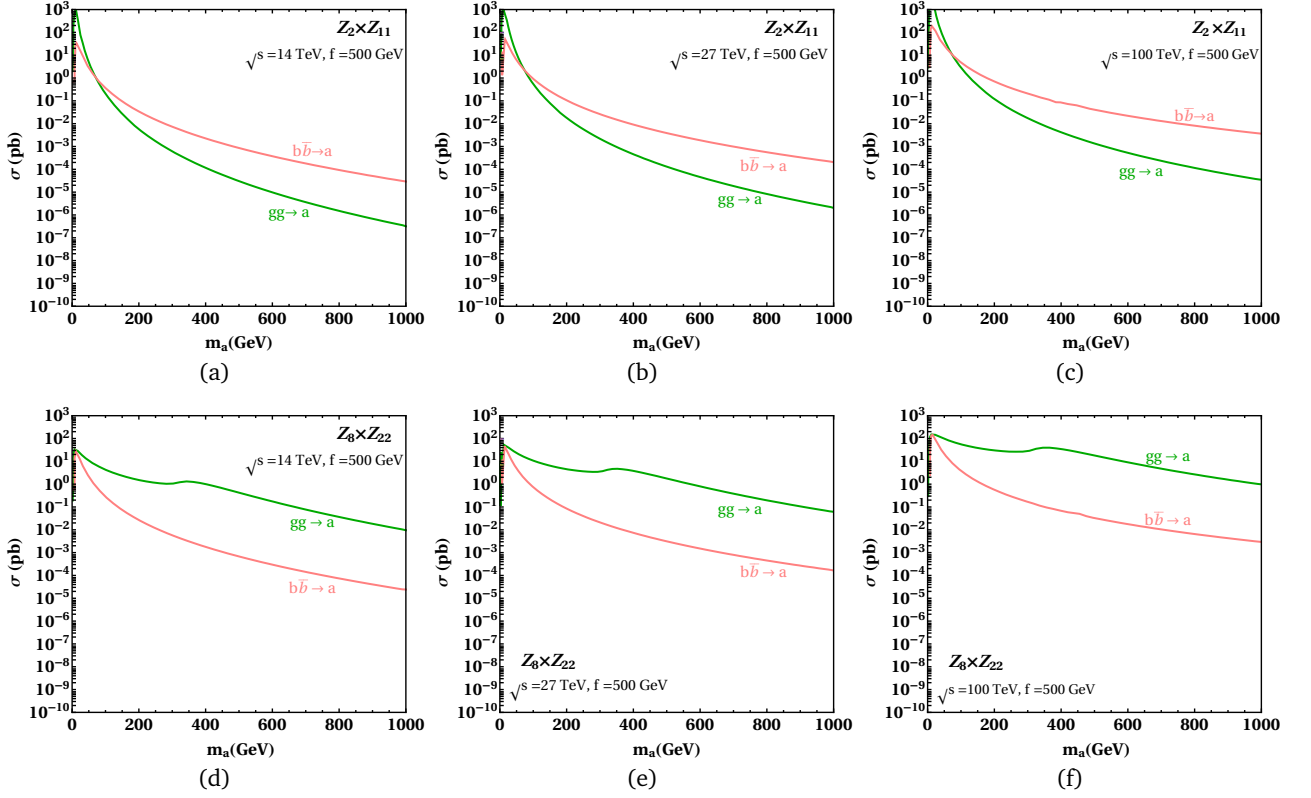


Figure 24: Production cross-sections of the flavon of $Z_2 \times Z_{11}$, and $Z_8 \times Z_{22}$ flavor symmetries with respect to its mass through different channels for 14 TeV HL-LHC, 27 TeV HE-LHC, and future 100 TeV high-luminosity hadron collider, where the flavon VEV $f = 500$ GeV.

From table 14, we observe that only the $Z_2 \times Z_5$ and the $Z_8 \times Z_{22}$ flavor symmetries are accessible to the HL-LHC, and both the symmetries can be differentiated due to the distinct accessible processes. This situation changes sufficiently for the HE-LHC as shown in table 15, as more processes are under the reach of the HE-LHC. However, even now, mainly the $Z_2 \times Z_5$ and the $Z_8 \times Z_{22}$ flavor symmetries are under the reach of the HE-LHC. The $Z_2 \times Z_9$ flavor symmetry can be probed through the $e\tau$ channel.

m_a [GeV]	Benchmark $\mathcal{Z}_2 \times \mathcal{Z}_5$		Benchmark $\mathcal{Z}_2 \times \mathcal{Z}_9$		Benchmark $\mathcal{Z}_2 \times \mathcal{Z}_{11}$		Benchmark $\mathcal{Z}_8 \times \mathcal{Z}_{22}$	
	500	1000	500	1000	500	1000	500	1000
jet-jet [pb]		$3.6 \cdot 10^{-2}$		$1.5 \cdot 10^{-6}$		$2.3 \cdot 10^{-7}$		$1.4 \cdot 10^{-3}$
$\tau\tau$ [pb]	$1.2 \cdot 10^{-3}$	$9.2 \cdot 10^{-5}$	$8.0 \cdot 10^{-5}$	$3.4 \cdot 10^{-6}$	$2.9 \cdot 10^{-5}$	$1.6 \cdot 10^{-6}$	$3.4 \cdot 10^{-3}$	$6.1 \cdot 10^{-5}$
$\mu\tau$ [pb]	$1.4 \cdot 10^{-3}$	$1.1 \cdot 10^{-4}$	$2.3 \cdot 10^{-4}$	$9.5 \cdot 10^{-6}$	$3 \cdot 10^{-5}$	$1.7 \cdot 10^{-6}$	$5.8 \cdot 10^{-3}$	$1 \cdot 10^{-4}$
$e\tau$ [pb]	$1.1 \cdot 10^{-3}$	$8.9 \cdot 10^{-5}$	$2.2 \cdot 10^{-4}$	$9.4 \cdot 10^{-6}$	$8.5 \cdot 10^{-5}$	$4.7 \cdot 10^{-6}$	$3.2 \cdot 10^{-4}$	$5.8 \cdot 10^{-6}$
$\mu\mu$ [pb]	$1.1 \cdot 10^{-6}$	$8.3 \cdot 10^{-8}$	$1.7 \cdot 10^{-6}$	$7.3 \cdot 10^{-8}$	$2.2 \cdot 10^{-7}$	$1.2 \cdot 10^{-8}$	$2.9 \cdot 10^{-5}$	$5.3 \cdot 10^{-7}$
μe [pb]	$2.9 \cdot 10^{-6}$	$2.3 \cdot 10^{-7}$	$6.3 \cdot 10^{-7}$	$2.6 \cdot 10^{-8}$	$4.8 \cdot 10^{-7}$	$2.7 \cdot 10^{-8}$	$3.3 \cdot 10^{-6}$	$5.8 \cdot 10^{-8}$
ee [pb]	$2.5 \cdot 10^{-10}$	$2 \cdot 10^{-11}$	$3.4 \cdot 10^{-9}$	$1.4 \cdot 10^{-10}$	$6.7 \cdot 10^{-11}$	$3.7 \cdot 10^{-12}$	$1.7 \cdot 10^{-9}$	$3 \cdot 10^{-11}$
$\gamma\gamma$ [pb]	$1.3 \cdot 10^{-7}$	$3.6 \cdot 10^{-9}$	$8.2 \cdot 10^{-10}$	$1.2 \cdot 10^{-11}$	$1.5 \cdot 10^{-10}$	$3 \cdot 10^{-12}$	$6.6 \cdot 10^{-4}$	$1 \cdot 10^{-5}$
$b\bar{b}$ [pb]	$9.8 \cdot 10^{-3}$	$6.3 \cdot 10^{-4}$	$4.7 \cdot 10^{-4}$	$1.9 \cdot 10^{-5}$	$1.2 \cdot 10^{-4}$	$5.7 \cdot 10^{-6}$	$1.9 \cdot 10^{-2}$	$3.2 \cdot 10^{-4}$
tc [pb]	$3.6 \cdot 10^{-3}$	$2.8 \cdot 10^{-4}$	$2.5 \cdot 10^{-5}$	$1.2 \cdot 10^{-6}$	$1.5 \cdot 10^{-3}$	$8.5 \cdot 10^{-5}$	0.152	$3.1 \cdot 10^{-3}$
tu [pb]	$6.5 \cdot 10^{-8}$	$5.1 \cdot 10^{-9}$	$7.8 \cdot 10^{-10}$	$3.8 \cdot 10^{-11}$	$6.6 \cdot 10^{-4}$	$3.8 \cdot 10^{-5}$	$1.1 \cdot 10^{-3}$	$2.3 \cdot 10^{-5}$
$t\bar{t}$ [pb]							4.42	0.12

Table 14: Benchmark points for different $\mathcal{Z}_N \times \mathcal{Z}_M$ flavor symmetries for inclusive flavon production channels with high flavon mass (m_a) in case of the soft symmetry-breaking scenario at the 14 TeV HL-LHC, assuming $\text{VEV}(f) = 500$ GeV. Accessible channels are represented within the box.

m_a [GeV]	Benchmark $\mathcal{Z}_2 \times \mathcal{Z}_5$		Benchmark $\mathcal{Z}_2 \times \mathcal{Z}_9$		Benchmark $\mathcal{Z}_2 \times \mathcal{Z}_{11}$		Benchmark $\mathcal{Z}_8 \times \mathcal{Z}_{22}$	
	500	1000	500	1000	500	1000	500	1000
jet-jet [pb]		0.133		$8.2 \cdot 10^{-6}$		$9.4 \cdot 10^{-7}$		$9.8 \cdot 10^{-3}$
$\tau\tau$ [pb]	$2.6 \cdot 10^{-3}$	$2.8 \cdot 10^{-4}$	$2.9 \cdot 10^{-4}$	$1.7 \cdot 10^{-5}$	$8 \cdot 10^{-5}$	$5.6 \cdot 10^{-6}$	$1.5 \cdot 10^{-2}$	$4 \cdot 10^{-4}$
$\mu\tau$ [pb]	$3.2 \cdot 10^{-3}$	$3.5 \cdot 10^{-4}$	$8.3 \cdot 10^{-4}$	$4.8 \cdot 10^{-5}$	$8.4 \cdot 10^{-5}$	$5.8 \cdot 10^{-6}$	$2.5 \cdot 10^{-2}$	$6.8 \cdot 10^{-4}$
$e\tau$ [pb]	$2.6 \cdot 10^{-3}$	$2.8 \cdot 10^{-4}$	$8.2 \cdot 10^{-4}$	$4.8 \cdot 10^{-5}$	$2.3 \cdot 10^{-4}$	$1.6 \cdot 10^{-5}$	$1.4 \cdot 10^{-3}$	$3.8 \cdot 10^{-5}$
$\mu\mu$ [pb]	$2.4 \cdot 10^{-6}$	$2.6 \cdot 10^{-7}$	$6.4 \cdot 10^{-6}$	$3.7 \cdot 10^{-7}$	$6.2 \cdot 10^{-7}$	$4.3 \cdot 10^{-8}$	$1.3 \cdot 10^{-4}$	$3.5 \cdot 10^{-6}$
μe [pb]	$6.6 \cdot 10^{-6}$	$7.1 \cdot 10^{-7}$	$2.3 \cdot 10^{-6}$	$1.4 \cdot 10^{-7}$	$1.3 \cdot 10^{-6}$	$9.3 \cdot 10^{-8}$	$1.4 \cdot 10^{-5}$	$3.8 \cdot 10^{-7}$
ee [pb]	$5.6 \cdot 10^{-10}$	$6.1 \cdot 10^{-11}$	$1.3 \cdot 10^{-8}$	$7.4 \cdot 10^{-10}$	$1.8 \cdot 10^{-10}$	$1.3 \cdot 10^{-11}$	$7.2 \cdot 10^{-9}$	$1.9 \cdot 10^{-10}$
$\gamma\gamma$ [pb]	$2.9 \cdot 10^{-7}$	$1.1 \cdot 10^{-8}$	$3 \cdot 10^{-9}$	$6.3 \cdot 10^{-11}$	$4.2 \cdot 10^{-10}$	$1.1 \cdot 10^{-11}$	$2.8 \cdot 10^{-3}$	$6.7 \cdot 10^{-5}$
$b\bar{b}$ [pb]	$2.7 \cdot 10^{-2}$	$2.3 \cdot 10^{-3}$	$1.9 \cdot 10^{-3}$	$1 \cdot 10^{-4}$	$3.8 \cdot 10^{-4}$	$2.3 \cdot 10^{-5}$	$8.8 \cdot 10^{-2}$	$2.2 \cdot 10^{-3}$
tc [pb]	$1 \cdot 10^{-2}$	$1 \cdot 10^{-3}$	$1 \cdot 10^{-4}$	$6.6 \cdot 10^{-6}$	$4.6 \cdot 10^{-3}$	$3.4 \cdot 10^{-4}$	0.702	$2.1 \cdot 10^{-2}$
tu [pb]	$1.8 \cdot 10^{-7}$	$1.9 \cdot 10^{-8}$	$3.1 \cdot 10^{-9}$	$2 \cdot 10^{-10}$	$2 \cdot 10^{-3}$	$1.5 \cdot 10^{-4}$	$5.3 \cdot 10^{-3}$	$1.6 \cdot 10^{-4}$
$t\bar{t}$ [pb]							20.46	0.83

Table 15: Benchmark points for different $\mathcal{Z}_N \times \mathcal{Z}_M$ flavor symmetries for inclusive flavon production channels with high flavon mass (m_a) in case of the soft symmetry-breaking scenario at the 27 TeV HE-LHC, assuming $f = 500$ GeV.

A 100 TeV collider provides a more dramatic scenario for the $\mathcal{Z}_N \times \mathcal{Z}_M$ flavor symmetries. As shown in table 16, all symmetries except the $\mathcal{Z}_2 \times \mathcal{Z}_{11}$ become sensitive in most of the inclusive processes. The $\mathcal{Z}_2 \times \mathcal{Z}_{11}$ flavor symmetry is accessible only through the $e\tau$ channel.

The LHC is actively searching for light pseudoscalar particles. For a light flavon, present sensitivities of the LHC are given in table 17. Using these sensitivities given in table 17, the estimated sensitivities for the HL-LHC, HE-LHC, and a 100 TeV collider are given in table 18. The benchmark predictions for the processes given in

m_a [GeV]	Benchmark $\mathcal{Z}_2 \times \mathcal{Z}_5$		Benchmark $\mathcal{Z}_2 \times \mathcal{Z}_9$		Benchmark $\mathcal{Z}_2 \times \mathcal{Z}_{11}$		Benchmark $\mathcal{Z}_8 \times \mathcal{Z}_{22}$	
	500	1000	500	1000	500	1000	500	1000
jet-jet [pb]		0.95		$1.1 \cdot 10^{-4}$		$8.1 \cdot 10^{-6}$		0.18
$\tau\tau$ [pb]	$1.1 \cdot 10^{-2}$	$1.4 \cdot 10^{-3}$	$2.2 \cdot 10^{-3}$	$1.9 \cdot 10^{-4}$	$4.8 \cdot 10^{-4}$	$3.8 \cdot 10^{-5}$	0.14	$6.2 \cdot 10^{-3}$
$\mu\tau$ [pb]	$1.3 \cdot 10^{-2}$	$1.7 \cdot 10^{-3}$	$6.3 \cdot 10^{-3}$	$5.5 \cdot 10^{-4}$	$5 \cdot 10^{-4}$	$3.9 \cdot 10^{-5}$	0.23	$1.0 \cdot 10^{-2}$
$e\tau$ [pb]	$1.1 \cdot 10^{-2}$	$1.4 \cdot 10^{-3}$	$6.2 \cdot 10^{-3}$	$5.4 \cdot 10^{-4}$	$1.3 \cdot 10^{-3}$	$1.1 \cdot 10^{-4}$	$1.3 \cdot 10^{-2}$	$5.9 \cdot 10^{-4}$
$\mu\mu$ [pb]	$9.9 \cdot 10^{-5}$	$1.3 \cdot 10^{-6}$	$4.8 \cdot 10^{-5}$	$4.2 \cdot 10^{-6}$	$3.7 \cdot 10^{-6}$	$2.9 \cdot 10^{-7}$	$1.2 \cdot 10^{-3}$	$5.4 \cdot 10^{-5}$
μe [pb]	$2.8 \cdot 10^{-5}$	$3.5 \cdot 10^{-6}$	$1.7 \cdot 10^{-5}$	$1.5 \cdot 10^{-6}$	$8 \cdot 10^{-6}$	$6.3 \cdot 10^{-7}$	$1.3 \cdot 10^{-4}$	$5.9 \cdot 10^{-6}$
ee [pb]	$2.4 \cdot 10^{-9}$	$3.0 \cdot 10^{-10}$	$9.6 \cdot 10^{-8}$	$8.4 \cdot 10^{-9}$	$1.1 \cdot 10^{-9}$	$8.8 \cdot 10^{-11}$	$6.9 \cdot 10^{-8}$	$3.0 \cdot 10^{-9}$
$\gamma\gamma$ [pb]	$1.2 \cdot 10^{-6}$	$5.6 \cdot 10^{-8}$	$2.3 \cdot 10^{-8}$	$7.2 \cdot 10^{-10}$	$2.5 \cdot 10^{-9}$	$7.2 \cdot 10^{-11}$	$2.7 \cdot 10^{-2}$	$1 \cdot 10^{-3}$
$b\bar{b}$ [pb]	0.15	$1.7 \cdot 10^{-2}$	$1.7 \cdot 10^{-2}$	$1.3 \cdot 10^{-3}$	$2.7 \cdot 10^{-3}$	$2 \cdot 10^{-4}$	1.03	$4.1 \cdot 10^{-2}$
tc [pb]	$5.4 \cdot 10^{-2}$	$7.6 \cdot 10^{-3}$	$9.2 \cdot 10^{-4}$	$8.9 \cdot 10^{-5}$	$3.2 \cdot 10^{-2}$	$3 \cdot 10^{-3}$	8.26	0.39
tu [pb]	$9.8 \cdot 10^{-7}$	$1.4 \cdot 10^{-7}$	$2.8 \cdot 10^{-8}$	$2.7 \cdot 10^{-9}$	$1.4 \cdot 10^{-2}$	$1.3 \cdot 10^{-3}$	$6.2 \cdot 10^{-2}$	$2.9 \cdot 10^{-3}$
$t\bar{t}$ [pb]							241.4	15.4

Table 16: Benchmark points for different $\mathcal{Z}_N \times \mathcal{Z}_M$ flavor symmetries for inclusive flavon production channels with high flavon mass (m_a) in case of the soft symmetry-breaking scenario at a 100 TeV hadron collider, assuming $f = 500$ GeV.

table 17, for different $\mathcal{Z}_N \times \mathcal{Z}_M$ flavor symmetries, are given in tables 19- 21 for $m_a = 20, 60$ GeV for the soft symmetry-breaking scenario.

m_a [GeV]	$\mathcal{L}[fb^{-1}]$ [References]		ATLAS 13 TeV		CMS 13 TeV	
	ATLAS	CMS	20	60	20	60
$\tau\tau$ [pb]		138 [144]			4	
$\gamma\gamma$ [pb]	138 [145, 146]	[147]	6	7		

Table 17: Current limits of $\sigma \times BR$ at 13 TeV LHC by ATLAS and CMS in low mass resonance searches for inclusive flavon production channels.

m_a [GeV]	HL-LHC [14 TeV, 3 ab $^{-1}$]		HE-LHC [27 TeV, 15 ab $^{-1}$]		100 TeV, 30 ab $^{-1}$	
	20	60	20	60	20	60
$\tau\tau$ [pb]		0.9		0.5		0.6
$\gamma\gamma$ [pb]	1.3	1.5	0.7	0.8	0.8	0.9

Table 18: Estimated reach ($\sigma \times BR$) of the HL-LHC, HE-LHC and a 100 TeV collider for low flavon mass (m_a) in inclusive flavon production channels.

We observe from table 19 that the HL-LHC provides access only to probe the $\mathcal{Z}_8 \times \mathcal{Z}_{22}$ flavor symmetry through the $\tau\tau$ channel for the mass $m_a = 60$ GeV. The situation changes greatly as we approach the HE-LHC and a 100 TeV hadron collider, as shown in tables 20 and 21. Now, the $\tau\tau$ channel is accessible for all $\mathcal{Z}_N \times \mathcal{Z}_M$ flavor symmetries. The $\gamma\gamma$ channel and the flavon mass $m_a = 20$ GeV remain beyond the reach of the HL-LHC, HE-LHC and a 100 TeV collider for all flavor symmetries.

m_a [GeV]	Benchmark $\mathcal{Z}_2 \times \mathcal{Z}_5$		Benchmark $\mathcal{Z}_2 \times \mathcal{Z}_9$		Benchmark $\mathcal{Z}_2 \times \mathcal{Z}_{11}$		Benchmark $\mathcal{Z}_8 \times \mathcal{Z}_{22}$	
	20	60	20	60	20	60	20	60
$\tau\tau$ [pb]	$4.7 \cdot 10^{-3}$	0.58	$1.1 \cdot 10^{-2}$	0.62	$2.2 \cdot 10^{-2}$	0.69	$7.7 \cdot 10^{-3}$	9.62
$\gamma\gamma$ [pb]	$5.6 \cdot 10^{-4}$	$1 \cdot 10^{-3}$	$1.5 \cdot 10^{-4}$	$9.9 \cdot 10^{-5}$	$1.1 \cdot 10^{-4}$	$5.8 \cdot 10^{-5}$	$9 \cdot 10^{-5}$	$1.7 \cdot 10^{-2}$

Table 19: Benchmark points for different $\mathcal{Z}_N \times \mathcal{Z}_M$ flavor symmetries for inclusive flavon production channels with low flavon mass (m_a) in case of the soft symmetry-breaking scenario at the 14 TeV HL-LHC, assuming $f = 500$ GeV.

m_a [GeV]	Benchmark $\mathcal{Z}_2 \times \mathcal{Z}_5$		Benchmark $\mathcal{Z}_2 \times \mathcal{Z}_9$		Benchmark $\mathcal{Z}_2 \times \mathcal{Z}_{11}$		Benchmark $\mathcal{Z}_8 \times \mathcal{Z}_{22}$	
	20	60	20	60	20	60	20	60
$\tau\tau$ [pb]	$8 \cdot 10^{-3}$	1.06	$2.2 \cdot 10^{-2}$	1.38	$4.2 \cdot 10^{-2}$	1.55	$1.5 \cdot 10^{-2}$	21.78
$\gamma\gamma$ [pb]	$9.4 \cdot 10^{-4}$	$1.8 \cdot 10^{-3}$	$2.9 \cdot 10^{-4}$	$2.2 \cdot 10^{-4}$	$2.2 \cdot 10^{-4}$	$1.3 \cdot 10^{-4}$	$1.7 \cdot 10^{-4}$	$3.8 \cdot 10^{-2}$

Table 20: Benchmark points for different $\mathcal{Z}_N \times \mathcal{Z}_M$ flavor symmetries for inclusive flavon production channels with low flavon mass (m_a) in case of the soft symmetry-breaking scenario at the 27 TeV HE-LHC, assuming $f = 500$ GeV.

m_a [GeV]	Benchmark $\mathcal{Z}_2 \times \mathcal{Z}_5$		Benchmark $\mathcal{Z}_2 \times \mathcal{Z}_9$		Benchmark $\mathcal{Z}_2 \times \mathcal{Z}_{11}$		Benchmark $\mathcal{Z}_8 \times \mathcal{Z}_{22}$	
	20	60	20	60	20	60	20	60
$\tau\tau$ [pb]	$2.2 \cdot 10^{-2}$	3.29	$7.5 \cdot 10^{-2}$	5.72	0.15	6.43	$5.1 \cdot 10^{-2}$	92.23
$\gamma\gamma$ [pb]	$2.6 \cdot 10^{-3}$	$5.7 \cdot 10^{-3}$	$9.5 \cdot 10^{-4}$	$9.1 \cdot 10^{-4}$	$7.5 \cdot 10^{-4}$	$5.3 \cdot 10^{-4}$	$5.5 \cdot 10^{-4}$	0.16

Table 21: Benchmark points for different $\mathcal{Z}_N \times \mathcal{Z}_M$ flavor symmetries for inclusive flavon production channels with low flavon mass (m_a) in case of the soft symmetry-breaking scenario at a 100 TeV collider, assuming $f = 500$ GeV.

m_a [GeV]	Benchmark $\mathcal{Z}_2 \times \mathcal{Z}_5$		Benchmark $\mathcal{Z}_2 \times \mathcal{Z}_9$		Benchmark $\mathcal{Z}_2 \times \mathcal{Z}_{11}$	
	20	60	20	60	20	60
$\tau\tau$ [pb]	$1.9 \cdot 10^{-7}$	$5.1 \cdot 10^{-4}$	$1.1 \cdot 10^{-11}$	$2 \cdot 10^{-6}$	$2.4 \cdot 10^{-13}$	$3.3 \cdot 10^{-7}$
$\gamma\gamma$ [pb]	$3.8 \cdot 10^{-7}$	$8.8 \cdot 10^{-7}$	$4.5 \cdot 10^{-10}$	$3.2 \cdot 10^{-10}$	$3.8 \cdot 10^{-11}$	$2.7 \cdot 10^{-11}$

Table 22: Benchmark points for different $\mathcal{Z}_N \times \mathcal{Z}_M$ flavor symmetries for inclusive flavon production channels with low flavon mass (m_a) in case of the symmetry-conserving scenario at the 14 TeV HL-LHC.

In the symmetry-conserving case, we observe from figures 21 and 22 that the cross-section can be relatively significant only for a low flavon mass. Therefore, we investigate the symmetry-conserving scenario only for $m_a = 20, 60$ GeV. We show benchmark predictions of symmetry-conserving scenario for different $\mathcal{Z}_N \times \mathcal{Z}_M$ flavor symmetries in tables 22- 24 for $m_a = 20, 60$ GeV. It turns out that the inclusive processes in this scenario are beyond the reach of the HL-LHC, HE-LHC, and even a 100 TeV collider.

m_a [GeV]	Benchmark $\mathcal{Z}_2 \times \mathcal{Z}_5$		Benchmark $\mathcal{Z}_2 \times \mathcal{Z}_9$		Benchmark $\mathcal{Z}_2 \times \mathcal{Z}_{11}$	
	20	60	20	60	20	60
$\tau\tau$ [pb]	$2 \cdot 10^{-7}$	$9.2 \cdot 10^{-4}$	$1.8 \cdot 10^{-11}$	$4.5 \cdot 10^{-6}$	$4 \cdot 10^{-13}$	$7.3 \cdot 10^{-7}$
$\gamma\gamma$ [pb]	$6.3 \cdot 10^{-7}$	$1.6 \cdot 10^{-6}$	$8.8 \cdot 10^{-10}$	$7.2 \cdot 10^{-10}$	$7.4 \cdot 10^{-11}$	$6 \cdot 10^{-11}$

Table 23: Benchmark points for different $\mathcal{Z}_N \times \mathcal{Z}_M$ flavor symmetries for inclusive flavon production channels with low flavon mass (m_a) in case of the symmetry-conserving scenario at the 27 TeV HE-LHC.

m_a [GeV]	Benchmark $\mathcal{Z}_2 \times \mathcal{Z}_5$		Benchmark $\mathcal{Z}_2 \times \mathcal{Z}_9$		Benchmark $\mathcal{Z}_2 \times \mathcal{Z}_{11}$	
	20	60	20	60	20	60
$\tau\tau$ [pb]	$2.7 \cdot 10^{-10}$	$2.8 \cdot 10^{-3}$	$4.9 \cdot 10^{-11}$	$1.9 \cdot 10^{-5}$	$1.1 \cdot 10^{-12}$	$3 \cdot 10^{-6}$
$\gamma\gamma$ [pb]	$1.7 \cdot 10^{-6}$	$4.9 \cdot 10^{-6}$	$2.8 \cdot 10^{-9}$	$2.9 \cdot 10^{-9}$	$2.4 \cdot 10^{-10}$	$2.5 \cdot 10^{-10}$

Table 24: Benchmark points for different $\mathcal{Z}_N \times \mathcal{Z}_M$ flavor symmetries for inclusive flavon production channels with low flavon mass (m_a) in case of the symmetry-conserving scenario at a 100 TeV collider.

6.3.2 Associative production

We notice that there are other channels through which flavon can be produced, as shown in figure 25. For instance, the following associated production processes can be used to produce the flavon,

$$bg \rightarrow ba, ug, cg \rightarrow ta, b\bar{b}a \rightarrow b\bar{b}\tau^+\tau^-, t\bar{t}a \rightarrow t\bar{t}t\bar{t}, \quad (86)$$

where the first process undergoes through the flavor-diagonal coupling of the flavon to the $b\bar{b}$, and the second process occurs through the flavor-violating flavon-quark coupling.

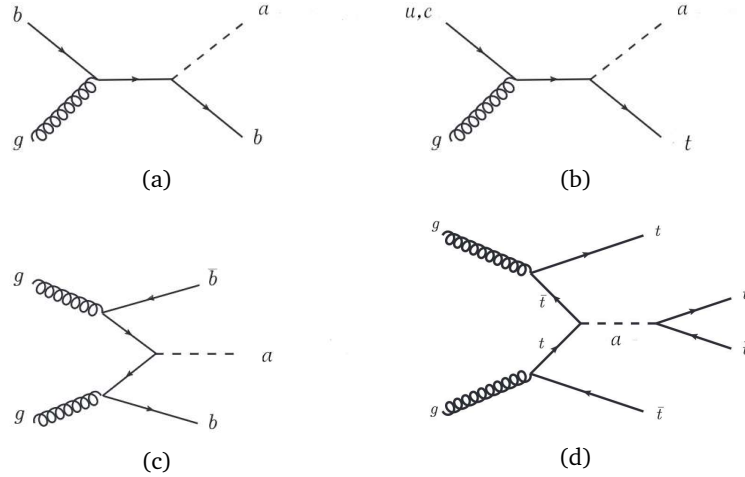


Figure 25: Feynman diagrams for the production of the flavon through different associative channels.

The cross-sections of different associative production channels are also shown in figures 26 and 27. We observe that the production cross sections are, in general, smaller for the soft symmetry-breaking as well as symmetry-conserving scenarios, and can be relatively large only for low flavon mass.

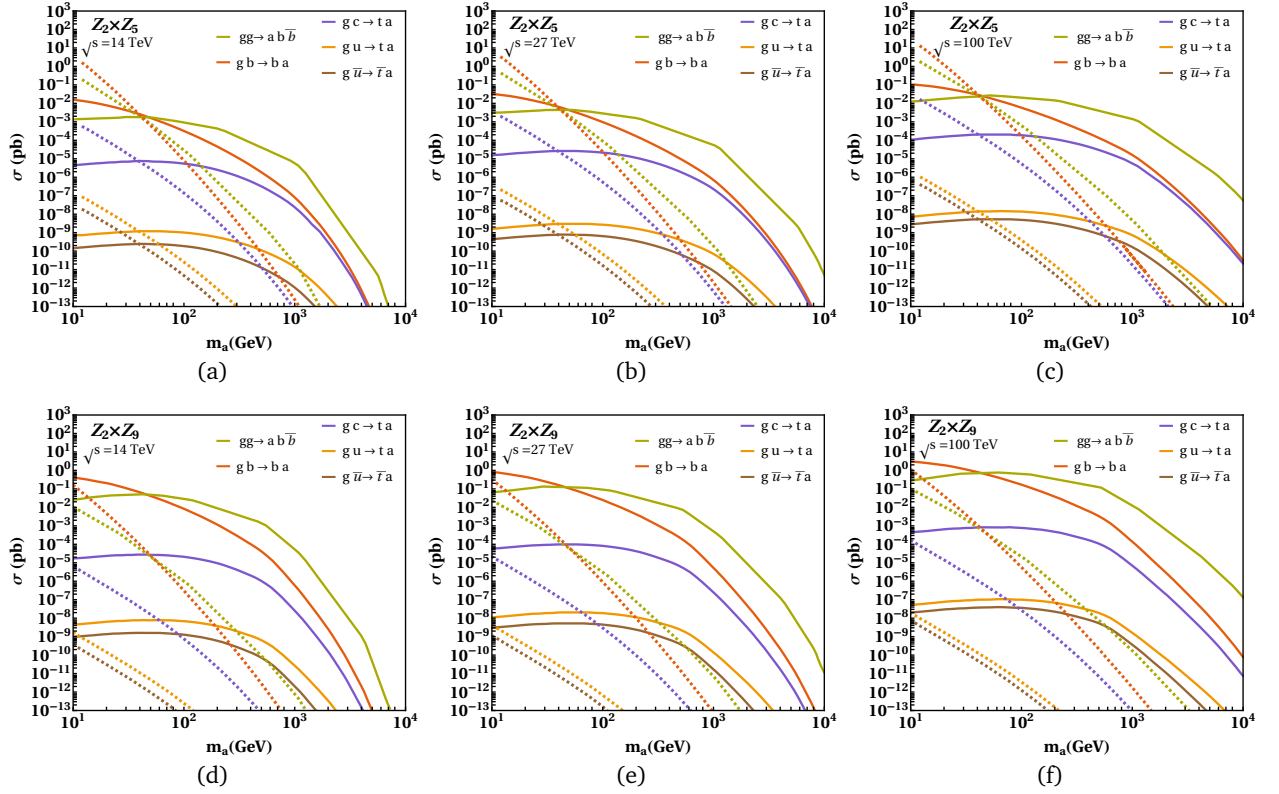


Figure 26: Production cross-sections of the flavon of $\mathcal{Z}_2 \times \mathcal{Z}_5$, and $\mathcal{Z}_2 \times \mathcal{Z}_9$ flavor symmetries with respect to its mass through different channels for 14 TeV HL-LHC, 27 TeV HE-LHC and future 100 TeV collider. The solid lines represents the production cross section along the boundaries of parameter space allowed by the observable $R_{\mu\mu}$ for soft symmetry-breaking scenario, while the dashed lines correspond to that in the symmetry-conserving scenario along the allowed parameter space by the observable $BR(K_L \rightarrow \mu\mu)_{SD}$.

The process $t\bar{t}a \rightarrow t\bar{t}t\bar{t}$ can occur only for the $\mathcal{Z}_8 \times \mathcal{Z}_{22}$ flavor symmetry where the flavor-diagonal coupling of the flavon to top quarks is allowed. This results in a relatively large cross-section involving $t\bar{t}$ channels. Thus, the $\mathcal{Z}_8 \times \mathcal{Z}_{22}$ flavor symmetry is very special in this sense.

As noticed in the case of inclusive production of the heavy flavon mass, we observe from figures 28 and 29 that the associative production cross-sections of the flavon of different $\mathcal{Z}_N \times \mathcal{Z}_M$ flavor symmetries for the VEV $f = 500$ GeV for the soft symmetry-breaking scenario can be sufficiently large. Therefore, we continue to use this choice even for the associative production of the heavy flavon of different $\mathcal{Z}_N \times \mathcal{Z}_M$ flavor symmetries.

m_a [GeV]	$\mathcal{L}[fb^{-1}]$ [References]		ATLAS 13 TeV		CMS 13 TeV	
	ATLAS	CMS	500	1000	500	1000
$t\bar{t}a \rightarrow t\bar{t}t\bar{t}$ [pb]	139 [148]	137 [149]	$1 \cdot 10^{-2}$	$6 \cdot 10^{-3}$	$2 \cdot 10^{-2}$	
$gg \rightarrow ab\bar{b} \rightarrow \tau\tau b\bar{b}$ [pb]	36.1 [133]	35.9 [134]	$8 \cdot 10^{-2}$	$9 \cdot 10^{-3}$	$6 \cdot 10^{-2}$	$1 \cdot 10^{-2}$
$gb \rightarrow ab \rightarrow \tau\tau b$ [pb]	36.1 [133]	35.9 [134]	$3 \cdot 10^{-2}$	$4 \cdot 10^{-3}$	$3 \cdot 10^{-2}$	$4 \cdot 10^{-3}$

Table 25: Current limits of $\sigma \times BR$ at 13 TeV LHC by ATLAS and CMS in resonance searches for associative flavon production channels.

The present reach of the LHC for the associative production channels is shown in table 25. We show the sensitivities of these modes at the HL-LHC, HE-LHC, and a 100 TeV collider in table 26. Our benchmark predictions for different $\mathcal{Z}_N \times \mathcal{Z}_M$ flavor symmetries, are given in tables 27- 29 for the soft symmetry-breaking scenario.

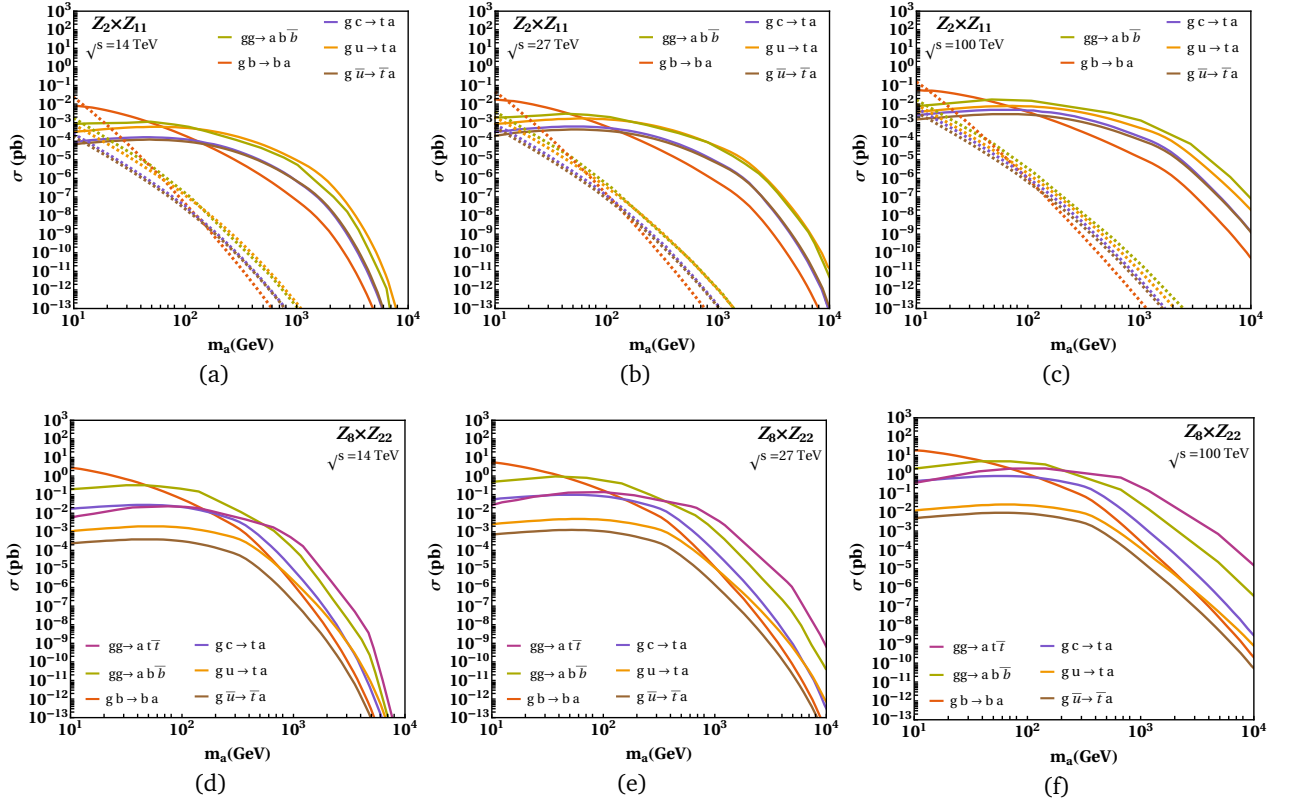


Figure 27: Production cross-sections of the flavon of $\mathcal{Z}_2 \times \mathcal{Z}_{11}$, and $\mathcal{Z}_8 \times \mathcal{Z}_{22}$ flavor symmetries with respect to its mass through different channels for 14 TeV HL-LHC, 27 TeV HE-LHC and future 100 TeV collider. The solid lines represents the production cross section along the boundaries of parameter space allowed by the observable $R_{\mu\mu}$ for soft symmetry-breaking scenario, while the dashed lines correspond to that in the symmetry-conserving scenario along the allowed parameter space by the observable $BR(K_L \rightarrow \mu\mu)_{SD}$.

m_a [GeV]	HL-LHC [14 TeV, 3 ab ⁻¹]		HE-LHC [27 TeV, 15 ab ⁻¹]		100 TeV, 30 ab ⁻¹	
	500	1000	500	1000	500	1000
$t\bar{t}a \rightarrow t\bar{t}t\bar{t}$ [pb]	$2 \cdot 10^{-3}$	$1 \cdot 10^{-3}$	$3 \cdot 10^{-3}$	$2 \cdot 10^{-3}$	$1 \cdot 10^{-2}$	$9 \cdot 10^{-3}$
$gg \rightarrow ab\bar{b} \rightarrow \tau\tau b\bar{b}$ [pb]	$7 \cdot 10^{-3}$	$1 \cdot 10^{-3}$	$5 \cdot 10^{-3}$	$8 \cdot 10^{-4}$	$8 \cdot 10^{-3}$	$1 \cdot 10^{-3}$
$gb \rightarrow ab \rightarrow \tau\tau b$ [pb]	$3 \cdot 10^{-3}$	$5 \cdot 10^{-4}$	$2 \cdot 10^{-3}$	$3 \cdot 10^{-4}$	$4 \cdot 10^{-3}$	$5 \cdot 10^{-4}$

Table 26: Estimated reach ($\sigma \times BR$) of HL-LHC, HE-LHC and the 100 TeV collider for high flavon mass (m_a) in associative flavon production channels.

We observe from table 27 that only the mode $t\bar{t}a \rightarrow t\bar{t}t\bar{t}$ is within the reach of the HL-LHC for the flavon mass $m_a = 500$ GeV for the $\mathcal{Z}_8 \times \mathcal{Z}_{22}$ flavor symmetry. This scenario improves slightly at the HE-LHC and at a 100 TeV collider for the $\mathcal{Z}_8 \times \mathcal{Z}_{22}$ flavor symmetry such that the flavon mass $m_a = 1000$ GeV becomes also accessible. The symmetry-conserving scenario remains beyond the reach of the HL-LHC, HE-LHC and a 100 TeV collider for the associative production modes. Therefore, we do not discuss it anymore in this case.

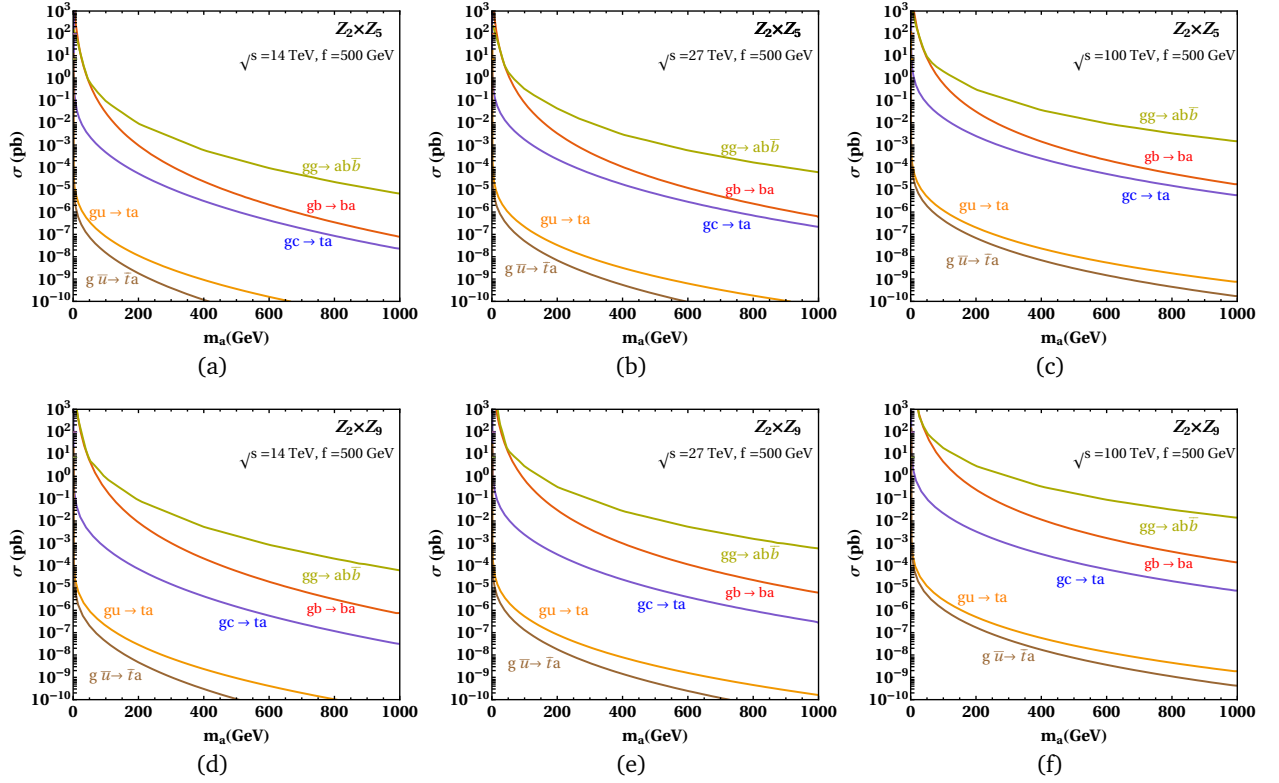


Figure 28: Production cross-sections of the flavon of $\mathcal{Z}_2 \times \mathcal{Z}_5$, and $\mathcal{Z}_2 \times \mathcal{Z}_9$ flavor symmetries with respect to its mass through different channels for 14 TeV HL-LHC, 27 TeV HE-LHC, and future 100 TeV hadron collider, where the flavon VEV $f = 500$ GeV.

m_a [GeV]	Benchmark $\mathcal{Z}_2 \times \mathcal{Z}_5$		Benchmark $\mathcal{Z}_2 \times \mathcal{Z}_9$		Benchmark $\mathcal{Z}_2 \times \mathcal{Z}_{11}$		Benchmark $\mathcal{Z}_8 \times \mathcal{Z}_{22}$	
	500	1000	500	1000	500	1000	500	1000
$t\bar{t}a \rightarrow t\bar{t}t\bar{t}$ [pb]							$1.6 \cdot 10^{-3}$	$1.6 \cdot 10^{-4}$
$gg \rightarrow ab\bar{b} \rightarrow \tau\tau b\bar{b}$ [pb]	$6 \cdot 10^{-7}$	$1.8 \cdot 10^{-8}$	$1 \cdot 10^{-4}$	$3.2 \cdot 10^{-6}$	$3.4 \cdot 10^{-5}$	$8.9 \cdot 10^{-7}$	$1.6 \cdot 10^{-6}$	$3.2 \cdot 10^{-8}$
$gb \rightarrow ab \rightarrow \tau\tau b$ [pb]	$1.7 \cdot 10^{-7}$	$5.6 \cdot 10^{-9}$	$2.9 \cdot 10^{-5}$	$9.7 \cdot 10^{-7}$	$9.4 \cdot 10^{-6}$	$2.7 \cdot 10^{-7}$	$4.5 \cdot 10^{-7}$	$9.7 \cdot 10^{-9}$

Table 27: Benchmark points for different $\mathcal{Z}_N \times \mathcal{Z}_M$ flavor symmetries for associative flavon production channels with high flavon mass (m_a) in case of the soft symmetry-breaking at the 14 TeV HL-LHC, assuming $f = 500$ GeV.

m_a [GeV]	Benchmark $\mathcal{Z}_2 \times \mathcal{Z}_5$		Benchmark $\mathcal{Z}_2 \times \mathcal{Z}_9$		Benchmark $\mathcal{Z}_2 \times \mathcal{Z}_{11}$		Benchmark $\mathcal{Z}_8 \times \mathcal{Z}_{22}$	
	500	1000	500	1000	500	1000	500	1000
$t\bar{t}a \rightarrow t\bar{t}t\bar{t}$ [pb]							$1.5 \cdot 10^{-2}$	$2.3 \cdot 10^{-3}$
$gg \rightarrow ab\bar{b} \rightarrow \tau\tau b\bar{b}$ [pb]	$3.3 \cdot 10^{-6}$	$1.6 \cdot 10^{-7}$	$5.8 \cdot 10^{-4}$	$2.8 \cdot 10^{-5}$	$1.9 \cdot 10^{-4}$	$7.9 \cdot 10^{-6}$	$9 \cdot 10^{-6}$	$2.8 \cdot 10^{-7}$
$gb \rightarrow ab \rightarrow \tau\tau b$ [pb]	$9.3 \cdot 10^{-7}$	$5.1 \cdot 10^{-8}$	$1.6 \cdot 10^{-4}$	$8.8 \cdot 10^{-6}$	$5.3 \cdot 10^{-5}$	$2.5 \cdot 10^{-6}$	$2.5 \cdot 10^{-6}$	$8.8 \cdot 10^{-8}$

Table 28: Benchmark points for different $\mathcal{Z}_N \times \mathcal{Z}_M$ flavor symmetries for associative flavon production channels with high flavon mass (m_a) in case of the soft symmetry-breaking at the 27 TeV HE-LHC, assuming $f = 500$ GeV.

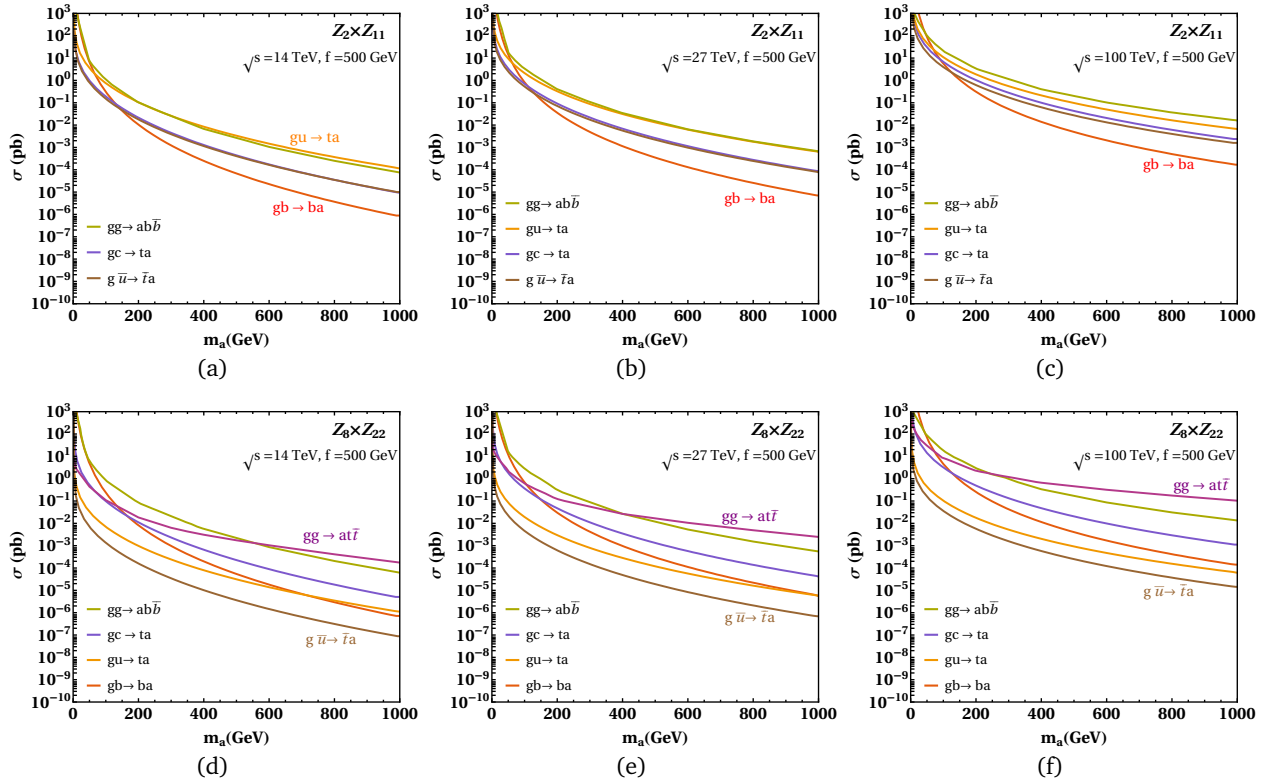


Figure 29: Production cross-sections of the flavon of $\mathcal{Z}_2 \times \mathcal{Z}_{11}$, and $\mathcal{Z}_8 \times \mathcal{Z}_{22}$ flavor symmetries with respect to its mass through different channels for 14 TeV HL-LHC, 27 TeV HE-LHC, and future 100 TeV hadron collider, where the flavon VEV $f = 500$ GeV.

m_a [GeV]	Benchmark $\mathcal{Z}_2 \times \mathcal{Z}_5$		Benchmark $\mathcal{Z}_2 \times \mathcal{Z}_9$		Benchmark $\mathcal{Z}_2 \times \mathcal{Z}_{11}$		Benchmark $\mathcal{Z}_8 \times \mathcal{Z}_{22}$	
	500	1000	500	1000	500	1000	500	1000
$t\bar{t}a \rightarrow t\bar{t}t\bar{t}$ [pb]							0.41	$9.6 \cdot 10^{-2}$
$gg \rightarrow ab\bar{b} \rightarrow \tau\tau b\bar{b}$ [pb]	$4.7 \cdot 10^{-5}$	$4.0 \cdot 10^{-6}$	$8.2 \cdot 10^{-3}$	$6.9 \cdot 10^{-4}$	$2.7 \cdot 10^{-3}$	$1.9 \cdot 10^{-4}$	$1.3 \cdot 10^{-4}$	$6.8 \cdot 10^{-6}$
$gb \rightarrow ab \rightarrow \tau\tau b$ [pb]	$1.34 \cdot 10^{-5}$	$1.23 \cdot 10^{-6}$	$2.3 \cdot 10^{-3}$	$2.1 \cdot 10^{-4}$	$7.5 \cdot 10^{-4}$	$6.0 \cdot 10^{-5}$	$3.6 \cdot 10^{-5}$	$2.1 \cdot 10^{-6}$

Table 29: Benchmark points for different $\mathcal{Z}_N \times \mathcal{Z}_M$ flavor symmetries for associative flavon production channels with high flavon mass (m_a) in case of the soft symmetry-breaking scenario at a 100 TeV collider, assuming $f = 500$ GeV.

6.3.3 Di-flavon production

In this section, we discuss the production of di-flavon, which is an important mode to explore the flavon physics of different $\mathcal{Z}_N \times \mathcal{Z}_M$ flavor symmetries. We show the present LHC sensitivities of di-flavon channels in table 30. The reach of the HL-LHC, HE-LHC and a 100 TeV collider is given in table 31. The di-flavon production cross-sections for different $\mathcal{Z}_N \times \mathcal{Z}_M$ flavor symmetries are shown in figure 30 in the case of soft symmetry-breaking scenario.

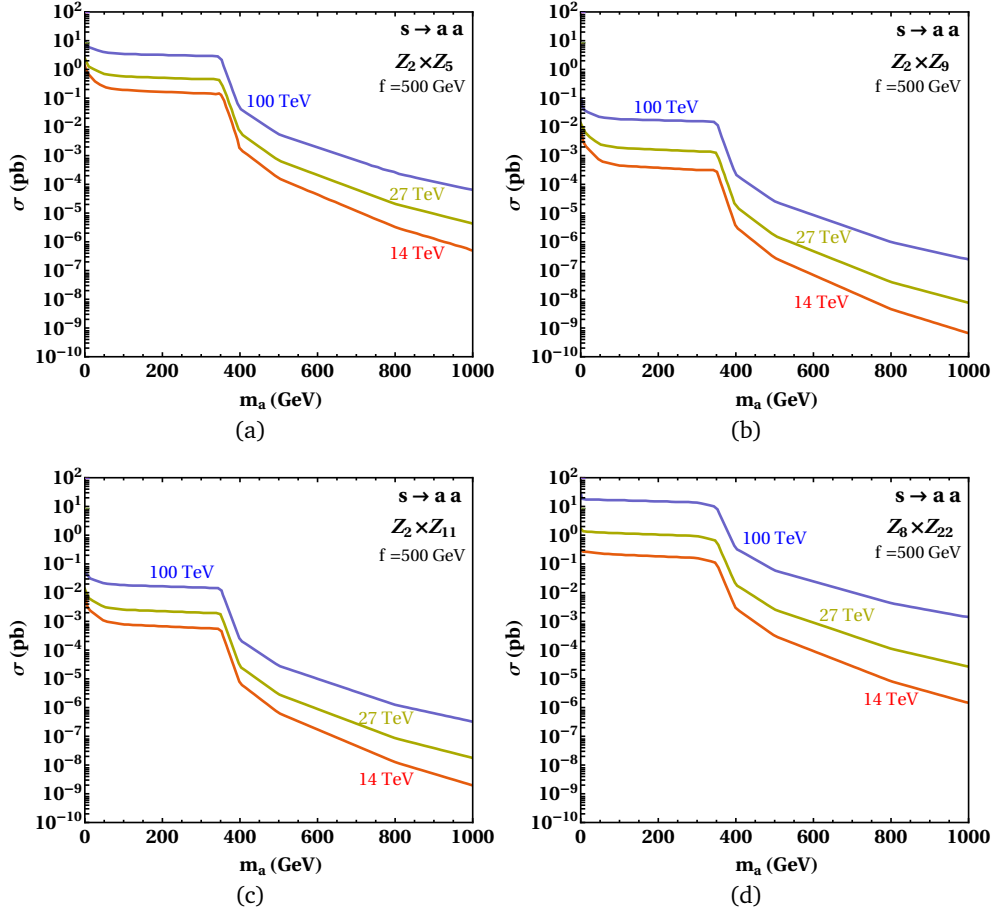


Figure 30: Production cross-sections of the di-flavon in $\mathcal{Z}_2 \times \mathcal{Z}_5$, $\mathcal{Z}_2 \times \mathcal{Z}_9$, $\mathcal{Z}_2 \times \mathcal{Z}_{11}$, and $\mathcal{Z}_8 \times \mathcal{Z}_{22}$ flavor symmetries with respect to its mass for 14 TeV HL-LHC, 27 TeV HE-LHC, and 100 TeV hadron collider, where the flavon VEV $f = 500$ GeV.

The benchmark predictions for different $\mathcal{Z}_N \times \mathcal{Z}_M$ flavor symmetries, are given in tables 32- 34 for the soft symmetry-breaking scenario and heavy flavon masses. We observe from tables 32- 34 that the di-flavon production for heavy flavon mass is insensitive to the HL-LHC, HE-LHC and even to a 100 TeV collider for all $\mathcal{Z}_N \times \mathcal{Z}_M$ flavor symmetries.

m_a [GeV]	$\mathcal{L}[fb^{-1}]$ [References]		ATLAS 13 TeV		CMS 13 TeV	
	ATLAS	CMS	500	1000	500	1000
$s \rightarrow aa \rightarrow b\bar{b}\ell\ell$ [pb]	36.1 [150]	19.7 [151] ^a	$2 \cdot 10^{-2}$	$1 \cdot 10^{-2}$	$2 \cdot 10^{-1}$	$2 \cdot 10^{-2}$
$s \rightarrow aa \rightarrow b\bar{b}b\bar{b}$ [pb]	36.1 [152]	35.9 [153]	$4 \cdot 10^{-2}$	$9 \cdot 10^{-3}$	$7 \cdot 10^{-2}$	$1 \cdot 10^{-2}$

^aThe reference [151] is at $\sqrt{s} = 8$ TeV.

Table 30: Current limits of $\sigma \times BR$ at 13 TeV LHC by ATLAS and CMS in high mass resonance searches for di-flavon production channels.

m_a [GeV]	HL-LHC [14 TeV, 3 ab ⁻¹]		HE-LHC [27 TeV, 15 ab ⁻¹]		100 TeV, 30 ab ⁻¹	
	500	1000	500	1000	500	1000
$s \rightarrow aa \rightarrow b\bar{b}\tau\tau$ [pb]	$2 \cdot 10^{-3}$	$1 \cdot 10^{-3}$	$2 \cdot 10^{-3}$	$8 \cdot 10^{-4}$	$3 \cdot 10^{-3}$	$1 \cdot 10^{-3}$
$s \rightarrow aa \rightarrow b\bar{b}b\bar{b}$ [pb]	$5 \cdot 10^{-3}$	$1 \cdot 10^{-3}$	$3 \cdot 10^{-3}$	$7 \cdot 10^{-4}$	$5 \cdot 10^{-3}$	$1 \cdot 10^{-3}$

Table 31: Estimated reach ($\sigma \times BR$) of HL-LHC, HE-LHC and the 100 TeV collider for high flavon mass (m_a) in di-flavon production channels.

m_a [GeV]	Benchmark $\mathcal{Z}_2 \times \mathcal{Z}_5$		Benchmark $\mathcal{Z}_2 \times \mathcal{Z}_9$		Benchmark $\mathcal{Z}_2 \times \mathcal{Z}_{11}$		Benchmark $\mathcal{Z}_8 \times \mathcal{Z}_{22}$	
	500	1000	500	1000	500	1000	500	1000
$s \rightarrow aa \rightarrow b\bar{b}\tau\tau$ [pb]	$1.4 \cdot 10^{-8}$	$4.4 \cdot 10^{-11}$	$7 \cdot 10^{-9}$	$1.7 \cdot 10^{-11}$	$7.5 \cdot 10^{-10}$	$1.7 \cdot 10^{-12}$	$2 \cdot 10^{-9}$	$3.7 \cdot 10^{-12}$
$s \rightarrow aa \rightarrow b\bar{b}\mu\mu$ [pb]	$1.3 \cdot 10^{-11}$	$4 \cdot 10^{-14}$	$1.5 \cdot 10^{-10}$	$3.6 \cdot 10^{-13}$	$5.8 \cdot 10^{-12}$	$1.3 \cdot 10^{-14}$	$1.8 \cdot 10^{-11}$	$3.2 \cdot 10^{-14}$
$s \rightarrow aa \rightarrow b\bar{b}b\bar{b}$ [pb]	$4 \cdot 10^{-8}$	$1.3 \cdot 10^{-10}$	$1.8 \cdot 10^{-8}$	$4.3 \cdot 10^{-11}$	$1.1 \cdot 10^{-9}$	$2.6 \cdot 10^{-12}$	$4.9 \cdot 10^{-9}$	$9.1 \cdot 10^{-12}$

Table 32: Benchmark points for different $\mathcal{Z}_N \times \mathcal{Z}_M$ flavor symmetries for di-flavon production channels with high flavon mass (m_a) in case of the soft symmetry-breaking scenario at the 14 TeV HL-LHC, assuming $f = 500$ GeV.

m_a [GeV]	Benchmark $\mathcal{Z}_2 \times \mathcal{Z}_5$		Benchmark $\mathcal{Z}_2 \times \mathcal{Z}_9$		Benchmark $\mathcal{Z}_2 \times \mathcal{Z}_{11}$		Benchmark $\mathcal{Z}_8 \times \mathcal{Z}_{22}$	
	500	1000	500	1000	500	1000	500	1000
$s \rightarrow aa \rightarrow b\bar{b}\tau\tau$ [pb]	$5.9 \cdot 10^{-8}$	$3.7 \cdot 10^{-10}$	$4.2 \cdot 10^{-8}$	$1.9 \cdot 10^{-10}$	$3.4 \cdot 10^{-9}$	$1.5 \cdot 10^{-11}$	$1.6 \cdot 10^{-8}$	$6.9 \cdot 10^{-11}$
$s \rightarrow aa \rightarrow b\bar{b}\mu\mu$ [pb]	$5.3 \cdot 10^{-11}$	$3.4 \cdot 10^{-13}$	$9.1 \cdot 10^{-10}$	$4.2 \cdot 10^{-12}$	$2.6 \cdot 10^{-11}$	$1.2 \cdot 10^{-13}$	$1.4 \cdot 10^{-10}$	$5.9 \cdot 10^{-13}$
$s \rightarrow aa \rightarrow b\bar{b}b\bar{b}$ [pb]	$1.7 \cdot 10^{-7}$	$1.1 \cdot 10^{-9}$	$1.1 \cdot 10^{-7}$	$4.9 \cdot 10^{-10}$	$5.1 \cdot 10^{-9}$	$2.3 \cdot 10^{-11}$	$4 \cdot 10^{-8}$	$1.7 \cdot 10^{-10}$

Table 33: Benchmark points for different $\mathcal{Z}_N \times \mathcal{Z}_M$ flavor symmetries for di-flavon production channels with high flavon mass (m_a) in case of the soft symmetry-breaking scenario at the 27 TeV HE-LHC, assuming $f = 500$ GeV.

m_a [GeV]	Benchmark $\mathcal{Z}_2 \times \mathcal{Z}_5$		Benchmark $\mathcal{Z}_2 \times \mathcal{Z}_9$		Benchmark $\mathcal{Z}_2 \times \mathcal{Z}_{11}$		Benchmark $\mathcal{Z}_8 \times \mathcal{Z}_{22}$	
	500	1000	500	1000	500	1000	500	1000
$s \rightarrow aa \rightarrow b\bar{b}\tau\tau$ [pb]	$4.8 \cdot 10^{-7}$	$5.5 \cdot 10^{-9}$	$6.5 \cdot 10^{-7}$	$6.2 \cdot 10^{-9}$	$3.3 \cdot 10^{-8}$	$2.8 \cdot 10^{-10}$	$3.7 \cdot 10^{-7}$	$3.5 \cdot 10^{-9}$
$s \rightarrow aa \rightarrow b\bar{b}\mu\mu$ [pb]	$4.2 \cdot 10^{-10}$	$4.9 \cdot 10^{-12}$	$1.4 \cdot 10^{-8}$	$1.3 \cdot 10^{-10}$	$2.5 \cdot 10^{-10}$	$2.2 \cdot 10^{-12}$	$3.2 \cdot 10^{-9}$	$3.1 \cdot 10^{-11}$
$s \rightarrow aa \rightarrow b\bar{b}b\bar{b}$ [pb]	$1.4 \cdot 10^{-6}$	$1.6 \cdot 10^{-8}$	$1.7 \cdot 10^{-6}$	$1.6 \cdot 10^{-8}$	$5 \cdot 10^{-8}$	$4.3 \cdot 10^{-10}$	$9.1 \cdot 10^{-7}$	$8.6 \cdot 10^{-9}$

Table 34: Benchmark points for different $\mathcal{Z}_N \times \mathcal{Z}_M$ flavor symmetries for di-flavon production channels with high flavon mass (m_a) in case of the soft symmetry-breaking scenario at a 100 TeV collider, assuming $f = 500$ GeV.

We observed earlier that the di-flavon production of a heavy mass flavon is beyond the reach of HL-LHC, HE-LHC, and a 100 TeV collider for different $\mathcal{Z}_N \times \mathcal{Z}_M$ flavor symmetries. However, this scenario changes in the case of a light flavon. We show the present sensitivities of the light di-flavon searches of the LHC in table 35. The sensitivities of the HL-LHC, HE-LHC, and a 100 TeV collider for a light di-flavon productions are shown in table 36.

m_a [GeV]	$\mathcal{L}[fb^{-1}]$ [References]		ATLAS 13 TeV		CMS 13 TeV	
	ATLAS	CMS	20	60	20	60
$s \rightarrow aa \rightarrow b\bar{b}\ell\ell$ [pb]	139 [154]	138 [155]	$1 \cdot 10^{-4}$	$1 \cdot 10^{-4}$	$9 \cdot 10^{-5}$	$8 \cdot 10^{-5}$
$s \rightarrow aa \rightarrow b\bar{b}b\bar{b}$ [pb]	36.1 [156]	138 [157]	3	1	1	$3 \cdot 10^{-1}$

Table 35: Current limits of $\sigma \times BR$ at 13 TeV LHC by ATLAS and CMS in low mass resonance searches for di-flavon channels.

m_a [GeV]	HL-LHC [14 TeV, 3 ab $^{-1}$]		HE-LHC [27 TeV, 15 ab $^{-1}$]		100 TeV, 30 ab $^{-1}$	
	20	60	20	60	20	60
$s \rightarrow aa \rightarrow b\bar{b}\ell\ell$ [pb]	$2 \cdot 10^{-5}$	$2 \cdot 10^{-5}$	$1 \cdot 10^{-5}$	$1 \cdot 10^{-5}$	$2 \cdot 10^{-5}$	$2 \cdot 10^{-5}$
$s \rightarrow aa \rightarrow b\bar{b}b\bar{b}$ [pb]	0.2	$7 \cdot 10^{-2}$	0.16	$5 \cdot 10^{-2}$	0.2	$7 \cdot 10^{-2}$

Table 36: Estimated reach ($\sigma \times BR$) of HL-LHC, HE-LHC and the 100 TeV collider for low flavon mass (m_a) in di-flavon production channels.

We show our benchmark predictions of di-flavon production cross-sections in tables 37-39 for low flavon masses in the soft symmetry-breaking scenario. We observe that $aa \rightarrow b\bar{b}\tau\tau$ mode is accessible for all $\mathcal{Z}_N \times \mathcal{Z}_M$ flavor symmetries at the HL-LHC, HE-LHC, and a 100 TeV collider. All three channels are sensitive to the HL-LHC, HE-LHC, and a 100 TeV collider only for the $\mathcal{Z}_8 \times \mathcal{Z}_{22}$ flavor symmetry. The production cross-sections in the symmetry-conserving scenario are too small to be under the reach of any collider, as observed in tables 40-42.

m_a [GeV]	Benchmark $\mathcal{Z}_2 \times \mathcal{Z}_5$		Benchmark $\mathcal{Z}_2 \times \mathcal{Z}_9$		Benchmark $\mathcal{Z}_2 \times \mathcal{Z}_{11}$		Benchmark $\mathcal{Z}_8 \times \mathcal{Z}_{22}$	
	20	60	20	60	20	60	20	60
$s \rightarrow aa \rightarrow b\bar{b}\tau\tau$ [pb]	$2.7 \cdot 10^{-5}$	$1.9 \cdot 10^{-5}$	$3.2 \cdot 10^{-5}$	$1.5 \cdot 10^{-5}$	$3.3 \cdot 10^{-5}$	$2 \cdot 10^{-5}$	$1.8 \cdot 10^{-2}$	$1.6 \cdot 10^{-2}$
$s \rightarrow aa \rightarrow b\bar{b}\mu\mu$ [pb]	$2.5 \cdot 10^{-8}$	$1.7 \cdot 10^{-8}$	$7.2 \cdot 10^{-7}$	$3.3 \cdot 10^{-7}$	$2.7 \cdot 10^{-7}$	$1.5 \cdot 10^{-7}$	$1.6 \cdot 10^{-4}$	$1.3 \cdot 10^{-4}$
$s \rightarrow aa \rightarrow b\bar{b}b\bar{b}$ [pb]	$6.8 \cdot 10^{-5}$	$5.4 \cdot 10^{-5}$	$6.1 \cdot 10^{-5}$	$3.7 \cdot 10^{-5}$	$4.1 \cdot 10^{-5}$	$2.9 \cdot 10^{-5}$	$3.6 \cdot 10^{-2}$	$3.7 \cdot 10^{-2}$

Table 37: Benchmark points for different $\mathcal{Z}_N \times \mathcal{Z}_M$ flavor symmetries for di-flavon production channels with low flavon mass (m_a) in case of the soft symmetry-breaking scenario at the 14 TeV HL-LHC, assuming $f = 500$ GeV.

m_a [GeV]	Benchmark $\mathcal{Z}_2 \times \mathcal{Z}_5$		Benchmark $\mathcal{Z}_2 \times \mathcal{Z}_9$		Benchmark $\mathcal{Z}_2 \times \mathcal{Z}_{11}$		Benchmark $\mathcal{Z}_8 \times \mathcal{Z}_{22}$	
	20	60	20	60	20	60	20	60
$s \rightarrow aa \rightarrow b\bar{b}\tau\tau$ [pb]	$6.8 \cdot 10^{-5}$	$5.5 \cdot 10^{-5}$	$9.5 \cdot 10^{-5}$	$5.8 \cdot 10^{-5}$	$8.9 \cdot 10^{-5}$	$6.1 \cdot 10^{-5}$	$8.8 \cdot 10^{-2}$	$8.1 \cdot 10^{-2}$
$s \rightarrow aa \rightarrow b\bar{b}\mu\mu$ [pb]	$6.4 \cdot 10^{-8}$	$5 \cdot 10^{-8}$	$2.2 \cdot 10^{-6}$	$1.3 \cdot 10^{-6}$	$7.1 \cdot 10^{-7}$	$4.7 \cdot 10^{-7}$	$8 \cdot 10^{-4}$	$7 \cdot 10^{-4}$
$s \rightarrow aa \rightarrow b\bar{b}b\bar{b}$ [pb]	$1.7 \cdot 10^{-4}$	$1.6 \cdot 10^{-4}$	$1.8 \cdot 10^{-4}$	$1.4 \cdot 10^{-4}$	$1.1 \cdot 10^{-4}$	$9.2 \cdot 10^{-5}$	0.18	0.19

Table 38: Benchmark points for different $\mathcal{Z}_N \times \mathcal{Z}_M$ flavor symmetries for di-flavon production channels with low flavon mass (m_a) in case of the soft symmetry-breaking scenario at the 27 TeV HE-LHC, assuming $f = 500$ GeV.

m_a [GeV]	Benchmark $\mathcal{Z}_2 \times \mathcal{Z}_5$		Benchmark $\mathcal{Z}_2 \times \mathcal{Z}_9$		Benchmark $\mathcal{Z}_2 \times \mathcal{Z}_{11}$		Benchmark $\mathcal{Z}_8 \times \mathcal{Z}_{22}$	
	20	60	20	60	20	60	20	60
$s \rightarrow aa \rightarrow b\bar{b}\tau\tau$ [pb]	$3.5 \cdot 10^{-4}$	$3.2 \cdot 10^{-4}$	$6.9 \cdot 10^{-4}$	$5.5 \cdot 10^{-4}$	$5.2 \cdot 10^{-4}$	$4.2 \cdot 10^{-4}$	1.17	1.11
$s \rightarrow aa \rightarrow b\bar{b}\mu\mu$ [pb]	$3.3 \cdot 10^{-7}$	$2.9 \cdot 10^{-7}$	$1.6 \cdot 10^{-5}$	$1.2 \cdot 10^{-5}$	$4.2 \cdot 10^{-6}$	$3.2 \cdot 10^{-6}$	$1.1 \cdot 10^{-2}$	$9.7 \cdot 10^{-3}$
$s \rightarrow aa \rightarrow b\bar{b}b\bar{b}$ [pb]	$8.8 \cdot 10^{-4}$	$9.2 \cdot 10^{-4}$	$1.3 \cdot 10^{-3}$	$1.3 \cdot 10^{-3}$	$6.4 \cdot 10^{-4}$	$6.3 \cdot 10^{-4}$	2.35	2.65

Table 39: Benchmark points for different $\mathcal{Z}_N \times \mathcal{Z}_M$ flavor symmetries for di-flavon production channels with low flavon mass (m_a) in case of the soft symmetry-breaking scenario at a 100 TeV collider, assuming $f = 500$ GeV.

m_a [GeV]	Benchmark $\mathcal{Z}_2 \times \mathcal{Z}_5$		Benchmark $\mathcal{Z}_2 \times \mathcal{Z}_9$		Benchmark $\mathcal{Z}_2 \times \mathcal{Z}_{11}$	
	20	60	20	60	20	60
$s \rightarrow aa \rightarrow b\bar{b}\tau\tau$ [pb]	$8.7 \cdot 10^{-10}$	$3.5 \cdot 10^{-12}$	$1.9 \cdot 10^{-14}$	$5.4 \cdot 10^{-17}$	$3.4 \cdot 10^{-16}$	$1.1 \cdot 10^{-18}$
$s \rightarrow aa \rightarrow b\bar{b}\mu\mu$ [pb]	$8.2 \cdot 10^{-13}$	$3.2 \cdot 10^{-15}$	$4.2 \cdot 10^{-16}$	$1.2 \cdot 10^{-18}$	$2.7 \cdot 10^{-18}$	$8.8 \cdot 10^{-21}$
$s \rightarrow aa \rightarrow b\bar{b}b\bar{b}$ [pb]	$2.2 \cdot 10^{-9}$	$1 \cdot 10^{-11}$	$3.6 \cdot 10^{-14}$	$1.3 \cdot 10^{-16}$	$4.2 \cdot 10^{-16}$	$1.7 \cdot 10^{-18}$

Table 40: Benchmark points for different $\mathcal{Z}_N \times \mathcal{Z}_M$ flavor symmetries for di-flavon production channels with low flavon mass (m_a) in case of the symmetry-conserving scenario at the 14 TeV HL-LHC.

m_a [GeV]	Benchmark $\mathcal{Z}_2 \times \mathcal{Z}_5$		Benchmark $\mathcal{Z}_2 \times \mathcal{Z}_9$		Benchmark $\mathcal{Z}_2 \times \mathcal{Z}_{11}$	
	20	60	20	60	20	60
$s \rightarrow aa \rightarrow b\bar{b}\tau\tau$ [pb]	$1.9 \cdot 10^{-9}$	$8.8 \cdot 10^{-12}$	$4.7 \cdot 10^{-14}$	$1.6 \cdot 10^{-16}$	$7.7 \cdot 10^{-16}$	$3 \cdot 10^{-18}$
$s \rightarrow aa \rightarrow b\bar{b}\mu\mu$ [pb]	$1.8 \cdot 10^{-12}$	$7.9 \cdot 10^{-15}$	$1.1 \cdot 10^{-15}$	$3.6 \cdot 10^{-18}$	$6.2 \cdot 10^{-18}$	$2.3 \cdot 10^{-20}$
$s \rightarrow aa \rightarrow b\bar{b}b\bar{b}$ [pb]	$4.7 \cdot 10^{-9}$	$2.5 \cdot 10^{-11}$	$9.1 \cdot 10^{-14}$	$4.1 \cdot 10^{-16}$	$9.5 \cdot 10^{-16}$	$3.1 \cdot 10^{-18}$

Table 41: Benchmark points for different $\mathcal{Z}_N \times \mathcal{Z}_M$ flavor symmetries for di-flavon production channels with low flavon mass (m_a) in case of the symmetry-conserving scenario at the 27 TeV HE-LHC.

m_a [GeV]	Benchmark $\mathcal{Z}_2 \times \mathcal{Z}_5$		Benchmark $\mathcal{Z}_2 \times \mathcal{Z}_9$		Benchmark $\mathcal{Z}_2 \times \mathcal{Z}_{11}$	
	20	60	20	60	20	60
$s \rightarrow aa \rightarrow b\bar{b}\tau\tau$ [pb]	$7.8 \cdot 10^{-9}$	$4.5 \cdot 10^{-11}$	$2.4 \cdot 10^{-13}$	$1.2 \cdot 10^{-15}$	$3.4 \cdot 10^{-15}$	$1.7 \cdot 10^{-17}$
$s \rightarrow aa \rightarrow b\bar{b}\mu\mu$ [pb]	$7.4 \cdot 10^{-12}$	$4 \cdot 10^{-14}$	$5.5 \cdot 10^{-15}$	$2.5 \cdot 10^{-17}$	$2.8 \cdot 10^{-17}$	$1.3 \cdot 10^{-19}$
$s \rightarrow aa \rightarrow b\bar{b}b\bar{b}$ [pb]	$2 \cdot 10^{-8}$	$1.3 \cdot 10^{-10}$	$4.7 \cdot 10^{-13}$	$2.8 \cdot 10^{-15}$	$4.2 \cdot 10^{-15}$	$2.6 \cdot 10^{-17}$

Table 42: Benchmark points for different $\mathcal{Z}_N \times \mathcal{Z}_M$ flavor symmetries for di-flavon production channels with low flavon mass (m_a) in case of the symmetry-conserving scenario at a 100 TeV collider.

7 Summary

The $\mathcal{Z}_N \times \mathcal{Z}_M$ flavor symmetry is a unique and novel framework that may have its origin either in a $U(1) \times U(1)$ symmetry or in an anomalous global $U(1)_A \times U(1)_A$ symmetry. This symmetry provides a unique way to realize the FN mechanism, resulting in an explanation to the flavor problem of the SM. In this work, we have thoroughly investigated the flavor phenomenology and the collider signatures of different realizations of the $\mathcal{Z}_N \times \mathcal{Z}_M$ flavor symmetry motivated by different theoretical demands.

In the case of quark flavor physics, the $K^0 - \bar{K}^0$ mixing places the strongest bounds on the parameter space of the flavon of the $\mathcal{Z}_2 \times \mathcal{Z}_9$ flavor symmetry in the case of the soft symmetry-breaking scenario. The $\mathcal{Z}_2 \times \mathcal{Z}_5$ flavor symmetry is subjected to the weakest constraints from the $K^0 - \bar{K}^0$ mixing. This scenario continues to remain the same even for the symmetry-conserving case, where the allowed parameter space is only along a straight dashed line. The $B_s - \bar{B}_s$ mixing better constraints the parameter space of the flavon of the $\mathcal{Z}_2 \times \mathcal{Z}_{11}$ and $\mathcal{Z}_8 \times \mathcal{Z}_{22}$ flavor symmetries for the soft symmetry-breaking scenario. In the case of the symmetry-conserving potential, the $B_s - \bar{B}_s$ mixing provides more stringent bounds on the $\mathcal{Z}_2 \times \mathcal{Z}_{11}$ flavor symmetry. The $B_d - \bar{B}_d$ mixing places more tight bounds on the parameter space of the flavon of the $\mathcal{Z}_2 \times \mathcal{Z}_{11}$ and $\mathcal{Z}_2 \times \mathcal{Z}_{5,9}$ flavor symmetries for the soft symmetry-breaking scenario. This feature continues to hold even for the symmetry-conserving potential. The $D^0 - \bar{D}^0$ mixing works remarkably well in constraining the parameter space of the flavon of the $\mathcal{Z}_2 \times \mathcal{Z}_5$ flavor symmetry for the soft symmetry-breaking scenario. This is also true for the symmetry-conserving case. The $B_{d,s} \rightarrow \mu^+ \mu^-$ decays impose relatively better bounds on the parameter space of the flavon of the $\mathcal{Z}_2 \times \mathcal{Z}_{11}$ symmetry. On the other side, the $K_L \rightarrow \mu^+ \mu^-$ decays are more sensitive to the parameter space of the flavon of the $\mathcal{Z}_2 \times \mathcal{Z}_9$ symmetry. The $B_{d,s} \rightarrow \mu^+ \mu^-$ and $K_L \rightarrow \mu^+ \mu^-$ decays place tighter constraints on the parameter space of the flavon of the $\mathcal{Z}_2 \times \mathcal{Z}_{11}$ symmetry for the symmetry-conserving scenario. The lifetime $\tau_{\mu\mu}$ is important in constraining the parameter space of the flavon of the $\mathcal{Z}_2 \times \mathcal{Z}_5$ symmetry. For the soft symmetry-breaking scenario, the lifetime $\tau_{\mu\mu}$ places more significant bounds on the parameter space of the flavon of the $\mathcal{Z}_2 \times \mathcal{Z}_{11}$ symmetry. The ratio $R_{\mu\mu}$ is a powerful observable to constrain the parameter space of the flavon of all $\mathcal{Z}_N \times \mathcal{Z}_M$ flavor symmetries for the soft symmetry-breaking as well as symmetry-conserving scenarios, and will play a crucial role in determining the parameter space of the flavon of different $\mathcal{Z}_N \times \mathcal{Z}_M$ flavor symmetries. A global fit to diverse data coming from the observables having $b \rightarrow s\mu^+ \mu^-$ transitions is performed, and allowed

ranges of the Wilson coefficients are derived. This results in bounds on the parameter space of the flavon of all $\mathcal{Z}_N \times \mathcal{Z}_M$ flavor symmetries for the soft symmetry-breaking as well as symmetry-conserving scenarios. We also predict muon forward-backward asymmetry in $B \rightarrow K \mu^+ \mu^-$ decays for $f < 200$ GeV.

On the leptonic flavor side, the decay $\mu \rightarrow e \gamma$ is able to constrain more the parameter space of the flavon of the $\mathcal{Z}_2 \times \mathcal{Z}_9$ and the $\mathcal{Z}_8 \times \mathcal{Z}_{22}$ flavor symmetries for the soft symmetry-breaking case. However, the parameter space of the flavon of the $\mathcal{Z}_2 \times \mathcal{Z}_{11}$ is more constrained for the symmetry-conserving scenario. The $A \mu \rightarrow A e$ conversion is more effective in constraining the parameter space of the flavon of the $\mathcal{Z}_8 \times \mathcal{Z}_{22}$ flavor symmetry for the soft symmetry-breaking scenario. In the case of symmetry-conserving scenario, the parameter space of the flavon of the $\mathcal{Z}_2 \times \mathcal{Z}_{11}$ is more constrained. Similar results are obtained for the $\mu \rightarrow 3e$ and $\tau \rightarrow 3\mu$ decays.

In the study of collider physics of the flavon of different $\mathcal{Z}_N \times \mathcal{Z}_M$ flavor symmetries, we computed flavon decays as well as $t \rightarrow (c, u)a$ decays. The $t \rightarrow ca$ decays are within the reach of the HL-LHC, HE-LHC, and a 100 TeV collider only for the $\mathcal{Z}_2 \times \mathcal{Z}_{11}$ and the $\mathcal{Z}_8 \times \mathcal{Z}_{22}$ flavor symmetries for the soft symmetry-breaking scenario. Furthermore, we have investigated inclusive, associative, and di-flavon production signatures of flavon for the soft symmetry-breaking as well as symmetry-conserving scenarios. We have predicted the sensitivities of these channels for the HL-LHC, HE-LHC, and a 100 TeV collider in a model-independent way using the square root scaling of luminosity. We compare our benchmark predictions for heavy and light flavon at the HL-LHC, HE-LHC, and a 100 TeV collider to estimated sensitivities of the HL-LHC, HE-LHC and a 100 TeV collider for all the $\mathcal{Z}_N \times \mathcal{Z}_M$ flavor symmetries discussed in this work. In the case of inclusive production channels, a 100 TeV collider can probe the $\mathcal{Z}_2 \times \mathcal{Z}_{5,9}$ and the $\mathcal{Z}_8 \times \mathcal{Z}_{22}$ flavor symmetries for the soft symmetry-breaking scenario for a heavy flavon. The HE-LHC will be able to probe the $\mathcal{Z}_2 \times \mathcal{Z}_5$ and the $\mathcal{Z}_8 \times \mathcal{Z}_{22}$ flavor symmetries better than the HL-LHC for the soft symmetry-breaking scenario. In the case of a light flavon, the HE-LHC and a 100 TeV collider can probe all the $\mathcal{Z}_N \times \mathcal{Z}_M$ flavor symmetries in the $\tau\tau$ channel for the soft symmetry-breaking scenario. A few specific inclusive signatures are within the reach of the 14 TeV high-luminosity LHC only for the $\mathcal{Z}_2 \times \mathcal{Z}_5$ and $\mathcal{Z}_8 \times \mathcal{Z}_{22}$ flavor symmetries. The symmetry-conserving scenario is beyond the reach of detection capabilities of any collider for the inclusive processes.

For associative production modes, only the parameter space of the flavon of the $\mathcal{Z}_8 \times \mathcal{Z}_{22}$ flavor is accessible to the HL-LHC, HE-LHC, and a 100 TeV collider through the $t\bar{t}a \rightarrow t\bar{t}t\bar{t}$ channel in the soft symmetry-breaking scenario for high flavon mass. The di-flavon production channels for heavy flavon are insensitive to the HL-LHC, HE-LHC, and even to a 100 TeV collider for all the $\mathcal{Z}_N \times \mathcal{Z}_M$ flavor symmetries in the case of soft symmetry-breaking scenario. However, a light flavon scenario can be probed for all the $\mathcal{Z}_N \times \mathcal{Z}_M$ flavor symmetries at the HL-LHC, HE-LHC, and a 100 TeV collider. In the case of the symmetry-conserving scenario, the di-flavon productions cross-sections are too small to be accessible at the HL-LHC, HE-LHC as well as a 100 TeV collider, and can be further constrained through the precision flavor physics in future. Collider simulations for some particular signatures, such as $pp \rightarrow a \rightarrow t\bar{t}$, could be an interesting future investigation, which is an expected sequel to the present work [158].

Acknowledgement

We acknowledge the use of JaxoDraw [159] for creating the Feynman diagrams in this work. This work is supported by the Council of Science and Technology, Govt. of Uttar Pradesh, India through the project “A new paradigm for flavor problem” no. CST/D-1301, and Science and Engineering Research Board, Department of Science and Technology, Government of India through the project “Higgs Physics within and beyond the Standard Model” no. CRG/2022/003237. NS acknowledges the support through the INSPIRE fellowship by the Department of Science and Technology, Government of India.

Benchmark points for the Yukawa couplings

We perform a χ^2 fit to the quark and charged-lepton masses, along with the quark mixing parameters, by defining,

$$\chi^2 = \frac{(m_q - m_q^{\text{model}})^2}{\sigma_{m_q}^2} + \frac{(m_\ell - m_\ell^{\text{model}})^2}{\sigma_{m_\ell}^2} + \frac{(\sin \theta_{ij} - \sin \theta_{ij}^{\text{model}})^2}{\sigma_{\sin \theta_{ij}}^2} + \frac{(\sin 2\beta - \sin 2\beta^{\text{model}})^2}{\sigma_{\sin 2\beta}^2}$$

$$+ \frac{(\alpha - \alpha^{\text{model}})^2}{(\sigma_\alpha)^2} + \frac{(\gamma - \gamma^{\text{model}})^2}{(\sigma_\gamma)^2}, \quad (87)$$

where $q = \{u, d, c, s, t, b\}$, $\ell = \{e, \mu, \tau\}$, and $i, j = 1, 2, 3$. The CKM matrix phases in the standard parametrization are given by

$$\beta^{\text{model}} = \arg\left(-\frac{V_{cd}V_{cb}^*}{V_{td}V_{tb}^*}\right), \quad \alpha^{\text{model}} = \arg\left(-\frac{V_{td}V_{tb}^*}{V_{ud}V_{ub}^*}\right), \quad \gamma^{\text{model}} = \arg\left(-\frac{V_{ud}V_{ub}^*}{V_{cd}V_{cb}^*}\right). \quad (88)$$

To reproduce the fermion masses, we use the following values of the quark and charged-lepton masses at 1TeV[160],

$$\begin{aligned} \{m_t, m_c, m_u\} &\simeq \{150.7 \pm 3.4, 0.532_{-0.073}^{+0.074}, (1.10_{-0.37}^{+0.43}) \times 10^{-3}\} \text{ GeV}, \\ \{m_b, m_s, m_d\} &\simeq \{2.43 \pm 0.08, 4.7_{-1.3}^{+1.4} \times 10^{-2}, 2.50_{-1.03}^{+1.08} \times 10^{-3}\} \text{ GeV}, \\ \{m_\tau, m_\mu, m_e\} &\simeq \{1.78 \pm 0.2, 0.105_{-9.3 \times 10^{-9}}^{+9.4 \times 10^{-9}}, 4.96 \pm 0.00000043 \times 10^{-4}\} \text{ GeV}. \end{aligned} \quad (89)$$

The magnitudes and phases of the CKM mixing elements are [51],

$$\begin{aligned} |V_{ud}| &= 0.97370 \pm 0.00014, |V_{cb}| = 0.0410 \pm 0.0014, |V_{ub}| = 0.00382 \pm 0.00024, \\ \sin 2\beta &= 0.699 \pm 0.017, \alpha = (84.9_{-4.5}^{+5.1})^\circ, \gamma = (72.1_{-4.5}^{+4.1})^\circ, \delta = 1.196_{-0.043}^{+0.045} \end{aligned} \quad (90)$$

The $\mathcal{Z}_2 \times \mathcal{Z}_5$ model

The dimensionless coefficients $y_{ij}^{u,d,\ell,\nu} = |y_{ij}^{u,d,\ell,\nu}| e^{i\phi_{ij}^{q,\ell,\nu}}$ are scanned with $|y_{ij}^{u,d,\ell,\nu}| \in [0.1, 4\pi]$ and $\phi_{ij}^{q,\ell,\nu} \in [0, 2\pi]$. The fit results are,

$$\begin{aligned} Y_u &= \begin{pmatrix} -1.68 - 3.37i & -0.09 + 0.03i & -0.1 - 0.02i \\ 1.53 + 4.95i & -0.57 + 0.55i & 0.48 + 0.002i \\ 0.76 + 0.18i & -1.04 + 0.46i & 0.58 - 0.65i \end{pmatrix}, Y_d = \begin{pmatrix} -4.15 + 3.58i & 2.20 - 0.89i & 2.62 - 4.20i \\ -0.33 - 0.36i & 0.07 - 0.075i & 0.17 + 0.47i \\ -0.24 - 0.07i & -0.06 - 0.084i & -0.07 - 0.12i \end{pmatrix}, \\ Y_l &= \begin{pmatrix} -0.07 - 0.06i & 0.099 - 0.004i & 0.45 - 0.32i \\ -0.14 - 0.09i & 0.08 - 0.06i & -0.63 + 0.24i \\ -0.04 + 0.09i & -0.09 + 0.06i & 0.10 - 0.0003i \end{pmatrix} \end{aligned}$$

with $\epsilon = 0.1$, $\delta = 1.196$, and $\chi_{min}^2 = 3.16$.

The $\mathcal{Z}_2 \times \mathcal{Z}_9$ model

The dimensionless coefficients $y_{ij}^{u,d,\ell,\nu} = |y_{ij}^{u,d,\ell,\nu}| e^{i\phi_{ij}^{q,\ell,\nu}}$ are scanned with $|y_{ij}^{u,d,\ell,\nu}| \in [0.9, 2\pi]$ and $\phi_{ij}^{q,\ell,\nu} \in [0, 2\pi]$. The fit results are,

$$\begin{aligned} Y_u &= \begin{pmatrix} 1 & 0.87 - 0.49i & -0.23 + 0.97i \\ -0.9 + 1.05i & -0.7 - 0.72i & 1 \\ 0.94 - 0.33i & 0.55 + 0.84i & 0.9 \end{pmatrix}, Y_d = \begin{pmatrix} 0.99 - 0.09i & 3.24 - 1.05i & 1 \\ 0.99 - 0.10i & 0.92 + 0.39i & 0.9 \\ 1 & 1 & -1.04 + 0.54i \end{pmatrix}, \\ Y_l &= \begin{pmatrix} 0.9 & 0.9 & 1.5 \\ 0.9 & 1.5 & 1.5 \\ 1.5 & 1.5 & 0.9 \end{pmatrix} \end{aligned}$$

with $\epsilon = 0.23$, $\delta = 1.196$, and $\chi_{min}^2 = 5.91$.

The $\mathcal{Z}_2 \times \mathcal{Z}_{11}$ model

The dimensionless coefficients $y_{ij}^{u,d,\ell,\nu} = |y_{ij}^{u,d,\ell,\nu}| e^{i\phi_{ij}^{q,\ell,\nu}}$ are scanned with $|y_{ij}^{u,d,\ell,\nu}| \in [0.7, 2\pi]$ and $\phi_{ij}^{q,\ell,\nu} \in [0, 2\pi]$. The fit results are,

$$Y_u = \begin{pmatrix} 2.19 - 0.18i & 1.40 - 0.09i & 0.70 - 0.002i \\ 2.12 + 0.02i & -1.02 + 2.12i & 4.45 - 1.01i \\ 0.33 - 0.71i & 0.92 + 0.42i & 0.82 - 0.26i \end{pmatrix}, Y_d = \begin{pmatrix} 0.40 + 0.59i & 3.61 - 0.16i & 3.34 - 4.06i \\ 1.02 + 0.01i & -0.36 + 1.18i & 1.29 + 0.36i \\ -0.77 + 0.33i & 0.82 + 0.02i & -0.51 + 0.48i \end{pmatrix}$$

$$Y_l = \begin{pmatrix} -0.73 + 0.001i & -0.58 + 0.53i & 0.001 + 1.29i \\ 6.24 + 0.37i & 3.48 - 2.44i & 1.71 + 1.7 \times 10^{-5}i \\ 0.24 - 1.16i & -0.36 - 0.61i & -0.60 + 0.35i \end{pmatrix}$$

with $\epsilon = 0.28$, $\delta = 1.196$, and $\chi_{min}^2 = 11.82$.

The $\mathcal{Z}_8 \times \mathcal{Z}_{22}$ model

The dimensionless coefficients $y_{ij}^{u,d,\ell,\nu} = |y_{ij}^{u,d,\ell,\nu}| e^{i\phi_{ij}^{q,\ell,\nu}}$ are scanned with $|y_{ij}^{u,d,\ell,\nu}| \in [0.9, 2]$ and $\phi_{ij}^{q,\ell,\nu} \in [0, 2\pi]$. The fit results are,

$$Y_u = \begin{pmatrix} 0.12 + 1.44i & -0.38 - 0.82i & 0.989 + 0.004i \\ -1.27 - 1.38i & -0.56 + 0.82i & -1.22 - 0.24i \\ -1.12 - 0.25i & -1.12 - 0.43i & -2.70 - 2.61i \end{pmatrix}, Y_d = \begin{pmatrix} -1.36 + 0.39i & 0.31 - 1.28i & 0.71 + 0.61i \\ -1.05 + 0.27i & -0.44 + 0.85i & 0.47 - 0.79i \\ -1.11 - 0.37i & -0.81 + 0.42i & 0.80 + 0.82i \end{pmatrix}$$

$$Y_l = \begin{pmatrix} -1.40 - 0.21i & 1.14 - 0.004i & -0.78 + 0.45i \\ -0.88 + 0.16i & -0.54 + 0.78i & -1.16 + 0.11i \\ 0.85 + 0.34i & 0.899 + 0.003i & 0.899 - 0.003i \end{pmatrix}$$

with $\epsilon = 0.23$, $\delta = 1.196$, and $\chi_{min}^2 = 1.62$.

The SM background

Production mode	Channel	SM Backgrounds
Inclusive production	jet-jet	$pp \rightarrow jj$
	$\ell^+ \ell^- (\ell = e, \mu, \tau)$	$pp \rightarrow \ell^+ \ell^-$
	μe	$pp \rightarrow tt, pp \rightarrow VV (V = W^+, W^-, Z),$ $pp \rightarrow \ell^+ \ell^-, pp \rightarrow tWb$
	$\mu\tau, e\tau$	$pp \rightarrow \text{multijets}, pp \rightarrow W + \text{jets},$ $pp \rightarrow t\bar{t}, pp \rightarrow VV (V = W^+, W^-, Z),$ $pp \rightarrow \ell^+ \ell^-, pp \rightarrow tWb$
	$b\bar{b}$	$pp \rightarrow b\bar{b}$
	$\gamma\gamma$	$pp \rightarrow \gamma\gamma$
	$t\bar{t}$	$pp \rightarrow t\bar{t}$
Associative production	$t\bar{t}a \rightarrow t\bar{t}t\bar{t}$	$pp \rightarrow t\bar{t}t\bar{t}$
	$abb \rightarrow \tau\tau b\bar{b}$	$pp \rightarrow \tau\tau b\bar{b}$
	$ab \rightarrow \tau\tau b$	$pp \rightarrow \text{multijets}, pp \rightarrow W + \text{jets}, pp \rightarrow t\bar{t}$ $pp \rightarrow \ell^+ \ell^-, pp \rightarrow tWb, pp \rightarrow VV$
Di-flavon production	$aa \rightarrow b\bar{b}\ell\ell (\ell = \mu, \tau)$	$pp \rightarrow b\bar{b}\ell\ell$
	$aa \rightarrow b\bar{b}b\bar{b}$	$pp \rightarrow b\bar{b}b\bar{b}$

Table 43: SM Backgrounds for the flavon production through various channels.

The dark-technicolor paradigm

In this appendix, we show how the $\mathcal{Z}_N \times \mathcal{Z}_M$ flavor symmetry and the FN mechanism of the $\mathcal{Z}_8 \times \mathcal{Z}_{22}$ model naturally emerge from a dark-technicolour paradigm [3, 4, 6]. The technicolour paradigm is obtained by $SU(N_{\text{TC}}) \times SU(N_{\text{DTC}}) \times SU(N_{\text{F}})$, where TC denotes the standard technicolour gauge group, DTC is for the dark-technicolour, and the F stands for the strong dynamics of vector-like fermions.

The TC fermions transform under the symmetry $\text{SM} \times \mathcal{G}$ as [4],

$$\begin{aligned} T_q^i &\equiv \begin{pmatrix} T \\ B \end{pmatrix}_L : (1, 2, 0, N_{\text{TC}}, 1, 1), \\ T_R^i &: (1, 1, 1, N_{\text{TC}}, 1, 1), B_R^i : (1, 1, -1, N_{\text{TC}}, 1, 1), \end{aligned} \quad (91)$$

where $i = 1, 2, 3 \dots$, and $+\frac{1}{2}$ is the electric charge for T , and $-\frac{1}{2}$ is that of the B .

The transformation of the DTC fermions under the $\text{SM} \times \mathcal{G}$ symmetry is [4],

$$\mathcal{D}_q^i \equiv \mathcal{C}_{L,R}^i : (1, 1, 1, 1, N_{\text{DTC}}, 1), \mathcal{S}_{L,R}^i : (1, 1, -1, 1, N_{\text{DTC}}, 1), \quad (92)$$

where $i = 1, 2, 3 \dots$, and electric charges are $+\frac{1}{2}$ for \mathcal{C} and $-\frac{1}{2}$ for \mathcal{S} .

The fermions of the $SU(N_{\text{F}})$ symmetry have the following behavior under the $\text{SM} \times \mathcal{G}$ symmetry [4],

$$\begin{aligned} F_{L,R} &\equiv U_{L,R}^i \equiv (3, 1, \frac{4}{3}, 1, 1, N_{\text{F}}), D_{L,R}^i \equiv (3, 1, -\frac{2}{3}, 1, 1, N_{\text{F}}), \\ N_{L,R}^i &\equiv (1, 1, 0, 1, 1, N_{\text{F}}), E_{L,R}^i \equiv (1, 1, -2, 1, 1, N_{\text{F}}), \end{aligned} \quad (93)$$

where $i = 1, 2, 3 \dots$.

We notice that there are three axial $U(1)_{\text{A}}^{\text{TC,DTC,F}}$ symmetries in the dark-technicolor paradigm. They are broken by instanton effects to a cyclic discrete group as $U(1)_{\text{A}}^{\text{TC,DTC,F}} \rightarrow \mathcal{Z}_{2K_{\text{TC,DTC,F}}}$ [161], where $K_{\text{TC,DTC,F}}$ show the number of massless flavors of the TC, DTC and F gauge symmetries in the N -dimensional representation of the gauge group $SU(N)_{\text{TC,DTC,F}}$. Thus, we observe a natural emergence of a generic $\mathcal{Z}_N \times \mathcal{Z}_M \times \mathcal{Z}_P$ flavor symmetry, whose subset is the $\mathcal{Z}_N \times \mathcal{Z}_M$ flavor symmetry.

In the next step, we assume the existence of an extended technicolour dynamics (ETC) which accommodates the SM, TC, and DTC sectors. This provides the required interactions for the masses of fermions in the FN mechanism. These interactions are shown in figure 31, where $\langle \varphi \rangle$ and $\langle \chi \rangle$ show the Higgs and flavon VEVs, respectively, in the form of an on-shell chiral condensate.

The multi-fermion condensate can be written as [162],

$$\langle (\bar{\psi}_L \psi_R)^n \rangle \sim (\Lambda \exp(k \Delta \chi))^{3n}, \quad (94)$$

where $\Delta \chi$ is the chirality of an operator, k is a constant, and Λ represents the scale of the underlying gauge theory.

Now, the masses of the SM fermions in the FN mechanism can be written as,

$$m_f \approx \frac{\Lambda_{\text{TC}}^3}{\Lambda_{\text{ETC}}^2} \left(\frac{1}{\Lambda} \frac{\Lambda_{\text{DTC}}^3}{\Lambda_{\text{ETC}}^2} \exp(2k) \right)^{n_{ij}^f}, \quad (95)$$

where $f = u, d$, and Λ_{TC} , Λ_{DTC} and Λ are the scale of the TC, DTC, and F dynamics, respectively. We can now identify the order parameter ϵ as,

$$\epsilon = \frac{\langle \chi \rangle}{\Lambda} \propto \frac{1}{\Lambda} \frac{\Lambda_{\text{DTC}}^3}{\Lambda_{\text{ETC}}^2} \exp(2k), \quad (96)$$

and the SM Higgs VEV is given by,

$$\langle \varphi \rangle \propto \frac{\Lambda_{\text{TC}}^3}{\Lambda_{\text{ETC}}^2}. \quad (97)$$

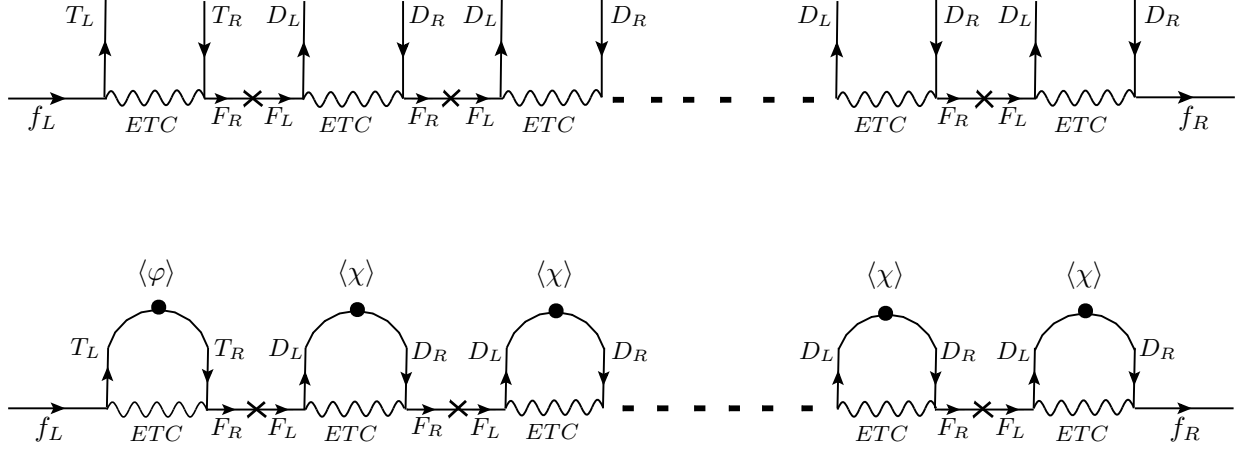


Figure 31: Feynman diagrams for the masses of the quarks and charged leptons in the dark-technicolour paradigm. On the top, the generic interactions of the SM, TC, F and DTC fermions are shown. In the bottom, we see the formations of the on-shell condensates $\langle\varphi\rangle$ and $\langle\chi\rangle$ (circular blobs), and the resulting mass of the SM fermions.

References

- [1] G. Abbas, R. Adhikari, E. J. Chun and N. Singh, [arXiv:2308.14811 [hep-ph]].
- [2] G. Abbas, doi:10.31526/ACP.BSM-2023.3 [arXiv:2404.03232 [hep-ph]].
- [3] G. Abbas, Int. J. Mod. Phys. A **34** (2019) no.20, 1950104 doi:10.1142/S0217751X19501045 [arXiv:1712.08052 [hep-ph]].
- [4] G. Abbas, Int. J. Mod. Phys. A **37**, no.11n12, 2250056 (2022) doi:10.1142/S0217751X22500567 [arXiv:2012.11283 [hep-ph]].
- [5] G. Abbas, [arXiv:2310.12915 [hep-ph]].
- [6] G. Abbas and N. Singh, [arXiv:2312.16532 [hep-ph]].
- [7] C. D. Froggatt and H. B. Nielsen, Nucl. Phys. B **147**, 277 (1979). doi:10.1016/0550-3213(79)90316-X
- [8] M. Leurer, Y. Nir and N. Seiberg, Nucl. Phys. B **398**, 319 (1993); M. Leurer, Y. Nir and N. Seiberg, Nucl. Phys. B **420**, 468 (1994).
- [9] E. J. Chun and A. Lukas, Phys. Lett. B **387**, 99-106 (1996) doi:10.1016/0370-2693(96)01015-5 [arXiv:hep-ph/9605377 [hep-ph]].
- [10] K. S. Babu and S. Nandi, Phys. Rev. D **62**, 033002 (2000) doi:10.1103/PhysRevD.62.033002 [hep-ph/9907213].
- [11] G. G. Ross and L. Velasco-Sevilla, Nucl. Phys. B **653**, 3-26 (2003) doi:10.1016/S0550-3213(03)00041-5 [arXiv:hep-ph/0208218 [hep-ph]]. S. F. King, JHEP **01**, 119 (2014) doi:10.1007/JHEP01(2014)119 [arXiv:1311.3295 [hep-ph]]. G. F. Giudice and O. Lebedev, Phys. Lett. B **665**, 79-85 (2008) doi:10.1016/j.physletb.2008.05.062 [arXiv:0804.1753 [hep-ph]].
- [12] A. Davidson, V. P. Nair and K. C. Wali, Phys. Rev. D **29**, 1504 (1984) doi:10.1103/PhysRevD.29.1504
- [13] A. Davidson and K. C. Wali, Phys. Rev. Lett. **60**, 1813 (1988) doi:10.1103/PhysRevLett.60.1813

- [14] Z. G. Berezhiani and M. Y. Khlopov, Sov. J. Nucl. Phys. **51**, 739-746 (1990)
- [15] Z. G. Berezhiani and M. Y. Khlopov, Sov. J. Nucl. Phys. **51**, 935-942 (1990)
- [16] Z. G. Berezhiani and M. Y. Khlopov, Z. Phys. C **49**, 73-78 (1991) doi:10.1007/BF01570798
- [17] A. S. Sakharov and M. Y. Khlopov, Phys. Atom. Nucl. **57**, 651-658 (1994)
- [18] A. R. Shaikh and R. Adhikari, [arXiv:2404.11570 [hep-ph]].
- [19] J. L. Yang, H. B. Zhang and T. F. Feng, Eur. Phys. J. C **84**, no.6, 616 (2024) doi:10.1140/epjc/s10052-024-12958-5 [arXiv:2405.17807 [hep-ph]].
- [20] A. Hinata, JHEP **07**, 147 (2020) doi:10.1007/JHEP07(2020)147 [arXiv:2004.08824 [hep-ph]].
- [21] G. Abbas, Int. J. Mod. Phys. A **36**, 2150090 (2021) doi:10.1142/S0217751X21500901 [arXiv:1807.05683 [hep-ph]].
- [22] G. Abbas, V. Singh, N. Singh and R. Sain, Eur. Phys. J. C **83**, no.4, 305 (2023) doi:10.1140/epjc/s10052-023-11471-5 [arXiv:2208.03733 [hep-ph]].
- [23] T. Higaki and J. Kawamura, JHEP **03**, 129 (2020) doi:10.1007/JHEP03(2020)129 [arXiv:1911.09127 [hep-ph]].
- [24] H. Georgi and S. L. Glashow, Phys. Rev. D **7**, 2457 (1973).
- [25] T. Gherghetta and A. Pomarol, Nucl. Phys. B **586**, 141 (2000); Y. Grossman and M. Neubert, Phys. Lett. B **474**, 361 (2000); M. Blanke, A. J. Buras, B. Duling, S. Gori and A. Weiler, JHEP **0903**, 001 (2009); S. Casagrande, F. Goertz, U. Haisch, M. Neubert and T. Pfoh, JHEP **0810**, 094 (2008); M. Bauer, S. Casagrande, U. Haisch and M. Neubert, JHEP **1009**, 017 (2010).
- [26] D. B. Kaplan, Nucl. Phys. B **365**, 259 (1991).
- [27] J. Fuentes-Martin, G. Isidori, J. M. Lizana, N. Selimovic and B. A. Stefanek, Phys. Lett. B **834**, 137382 (2022) doi:10.1016/j.physletb.2022.137382 [arXiv:2203.01952 [hep-ph]].
- [28] G. Abbas, Phys. Lett. B **773**, 252-257 (2017) doi:10.1016/j.physletb.2017.08.028 [arXiv:1706.02564 [hep-ph]].
- [29] G. Abbas, Mod. Phys. Lett. A **34**, no.15, 1950119 (2019) doi:10.1142/S0217732319501190 [arXiv:1706.01052 [hep-ph]].
- [30] G. Abbas, Phys. Rev. D **95**, no.1, 015029 (2017) doi:10.1103/PhysRevD.95.015029 [arXiv:1609.02899 [hep-ph]].
- [31] G. Abbas, Mod. Phys. Lett. A **31**, no.19, 1650117 (2016) doi:10.1142/S0217732316501170 [arXiv:1605.02497 [hep-ph]].
- [32] I. Dorsner and S. M. Barr, Phys. Rev. D **65**, 095004 (2002) doi:10.1103/PhysRevD.65.095004 [arXiv:hep-ph/0201207 [hep-ph]].
- [33] M. Bauer, M. Carena and K. Gemmler, Phys. Rev. D **94**, no.11, 115030 (2016) doi:10.1103/PhysRevD.94.115030 [arXiv:1512.03458 [hep-ph]].
- [34] M. Bauer, T. Schell and T. Plehn, Phys. Rev. D **94**, no.5, 056003 (2016) doi:10.1103/PhysRevD.94.056003 [arXiv:1603.06950 [hep-ph]].
- [35] L. Calibbi, A. Crivellin and B. Zaldívar, Phys. Rev. D **92**, no.1, 016004 (2015) doi:10.1103/PhysRevD.92.016004 [arXiv:1501.07268 [hep-ph]].

- [36] M. Fedele, A. Mastroddi and M. Valli, JHEP **03**, 135 (2021) doi:10.1007/JHEP03(2021)135 [arXiv:2009.05587 [hep-ph]].
- [37] K. Tsumura and L. Velasco-Sevilla, Phys. Rev. D **81**, 036012 (2010) doi:10.1103/PhysRevD.81.036012 [arXiv:0911.2149 [hep-ph]].
- [38] E. L. Berger, S. B. Giddings, H. Wang and H. Zhang, Phys. Rev. D **90**, no. 7, 076004 (2014) doi:10.1103/PhysRevD.90.076004 [arXiv:1406.6054 [hep-ph]].
- [39] K. Huitu, V. Keus, N. Koivunen and O. Lebedev, JHEP **05**, 026 (2016) doi:10.1007/JHEP05(2016)026 [arXiv:1603.06614 [hep-ph]].
- [40] J. L. Diaz-Cruz and U. J. Saldaña-Salazar, Nucl. Phys. B **913**, 942-963 (2016) doi:10.1016/j.nuclphysb.2016.10.018 [arXiv:1405.0990 [hep-ph]].
- [41] M. A. Arroyo-Ureña, J. L. Díaz-Cruz, G. Tavares-Velasco, A. Bolaños and G. Hernández-Tomé, Phys. Rev. D **98**, no.1, 015008 (2018) doi:10.1103/PhysRevD.98.015008 [arXiv:1801.00839 [hep-ph]].
- [42] M. A. Arroyo-Ureña, A. Fernández-Télez and G. Tavares-Velasco, [arXiv:1906.07821 [hep-ph]].
- [43] M. A. Arroyo-Ureña, A. Chakraborty, J. L. Díaz-Cruz, D. K. Ghosh, N. Khan and S. Moretti, [arXiv:2205.12641 [hep-ph]].
- [44] A. Alves, A. G. Dias, E. da Silva Almeida and D. S. V. Gonçalves, Phys. Rev. D **109**, no.5, 055013 (2024) doi:10.1103/PhysRevD.109.055013 [arXiv:2306.14957 [hep-ph]].
- [45] A. Chakraborty, D. K. Ghosh, N. Khan and S. Moretti, [arXiv:2405.16939 [hep-ph]].
- [46] A. Abada *et al.* [FCC], Eur. Phys. J. ST **228**, no.5, 1109-1382 (2019) doi:10.1140/epjst/e2019-900088-6
- [47] A. Abada *et al.* [FCC], Eur. Phys. J. C **79**, no.6, 474 (2019) doi:10.1140/epjc/s10052-019-6904-3
- [48] A. Rasin, Phys. Rev. D **58**, 096012 (1998) doi:10.1103/PhysRevD.58.096012 [arXiv:hep-ph/9802356 [hep-ph]].
- [49] G. G. Ross in “flavor Physics for the Millennium”, Editor Jonathan L. Rosner, World Scientific, Singapore, 2001
- [50] G. Abbas, R. Adhikari and E. J. Chun, [arXiv:2303.10125 [hep-ph]].
- [51] P.A. Zyla *et al.* (Particle Data Group), Prog. Theor. Exp. Phys. 2020, 083C01 (2020) and 2021 update
- [52] Y. Aoki *et al.*, [arXiv:2111.09849v1 [hep-lat]].
- [53] M. Ciuchini *et al.*, JHEP **9810** (1998) 008 doi:10.1088/1126-6708/1998/10/008 [hep-ph/9808328].
- [54] J. Brod and M. Gorbahn, Next-to-next-to-leading-order charm-quark contribution to the CP violation parameter ϵ_K and ΔM_K , Phys.Rev.Lett. 108 (2012) 121801, [1108.2036]
- [55] Buchalla, Gerhard and Buras, Andrzej J. and Lautenbacher, Markus E., doi:10.1103/RevModPhys.68.1125, <https://link.aps.org/doi/10.1103/RevModPhys.68.1125>
- [56] J. Brod and M. Gorbahn, ϵ_K at next-to-next-to-leading order: the charm-top-quark contribution, Phys. Rev. D **82** (2010) 094026, [1007.0684].
- [57] D. Becirevic, V. Gimenez, G. Martinelli, M. Papinutto and J. Reyes, JHEP **04** (2002), 025 doi:10.1088/1126-6708/2002/04/025 [arXiv:hep-lat/0110091 [hep-lat]].
- [58] M. Bona *et al.* [UTfit Collaboration], JHEP **0803**, 049 (2008), <http://www.utfit.org/UTfit/>
- [59] Y. Amhis *et al.* [HFLAV], Eur. Phys. J. C **77**, no.12, 895 (2017) doi:10.1140/epjc/s10052-017-5058-4 [arXiv:1612.07233 [hep-ex]].

- [60] A. J. Buras, F. De Fazio, J. Girrbach, R. Kneijens and M. Nagai, JHEP **1306**, 111 (2013).
- [61] A. Crivellin, A. Kokulu and C. Greub, Phys. Rev. D **87**, no. 9, 094031 (2013).
- [62] D. Becirevic, M. Ciuchini, E. Franco, V. Gimenez, G. Martinelli, A. Masiero, M. Papinutto, J. Reyes and L. Silvestrini, Nucl. Phys. B **634** (2002), 105-119 doi:10.1016/S0550-3213(02)00291-2 [arXiv:hep-ph/0112303 [hep-ph]].
- [63] A. Donini, V. Gimenez, L. Giusti and G. Martinelli, Phys. Lett. B **470**, 233-242 (1999) doi:10.1016/S0370-2693(99)01300-3 [arXiv:hep-lat/9910017 [hep-lat]].
- [64] J. Charles, S. Descotes-Genon, Z. Ligeti, S. Monteil, M. Papucci, K. Trabelsi and L. Vale Silva, Phys. Rev. D **102**, no.5, 056023 (2020) doi:10.1103/PhysRevD.102.056023 [arXiv:2006.04824 [hep-ph]].
- [65] J. Charles, S. Descotes-Genon, Z. Ligeti, S. Monteil, M. Papucci and K. Trabelsi, Phys. Rev. D **89**, no.3, 033016 (2014) doi:10.1103/PhysRevD.89.033016 [arXiv:1309.2293 [hep-ph]].
- [66] M. Bona [UTfit], PoS **CKM2016**, 143 (2017) doi:10.22323/1.291.0143
- [67] T. Inami and C. S. Lim, Prog. Theor. Phys. **65**, 297 (1981) [erratum: Prog. Theor. Phys. **65**, 1772 (1981)] doi:10.1143/PTP.65.297
- [68] A. J. Buras, J. Girrbach, D. Guadagnoli and G. Isidori, Eur. Phys. J. C **72**, 2172 (2012) doi:10.1140/epjc/s10052-012-2172-1 [arXiv:1208.0934 [hep-ph]].
- [69] Y. Amhis *et al.* [HFLAV], [arXiv:2206.07501 [hep-ex]].
- [70] R. Aaij *et al.* [LHCb], Phys. Rev. Lett. **128**, no.4, 041801 (2022) doi:10.1103/PhysRevLett.128.041801 [arXiv:2108.09284 [hep-ex]].
- [71] R. Aaij *et al.* [LHCb], Phys. Rev. D **105**, no.1, 012010 (2022) doi:10.1103/PhysRevD.105.012010 [arXiv:2108.09283 [hep-ex]].
- [72] K. De Bruyn, R. Fleischer, R. Kneijens, P. Koppenburg, M. Merk, A. Pellegrino and N. Tuning, Phys. Rev. Lett. **109**, 041801 (2012) doi:10.1103/PhysRevLett.109.041801 [arXiv:1204.1737 [hep-ph]].
- [73] R. Fleischer, [arXiv:1212.4967 [hep-ph]].
- [74] [CMS], CMS-PAS-BPH-21-006.
- [75] W. Altmannshofer and F. Archilli, [arXiv:2206.11331 [hep-ph]].
- [76] K. De Bruyn, R. Fleischer, R. Kneijens, P. Koppenburg, M. Merk and N. Tuning, Phys. Rev. D **86** (2012), 014027 doi:10.1103/PhysRevD.86.014027 [arXiv:1204.1735 [hep-ph]].
- [77] M. Gorbahn and U. Haisch, Phys. Rev. Lett. **97**, 122002 (2006) doi:10.1103/PhysRevLett.97.122002 [arXiv:hep-ph/0605203 [hep-ph]].
- [78] R. Aaij *et al.* [LHCb], Phys. Lett. B **725**, 15-24 (2013) doi:10.1016/j.physletb.2013.06.037 [arXiv:1305.5059 [hep-ex]].
- [79] M. Ciuchini, M. Fedele, E. Franco, A. Paul, L. Silvestrini and M. Valli, Phys. Rev. D **107** (2023) no.5, 055036 [arXiv:2212.10516 [hep-ph]].
- [80] J. P. Lees *et al.* [BaBar Collaboration], Phys. Rev. Lett. **112**, 211802 (2014) [arXiv:1312.5364 [hep-ex]].
- [81] R. Aaij *et al.* [LHCb], JHEP **11** (2016), 047 [arXiv:1606.04731 [hep-ex]].
- [82] CDF Collaboration, CDF public note 10894.
- [83] V. Khachatryan *et al.* [CMS Collaboration], Phys. Lett. B **753**, 424 (2016) [arXiv:1507.08126 [hep-ex]].

- [84] R. Aaij *et al.* [LHCb Collaboration], JHEP **1406**, 133 (2014) [arXiv:1403.8044 [hep-ex]].
- [85] R. Aaij *et al.* [LHCb], Phys. Rev. Lett. **127** (2021) no.15, 151801 [arXiv:2105.14007 [hep-ex]].
- [86] R. Aaij *et al.* [LHCb], Phys. Rev. Lett. **125** (2020) no.1, 011802 [arXiv:2003.04831 [hep-ex]].
- [87] M. Aaboud *et al.* [ATLAS], JHEP **10**, 047 (2018) [arXiv:1805.04000 [hep-ex]].
- [88] A. M. Sirunyan *et al.* [CMS], Phys. Lett. B **781**, 517-541 (2018) [arXiv:1710.02846 [hep-ex]].
- [89] R. Aaij *et al.* [LHCb], Phys. Rev. Lett. **126**, no.16, 161802 (2021) [arXiv:2012.13241 [hep-ex]].
- [90] R. Aaij *et al.* [LHCb], JHEP **11**, 043 (2021) [arXiv:2107.13428 [hep-ex]].
- [91] F. James and M. Roos, Comput. Phys. Commun. **10**, 343-367 (1975)
- [92] D. M. Straub, arXiv:1810.08132 [hep-ph].
- [93] A. Bharucha, D. M. Straub and R. Zwicky, JHEP **08**, 098 (2016) [arXiv:1503.05534 [hep-ph]].
- [94] N. Gubernari, A. Kokulu and D. van Dyk, JHEP **01**, 150 (2019) [arXiv:1811.00983 [hep-ph]].
- [95] A. K. Alok, N. R. Singh Chundawat, S. Gangal and D. Kumar, Eur. Phys. J. C **82** (2022) no.10, 967 [arXiv:2203.13217 [hep-ph]].
- [96] N. R. Singh Chundawat, Phys. Rev. D **107** (2023), 075014 [arXiv:2207.10613 [hep-ph]].
- [97] N. R. Singh Chundawat, Phys. Rev. D **107** (2023) no.5, 055004 [arXiv:2212.01229 [hep-ph]].
- [98] C. Bobeth, G. Hiller and G. Piranishvili, JHEP **12** (2007), 040 [arXiv:0709.4174 [hep-ph]].
- [99] A. K. Alok, A. Dighe and S. U. Sankar, Phys. Rev. D **78** (2008), 114025 [arXiv:0810.3779 [hep-ph]].
- [100] J. Charles, A. Le Yaouanc, L. Oliver, O. Pene and J. C. Raynal, Phys. Rev. D **60** (1999), 014001 [arXiv:hep-ph/9812358 [hep-ph]].
- [101] M. Beneke and T. Feldmann, Nucl. Phys. B **592** (2001), 3-34 [arXiv:hep-ph/0008255 [hep-ph]].
- [102] A. M. Baldini *et al.* [MEG], Eur. Phys. J. C **76**, no.8, 434 (2016) doi:10.1140/epjc/s10052-016-4271-x [arXiv:1605.05081 [hep-ex]].
- [103] A. M. Baldini *et al.* [MEG II], Eur. Phys. J. C **78**, no.5, 380 (2018) doi:10.1140/epjc/s10052-018-5845-6 [arXiv:1801.04688 [physics.ins-det]].
- [104] B. Aubert *et al.* [BaBar], Phys. Rev. Lett. **104**, 021802 (2010) doi:10.1103/PhysRevLett.104.021802 [arXiv:0908.2381 [hep-ex]].
- [105] E. Kou *et al.* [Belle-II], PTEP **2019**, no.12, 123C01 (2019) [erratum: PTEP **2020**, no.2, 029201 (2020)] doi:10.1093/ptep/ptz106 [arXiv:1808.10567 [hep-ex]].
- [106] W. H. Bertl *et al.* [SINDRUM II], Eur. Phys. J. C **47**, 337-346 (2006) doi:10.1140/epjc/s2006-02582-x
- [107] M. L. Wong [COMET], PoS FPCP2015, 059 (2015) doi:10.22323/1.248.0059
- [108] Akiro SATO https://indico.fnal.gov/event/46669/contributions/203149/attachments/138299/173056/201210_PRISM_sato.pdf
- [109] R. M. Carey *et al.* [Mu2e], doi:10.2172/952028
- [110] N. Teshima [DeeMe], SciPost Phys. Proc. **1**, 051 (2019) doi:10.21468/SciPostPhysProc.1.051 [arXiv:1811.04235 [physics.ins-det]].

- [111] S. Davidson and B. Echenard, Eur. Phys. J. C **82**, no.9, 836 (2022) doi:10.1140/epjc/s10052-022-10773-4 [arXiv:2204.00564 [hep-ph]].
- [112] Y. Kuno, Nucl. Phys. B Proc. Suppl. **225-227**, 228-231 (2012) doi:10.1016/j.nuclphysbps.2012.02.047
- [113] U. Bellgardt *et al.* [SINDRUM], Nucl. Phys. B **299**, 1-6 (1988) doi:10.1016/0550-3213(88)90462-2
- [114] A. Blondel, A. Bravar, M. Pohl, S. Bachmann, N. Berger, M. Kiehn, A. Schoning, D. Wiedner, B. Windelband and P. Eckert, *et al.* [arXiv:1301.6113 [physics.ins-det]].
- [115] K. Hayasaka, K. Inami, Y. Miyazaki, K. Arinstein, V. Aulchenko, T. Aushev, A. M. Bakich, A. Bay, K. Belous and V. Bhardwaj, *et al.* Phys. Lett. B **687**, 139-143 (2010) doi:10.1016/j.physletb.2010.03.037 [arXiv:1001.3221 [hep-ex]].
- [116] M. A. Shifman, A. I. Vainshtein and V. I. Zakharov, Phys. Lett. B **78**, 443-446 (1978) doi:10.1016/0370-2693(78)90481-1
- [117] A. Crivellin, M. Hoferichter and M. Procura, Phys. Rev. D **89**, 054021 (2014) doi:10.1103/PhysRevD.89.054021 [arXiv:1312.4951 [hep-ph]].
- [118] A. Crivellin, M. Hoferichter and M. Procura, Phys. Rev. D **89**, 093024 (2014) doi:10.1103/PhysRevD.89.093024 [arXiv:1404.7134 [hep-ph]].
- [119] P. Junnarkar and A. Walker-Loud, Phys. Rev. D **87**, 114510 (2013) doi:10.1103/PhysRevD.87.114510 [arXiv:1301.1114 [hep-lat]].
- [120] R. Kitano, M. Koike and Y. Okada, Phys. Rev. D **66**, 096002 (2002) [erratum: Phys. Rev. D **76**, 059902 (2007)] doi:10.1103/PhysRevD.76.059902 [arXiv:hep-ph/0203110 [hep-ph]].
- [121] T. Goto, R. Kitano and S. Mori, Phys. Rev. D **92**, 075021 (2015) doi:10.1103/PhysRevD.92.075021 [arXiv:1507.03234 [hep-ph]].
- [122] A. M. Sirunyan *et al.* [CMS], JHEP **06** (2018), 127 [erratum: JHEP **03** (2019), 128] doi:10.1007/JHEP06(2018)127 [arXiv:1804.01939 [hep-ex]].
- [123] G. Aad *et al.* [ATLAS], JHEP **07**, 200 (2023) doi:10.1007/JHEP07(2023)200 [arXiv:2211.02617 [hep-ex]].
- [124] A. M. Sirunyan *et al.* [CMS], JHEP **03**, 034 (2020) doi:10.1007/JHEP03(2020)034 [arXiv:1912.01594 [hep-ex]].
- [125] G. Aad *et al.* [ATLAS], Phys. Lett. B **822**, 136651 (2021) doi:10.1016/j.physletb.2021.136651 [arXiv:2102.13405 [hep-ex]].
- [126] A. M. Sirunyan *et al.* [CMS], Phys. Rev. D **98** (2018) no.9, 092001 doi:10.1103/PhysRevD.98.092001 [arXiv:1809.00327 [hep-ex]].
- [127] J. A. Aguilar-Saavedra and G. C. Branco, Phys. Lett. B **495**, 347 (2000).
- [128] A. D. Martin, W. J. Stirling, R. S. Thorne and G. Watt, Eur. Phys. J. C **63**, 189-285 (2009) doi:10.1140/epjc/s10052-009-1072-5 [arXiv:0901.0002 [hep-ph]].
- [129] A. Alloul, N. D. Christensen, C. Degrande, C. Duhr and B. Fuks, Comput. Phys. Commun. **185**, 2250-2300 (2014) doi:10.1016/j.cpc.2014.04.012 [arXiv:1310.1921 [hep-ph]].
- [130] J. Alwall, R. Frederix, S. Frixione, V. Hirschi, F. Maltoni, O. Mattelaer, H. S. Shao, T. Stelzer, P. Torrielli and M. Zaro, JHEP **07**, 079 (2014) doi:10.1007/JHEP07(2014)079 [arXiv:1405.0301 [hep-ph]].
- [131] G. Aad *et al.* [ATLAS], JHEP **03**, 145 (2020) doi:10.1007/JHEP03(2020)145 [arXiv:1910.08447 [hep-ex]].

- [132] A. M. Sirunyan *et al.* [CMS], JHEP **05**, 033 (2020) doi:10.1007/JHEP05(2020)033 [arXiv:1911.03947 [hep-ex]].
- [133] M. Aaboud *et al.* [ATLAS], JHEP **01**, 055 (2018) doi:10.1007/JHEP01(2018)055 [arXiv:1709.07242 [hep-ex]].
- [134] A. M. Sirunyan *et al.* [CMS], JHEP **09** (2018), 007 doi:10.1007/JHEP09(2018)007 [arXiv:1803.06553 [hep-ex]].
- [135] G. Aad *et al.* [ATLAS], Phys. Lett. B **796** (2019), 68-87 doi:10.1016/j.physletb.2019.07.016 [arXiv:1903.06248 [hep-ex]].
- [136] A. M. Sirunyan *et al.* [CMS], JHEP **07** (2021), 208 doi:10.1007/JHEP07(2021)208 [arXiv:2103.02708 [hep-ex]].
- [137] G. Aad *et al.* [ATLAS], JHEP **23** (2020), 082 doi:10.1007/JHEP10(2023)082 [arXiv:2307.08567 [hep-ex]].
- [138] A. Tumasyan *et al.* [CMS], JHEP **05** (2023), 227 doi:10.1007/JHEP05(2023)227 [arXiv:2205.06709 [hep-ex]].
- [139] A. Tumasyan *et al.* [CMS], Phys. Rev. D **108** (2023) no.1, 012009 doi:10.1103/PhysRevD.108.012009 [arXiv:2205.01835 [hep-ex]].
- [140] M. Aaboud *et al.* [ATLAS], Phys. Rev. D **99** (2019) no.9, 092004 doi:10.1103/PhysRevD.99.092004 [arXiv:1902.10077 [hep-ex]].
- [141] G. Aad *et al.* [ATLAS], JHEP **10** (2020), 061 doi:10.1007/JHEP10(2020)061 [arXiv:2005.05138 [hep-ex]].
- [142] A. M. Sirunyan *et al.* [CMS], JHEP **04** (2019), 031 doi:10.1007/JHEP04(2019)031 [arXiv:1810.05905 [hep-ex]].
- [143] <https://indico.cern.ch/event/284800/contributions/1635340/attachments/527023/726700/collider-reach.pdf>
- [144] A. Tumasyan *et al.* [CMS], JHEP **07**, 073 (2023) doi:10.1007/JHEP07(2023)073 [arXiv:2208.02717 [hep-ex]].
- [145] G. Aad *et al.* [ATLAS], JHEP **07**, 155 (2023) doi:10.1007/JHEP07(2023)155 [arXiv:2211.04172 [hep-ex]].
- [146] ATLAS-CONF-2023-035, 15 Jun 2023.
- [147] [CMS], CMS-PAS-HIG-20-002.
- [148] G. Aad *et al.* [ATLAS], JHEP **07**, 203 (2023) doi:10.1007/JHEP07(2023)203 [arXiv:2211.01136 [hep-ex]].
- [149] A. M. Sirunyan *et al.* [CMS], Eur. Phys. J. C **80** (2020) no.2, 75 doi:10.1140/epjc/s10052-019-7593-7 [arXiv:1908.06463 [hep-ex]].
- [150] M. Aaboud *et al.* [ATLAS], Phys. Rev. Lett. **121**, no.19, 191801 (2018) [erratum: Phys. Rev. Lett. **122**, no.8, 089901 (2019)] doi:10.1103/PhysRevLett.121.191801 [arXiv:1808.00336 [hep-ex]].
- [151] A. M. Sirunyan *et al.* [CMS], Phys. Rev. D **96**, no.7, 072004 (2017) doi:10.1103/PhysRevD.96.072004 [arXiv:1707.00350 [hep-ex]].
- [152] M. Aaboud *et al.* [ATLAS], JHEP **01**, 030 (2019) doi:10.1007/JHEP01(2019)030 [arXiv:1804.06174 [hep-ex]].

- [153] A. M. Sirunyan *et al.* [CMS], JHEP **08**, 152 (2018) doi:10.1007/JHEP08(2018)152 [arXiv:1806.03548 [hep-ex]].
- [154] G. Aad *et al.* [ATLAS], Phys. Rev. D **105**, no.1, 012006 (2022) doi:10.1103/PhysRevD.105.012006 [arXiv:2110.00313 [hep-ex]].
- [155] A. Hayrapetyan *et al.* [CMS], [arXiv:2402.13358 [hep-ex]].
- [156] M. Aaboud *et al.* [ATLAS], JHEP **10**, 031 (2018) doi:10.1007/JHEP10(2018)031 [arXiv:1806.07355 [hep-ex]].
- [157] A. Hayrapetyan *et al.* [CMS], [arXiv:2403.10341 [hep-ex]].
- [158] Under progress.
- [159] D. Binosi, J. Collins, C. Kaufhold and L. Theussl, Comput. Phys. Commun. **180**, 1709-1715 (2009) doi:10.1016/j.cpc.2009.02.020 [arXiv:0811.4113 [hep-ph]].
- [160] Z. z. Xing, H. Zhang and S. Zhou, Phys. Rev. D **77**, 113016 (2008) doi:10.1103/PhysRevD.77.113016 [arXiv:0712.1419 [hep-ph]].
- [161] H. Harari and N. Seiberg, Phys. Lett. B **102**, 263-266 (1981) doi:10.1016/0370-2693(81)90871-6
- [162] K. I. Aoki and M. Bando, Prog. Theor. Phys. **70**, 272 (1983) doi:10.1143/PTP.70.272